THE HONG KONG
POLYTECHNIC UNIVERSITY
香港理工大學
Pao Yue-kong Library
包玉剛圖書館

Copyright Undertaking

This thesis is protected by copyright, with all rights reserved.

By reading and using the thesis, the reader understands and agrees to the following terms:

1. The reader will abide by the rules and legal ordinances governing copyright regarding the use of the thesis.

2. The reader will use the thesis for the purpose of research or private study only and not for distribution or further reproduction or any other purpose.

3. The reader agrees to indemnify and hold the University harmless from and against any loss, damage, cost, liability or expenses arising from copyright infringement or unauthorized usage.

Pao Yue-kong Library, The Hong Kong Polytechnic University, Hung Hom, Kowloon, Hong Kong

http://www.lib.polyu.edu.hk

MEASUREMENT UNCERTAINTY QUANTIFICATION AND

PROBABILITY-BASED CONTROL FOR BUILDING

CENTRAL COOLING AND AIR CONDITIONING SYSTEMS

SUN SHAOBO

PhD

The Hong Kong Polytechnic University

2023

The Hong Kong Polytechnic University

Department of Building Environment and Energy Engineering

Measurement Uncertainty Quantification and Probability-based Control for Building Central Cooling and Air Conditioning Systems

SUN SHAOBO

A thesis submitted in partial fulfilment of the requirements for the degree of

Doctor of Philosophy

October 2022

CERTIFICATE OF ORIGINALITY

I hereby declare that this thesis is my own work and that, to the best of my knowledge and belief, it reproduces no material previously published or written, nor material that has been accepted for the award of any other degree or diploma, except where due acknowledgement has been made in the text.

_____ (Signed)

_____ SUN Shaobo _____ (Name of student)

ABSTRACT

Abstract of thesis entitled: Measurement Uncertainty Quantification and Probability-based Control for Building Central Cooling and Air Conditioning Systems

Submitted by: SUN Shaobo

For the degree of: Doctor of Philosophy

at The Hong Kong Polytechnic University in October 2022

Measurements are of great importance to health monitoring, performance evaluation and online control of heating, ventilation, and air conditioning (HVAC) systems. The accuracy of the measurements used, to a certain extent, determines the reliability of the decision-making. Uncertainties inevitably exist in measurements. The uncertainties outside the normal/acceptable range may lead to significant negative impacts on the performance of HVAC systems. Existing studies tend to use indirect methods to reduce the impacts of measurement uncertainties on HVAC systems, such as control optimization, and sensor fault detection. Though these methods performed well in their respective application scenarios, their flexibility and generalization ability are poor. An effective and direct measurement uncertainty quantification method is urgently needed for HVAC systems, and online corrections of measurements with unacceptable uncertainties also need to be done for improving the reliability of HVAC systems and extending the service life of measuring instruments.

This PhD study proposes a measurement uncertainty quantification framework for HVAC systems using Bayesian inference and Markov chain Monte Carlo sampling methods.

Based on the framework, two measurement uncertainty quantification methods are developed, one based on physical models, and another one based on data-driven models. The physical model-based measurement uncertainty quantification method is tested and validated systematically on virtual water-cooled multiple chiller plants. The energy and mass balance models are established. The test results show that the measurement uncertainties (including the systematic uncertainty and random uncertainty) of chilled water and cooling water flow rates can be quantified successfully using the developed physical model-based method. The data-driven model-based measurement uncertainty quantification method is tested and validated systematically on an actual air-cooled chiller. A multiple quadratic non-linear regression model is established. The test results show that the developed data-driven model-based method can effectively quantify both the systematic and random uncertainties of chilled water flow rates, and the relative errors are within 10.00%. The two developed methods show satisfactory performance in quantifying measurement uncertainties of HVAC systems.

Based on the physical model-based measurement uncertainty quantification method, a probability-based chiller sequencing control strategy is proposed. The measured chilled water flow rate is corrected online, and the distribution of real-time cooling load can further be obtained. The control decisions are made according to the probability that the cooling load is distributed in different intervals, and the risk of decision-making can also be quantified. The results show that the root-mean-square error of cooling loads is reduced significantly by about 79% after the correction of chilled water flow rates. Compared with the conventional cooling load-based chiller sequencing control, the impacts of both positive and negative uncertainties on system operation can be reduced significantly when using the proposed control strategy.

Based on the data-driven model-based measurement uncertainty quantification method, a fresh air control optimization strategy for air handling units is proposed. The impacts of humidity measurement uncertainties on enthalpy-based fresh air control are evaluated. A multiple quadratic non-linear regression model is established to address the uncertainties of relative humidity measurements and optimize the fresh air control. The relative humidity values of fresh air and return air are corrected and used to calculate their enthalpies for control decision making. The proposed strategy is tested on a virtual platform. The test results show that the proposed fresh air control optimization strategy can significantly reduce the impacts of uncertainties of relative humidity measurements on system operation. Compared with the energy consumption before optimization, the energy consumption of the air handling unit is reduced by 1.02% - 24.58% after optimization.

PUBLICATIONS ARISING FROM THE THESIS

Journal papers published

[1] **Sun, S.B.**, Shan, K. & Wang, S.W., (2022). An online robust sequencing control strategy for identical chillers using a probabilistic approach concerning flow measurement uncertainties. *Applied Energy*, 317, 119198.

[2] **Sun, S.B.**, Wang, S.W. & Shan, K., (2022). Flow measurement uncertainty quantification for building central cooling systems with multiple water-cooled chillers using a Bayesian approach. *Applied Thermal Engineering*, 202, 117857.

[3] Tang, R., Wang, S.W. & **Sun, S.B.**, (2021). Impacts of technology-guided occupant behavior on air-conditioning system control and building energy use. *Building Simulation*, 14(1), 209-217.

Journal papers being processed

[1] **Sun, S.B.**, Shan, K. & Wang, S.W., (2022). Data-driven model-based flow measurement uncertainty quantification for building central cooling systems using a probabilistic approach. *Science and Technology for the Built Environment* (Accepted)

[2] **Sun, S.B.**, Wang, S.W. & Shan, K., Impact evaluation of measurement uncertainties and optimization for enthalpy-based fresh air control of air handling unit

ACKNOWLEDGEMENTS

I would like to express my sincerest appreciation to Professor Shengwei Wang, my supervisor, for his readily available supervision, valuable suggestions, patient encouragement and continuous support during my PhD study. Also, I would like to thank Professor Fu Xiao, for her valuable suggestions and support over the past few years.

I would also like to thank all members of the Building Energy and Automation Research Laboratory, especially Dr. Kui Shan, Dr. Hangxin Li and Dr. Bingxu Li. Their talents and diligence often inspire and encourage me to be better.

Finally, I am truly grateful for the selfless love and unconditional support from my family and friends. Without them, I can hardly finish my PhD program on time.

TABLE OF CONTENTS

LIST OF FIGURES

LIST OF TABLES

NOMENCLATURE

Abbreviations

AHU	air handling unit
BCI	Bayesian credible interval
BMS	building management system
CHWFM	chilled water flow meter
COP	coefficient of performance
CWFM	cooling water flow meter
cLHS	conditioned Latin hypercube sampling
ECDF	empirical cumulative distribution function
GP	Gaussian process
HMC	Hamiltonian Monte Carlo
HVAC	heating, ventilation and air conditioning
ICC	International Commerce Centre
IPLV	integrated part load value
MCMC	Markov chain Monte Carlo
MLR	multiple linear regression
NN	neural network
NUTS	No-U-Turn Sampler
OLS	ordinary least squares
PCA	principal component analysis
RE	relative error
RMSE	root-mean-square error
VIC	virtual in-situ calibration
VSD	variable speed drive

Notations

a	coefficients
c	specific heat capacity of water $(\text{kJ}/(\text{kg} \cdot {}^\circ\text{C}))$
C_{rated}	rated chiller capacity (kW)
COP_{FL}	full load coefficient of performance
d	dead band
d_m	humidity ratio of the moist air $(\text{kg}_w/\text{kg}_a)$
d_x	distance function
E	observation data
$\tilde{E}_{RMS}$	root-mean-square error of measured cooling loads (kW)
E'_{RMS}	root-mean-square error of quantified cooling loads (kW)
e	error of data-driven model
h	enthalpy (kJ/kg)
K	number of warmup iterations per chain
k	interval of samples saved
l	chiller capacity loss rate
N	number of operating chillers
N_{chain}	number of Markov chains
N_{iter}	number of iterations per chain
N_{sam}	number of post-warmup samples
n	number of unknown parameters or chillers
n_s	total number of samples
P	probability
P_{CH}	power consumption of chiller (kW)
P_{fan}	power consumption of fan (kW)
p	pressure (Pa)

Q	building cooling load (kW)
Q_{in}	heat absorption of the evaporator (kW)
Q_{out}	heat rejection of the condenser (kW)
Q_{unmet}	unmet cooling load (kW)
Q_N^{off}, Q_{N+1}^{on}	thresholds of cooling loads (kW)
q	water flow rate (L/s)
q_r	rated flow rate of pump (L/s)
r	risk
$\hat{R}$	potential scale reduction factor
R^2	coefficient of determination
r_b	risk boundary
r_p	part load ratio
T	temperature (°C)
T_{chws}	chilled water supply temperature (°C)
T_{chwr}	chilled water return temperature (°C)
T_{cwin}	cooling water inlet temperature (°C)
T_{cwout}	cooling water outlet temperature (°C)
x, y	known parameter/input/variable (°C)
u	uncertainty

Greek letters

α	ratio of the part-load chiller COP to its full load COP
δ	standard deviation of data-driven model error
θ	unknown parameter/input/variable
μ	mean of uncertainty (systematic uncertainty)
ρ	density of water (kg/m^3)
σ	standard deviation of uncertainty (random uncertainty)

φ	relative humidity (%)
ω	standard deviation of water flow rate (L/s)

Subscripts

air	outdoor air
chw	chilled water
chwq	chilled water flow rate
cor	corrected value
cum	cumulative
cw	cooling water
cwq	cooling water flow rate
FA	fresh air
i	chiller no.
ref	reference value
RA	return air
set	setpoint
t	time

Accents and superscript

~	measured value
—	mean value
′	quantified value

CHAPTER 1   INTRODUCTION

This chapter gives an overview of this thesis. Section 1.1 introduces the background and motivation of this study. Section 1.2 presents the aim and objectives of this study. Section 1.3 provides a brief description of each chapter and introduces the relationships between the main chapters of this thesis.

1.1 Background and motivation

Nowadays, almost all modern buildings are equipped with heating, ventilation and air conditioning (HVAC) systems for providing cooling or heating to indoor spaces and maintaining indoor thermal comfort at an acceptable level. HVAC systems are one of the most energy-consuming devices in most buildings. The building sector consumes about 40% of the total global end-use energy (Song et al., 2020), while the energy consumed by HVAC systems accounts for about 60% of the total building energy use (Omrany et al., 2016). It attracts considerable attention to the energy savings of HVAC systems.

The energy efficiency of HVAC systems highly depends on their control systems. In recent years, many optimal control strategies are developed for improving the energy efficiency of HVAC systems and achieving energy savings (Jia et al., 2021). For example, Karami and Wang (2018) achieved 10.5-13.6% of energy savings for an all-variable speed water-cooled chiller plant by employing the particle swarm optimization search algorithm to optimize the chilled water temperature setpoint, the condenser water temperature setpoint, and the threshold of cooling load. Thangavelu et al. (2017) proposed an energy optimization methodology to derive optimized operation decisions for a chiller plant and achieved 20-40% of energy savings. For the control systems of HVAC systems,

online control decisions are generally made based on real-time measurements. The control systems regulate the system behaviour/operation by detecting the changes in external conditions and/or the deviations of the process variables from their setpoints. A number of measuring instruments are installed in HVAC systems for achieving the expected control performance. Undoubtedly, the accuracy of the measuring instruments used is of vital importance to the reliability of the control systems. The performance of control systems must be affected by the uncertainties of measuring instruments.

Uncertainties inevitably exist in measurements. The uncertainties outside the acceptable range may lead to significant biases in making online control decisions, and further affect the performance of HVAC systems. In addition to the control systems, the performance evaluation and real-time monitoring of HVAC systems are also affected by measurement uncertainties, which may make managers or operators make incorrect decisions. Generally, the measuring instruments can achieve the expected performance after the initial commissioning and their uncertainties are acceptable. But the measurement uncertainties tend to be more and more significant with the performance degradation of the measuring instruments. It is recommended to calibrate the measuring instruments in situ annually for reducing the impacts of measurement uncertainties (ASHRAE, 2014), but field calibration of measuring instruments is often not carried out strictly due to site constraints and technical feasibility. There are even measuring instruments that are never calibrated in their life cycles and always work in unhealthy conditions. Apart from field calibration, there is no effective method to address the uncertainties of measuring instruments. A reliable and convenient alternative to field calibration of measuring instruments is urgently needed.

Online measurement uncertainty quantification is a very challenging task but can address the uncertainties of measuring instruments fundamentally. Effective methods to directly

quantify the uncertainties of measuring instruments in HVAC systems are still missing in the literature. Measurement uncertainties are not fixed or even random, which leads to a significant increase in the difficulty of quantifying them. In addition, the actual uncertainty of a measuring instrument always cannot be known exactly, because the uncertainty of the standard calibration instrument may also lead to a deviation between the calibration value and its true value. It raises a new problem. Even though the uncertainty of a measuring instrument can be quantified by a method, the reliability of the quantification results cannot be evaluated. The challenges in quantifying the uncertainties of measuring instruments in HVAC systems online include method development, performance evaluation, reliability analysis, online correction, and so on, and they are summarised as follows. This thesis is devoted to coping with these challenges and addressing the measurement uncertainties in HVAC systems effectively.

i. The uncertainties of measuring instruments in HVAC systems are barely investigated. An effective measurement uncertainty quantification method is difficult to be developed due to the inherent characteristics of measurement uncertainties.

ii. If a method is developed to quantify measurement uncertainties, it cannot evaluate the performance of the method without knowing the actual measurement uncertainties. A comprehensive validation and reliability analysis should be conducted for this method.

iii. The uncertainty of a measuring instrument generally follows a distribution. Even if the distribution parameters (for example, the mean and standard deviation of a normal distribution) are known or can be quantified, it is very difficult to correct the real-time measurements of the instrument online.

1.2 Aim and objectives

This PhD study, therefore, aims to develop online measurement uncertainty quantification methods for HVAC systems and use them to optimize the control systems of HVAC systems for reducing the impacts of measurement uncertainties. To achieve this aim, the following objectives are addressed effectively:

i. Develop a physical model-based measurement uncertainty quantification method and conduct a systematic validation of it. The method is applicable to quantify uncertainties of measuring instruments in the HVAC systems where one or more physical models can be established, such as multiple water-cooled chiller systems, where energy and mass balance models can be established.

ii. Propose a probability-based online robust sequencing control strategy for multiple water-cooled chiller systems. The developed physical model-based measurement uncertainty quantification method is used to correct the real-time cooling load measurements online. It can make up for the drawbacks of conventional cooling load-based chiller sequencing control strategy in confronting measurement uncertainties. In addition, the risks of control decision-making can also be assessed, and further the reliability of the control decisions made can be evaluated.

iii. Develop a data-driven model-based measurement uncertainty quantification method and conduct a systematic validation of it. The method makes up for the limitation of the developed physical model-based measurement uncertainty quantification method and is applicable to almost all types of HVAC systems.

iv. Propose a fresh air control optimization strategy for air handling unit systems, where the measurement uncertainties are quantified by the developed data-driven model-

based method. It can reduce energy waste due to measurement uncertainties and improve the reliability of fresh air control.

1.3 Organization of this thesis

This thesis consists of eight chapters, which is organized as follows.

Chapter 1 provides an overview of this thesis, including the background and motivation of this study, the aim and objectives of this study, and the organization/structure of this thesis.

Chapter 2 is a comprehensive literature review. Firstly, the impacts of measurement uncertainties on the performance of HVAC systems are presented. Secondly, the solutions to measurement uncertainties in existing studies are introduced and their limitations are analysed. Then the existing studies on uncertainty quantification for building energy models are introduced. Finally, a summary of these existing studies and the research gaps to be addressed in this study are presented.

Chapter 3 proposes a measurement uncertainty quantification framework. Firstly, the characteristics of measurement uncertainty and the measurement uncertainty quantification methods adopted in this study are introduced. Then the proposed framework of measurement uncertainty quantification is presented in detail, which is the foundation of this study. In addition, the convergence diagnostics and evaluation index are presented and will be used to check the convergence and evaluate the performance of the measurement uncertainty quantification methods proposed in this study.

Chapter 4 presents a physical model-based measurement uncertainty quantification method for multiple water-cooled chiller systems. It is validated systematically using a site test and four simulation tests. The energy and mass balance models are established to

realize it. The performance of the proposed method on quantifying measurement uncertainties is evaluated by comparing the quantified uncertainties with the "actual uncertainties" (they are known to the simulation tests).

Chapter 5 presents a probability-based online robust sequencing control strategy for multiple water-cooled chiller systems. It is developed based on the conventional total cooling load-based chiller sequencing control strategy. The physical model-based measurement uncertainty quantification method proposed in Chapter 4 is used to address the uncertainties of the measuring instruments concerned. The control decisions are made based on the probability distributions of total cooling loads and the risks are assessed. The proposed control strategy is validated systematically on a virtual test platform.

Chapter 6 presents a data-driven model-based measurement uncertainty quantification method for making up for the limitation of the physical model-based measurement uncertainty quantification method. It is validated systematically on an air-cooled chiller system by quantifying different levels of measurement uncertainties. The validation results are presented and analysed comprehensively.

Chapter 7 presents a fresh air control optimization strategy for air handling units, where the data-driven model-based measurement uncertainty quantification method proposed in Chapter 6 is used to address the uncertainties of measuring instruments concerned. The impacts of measurement uncertainties on enthalpy-based fresh air control are evaluated. And the performance of the proposed fresh air control optimization strategy is validated systematically on a virtual platform. The test results are presented and analysed in detail.

Chapter 8 summarizes the main contributions and conclusions of this PhD study and provides suggestions for future work on the research subjects concerned.

The relationships between the main chapters of this thesis are shown in Figure 1.1. The measurement uncertainty quantification framework is the foundation of this study and is presented in Chapter 3. In addition, the general information used throughout this study, such as the characteristics of measurement uncertainty, the uncertainty quantification methods adopted, and the indexes used for checking convergence and performance evaluation, are also presented in this chapter. In Chapter 4, a physical model-based measurement uncertainty quantification method is developed based on the framework proposed in Chapter 3. Based on the method developed in Chapter 3, a probability-based online robust chiller sequencing control strategy is proposed in Chapter 5. In Chapter 6, a data-driven model-based measurement uncertainty quantification method is developed. Based on the method developed in Chapter 6, a probability-based optimization strategy for fresh air control of air handling units is proposed in Chapter 7.
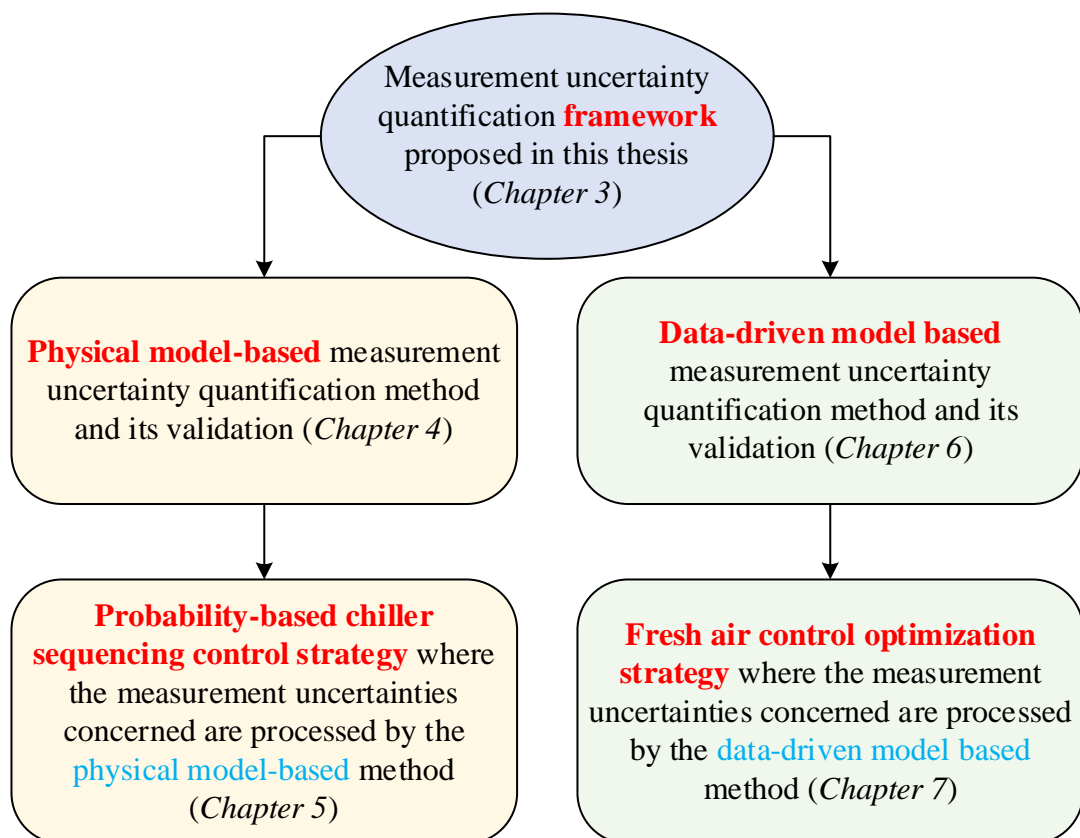
Figure 1.1 Relationships between the main chapters

CHAPTER 2   LITERATURE REVIEW

Measurements are essential to the normal operation of HVAC systems. Uncertainties in measurements certainly affect the system performance and may lead to a series of undesirable consequences (for example, high energy consumption, short service life, poor user experience, etc). The studies on measurement uncertainties of HVAC systems are of great interest in recent decades. This chapter conducts a comprehensive literature review on the uncertainty analysis of HVAC systems and gives an overview of the existing studies and the research gaps.

The organization of this chapter is as follows. Section 2.1 introduces the accuracy of commonly used measuring instruments in HVAC systems. Section 2.2 presents the impacts of measurement uncertainties on the operation performance (in the aspects of energy efficiency and reliability, etc.) of HVAC systems. Section 2.3 introduces the existing solutions to measurement uncertainties and their limitations, including the control optimization methods, sensor fault detection, and virtual sensor calibration. Section 2.4 focuses on the uncertainty quantification for building energy systems, especially the uncertainty analysis methods used. Section 2.5 gives a summary of the literature review and highlights the research gaps.

2.1 Accuracy of commonly used measuring instruments in HVAC systems

Measurement uncertainty is an inherent property of physical measuring instruments. With the development of technology, measurement uncertainty can be reduced but cannot be removed completely. Generally, there are accuracy requirements for measuring instruments. Table 2.1 shows the typical accuracy of commonly used measuring

instruments in HVAC systems (ASHRAE, 2014). In engineering practice, if the measuring instruments can meet their accuracy, their expected performance is achieved, and the measurement uncertainties are acceptable and can be ignored. However, the measurement uncertainties cannot be maintained at an acceptable range all the time due to performance degradation. The normal operation of HVAC systems must be affected with the increases of measurement uncertainties.

Table 2.1 Typical accuracy of commonly used measuring instruments in HVAC systems

Measuring instrument	Accuracy
Flow meter	2%
Power meter	1%
Temperature sensor	2%
Humidity sensor	2%-5%
Pressure sensor	1%-5%

2.2 Impacts of measurement uncertainties on HVAC systems

Measurements in HVAC systems are generally used for decision-making of control systems, performance evaluation of system running, real-time monitoring of system status, etc. Uncertainties of the measurements used certainly affect these functions and may lead to adverse consequences.

2.2.1 Impacts on control systems

Control systems are the core of HVAC systems for achieving energy-efficient and reliable operation. To some degree, the accuracy of control decisions depends on the measurements that participate in the decision-making of control systems. Uncertainties in

the measurements tend to make inaccurate control decisions and affect the operation performance of HVAC systems.

The impacts of measurement uncertainties on the main control systems of HVAC systems have been investigated systematically (Bae et al., 2021). Yan et al. (2017) found that the measurement uncertainties in outdoor air flow control led to a 17% increase in cooling energy consumption and a 43% increase in heating energy consumption. The study by Goyal et al. (2012) shows that total energy consumption increases by 18% and 16.5% during winter and summer days respectively due to the uncertainty in occupancy measurements. Lu et al. (2020) found that the measurement errors/uncertainties of the outdoor air flow sensor and supply air CO_2 sensor in an air handling unit using demand-controlled ventilation contribute to deviation rates of up to 16.9% and 94.32% in the annual energy consumption of an HVAC system and the outdoor air ratio respectively. Yoon (2020) reported that the supply air temperature sensor with a systematic error of +2 ℃ caused an increase of 38% in the total energy consumption of an air handling unit with an outside air economizer. Liao et al. (2014) systematically analysed the impacts of measurement uncertainties on the total cooling load-based, return water temperature-based, direct power-based and bypass flow-based chiller sequencing controls. Compared with the benchmark, the chiller switch number is reduced by 5.89% - 32.2%, while the supply air temperature tracking error increased dramatically by 50.95% - 14 682.83% due to measurement uncertainties concerned. Another study by Liao et al. (2015) also concluded that the total cooling load-based chiller sequencing control is affected by the measurement uncertainties heavily. The low level and high level of measurement uncertainties lead to increases of 20% and 57.1% respectively in the under-cooling percentage, which can make the indoor thermal comfort deteriorate severely.

Measurement uncertainties influence the reliability of control systems in decision-making, which may result in an increase in energy consumption, a decrease in indoor thermal comfort, etc. In addition, the higher the level of measurement uncertainties, the more significant the impacts.

2.2.2 Impacts on performance evaluation

The performance of HVAC systems under different conditions often needs to be evaluated based on the measurement data for energy-saving assessment and system health detection. The models developed and/or the measures adopted for improving the energy efficiency and reliability of HVAC systems need to be evaluated as well. The accuracy of the data used is of vital importance for the evaluations. Especially the data-driven prediction models, their performance is highly correlated with the quality of training data (Sun et al., 2017). Wrong evaluation results may be obtained as a result of the measurement uncertainties in the data used.

Shi et al. (2019) have reported that the measurement uncertainties of operation data affect the evaluation of the energy saving potential of an HVAC system, leading to erroneous evaluation results. Ohlsson et al. (2022) found that the uncertainty in the model prediction of energy savings in building retrofits is mainly caused by measurement uncertainty. The study by Li et al. (2021) shows that data uncertainty affects the performance of a data-driven fault diagnosis model significantly, it makes the accuracy decline from 82.4% to 61.5%. Measurement uncertainties also lead to risks in evaluating the energy performance of energy retrofit projects/measures (Lee et al., 2015). As a consequence, the maximum benefit may not be achieved.

The measurement uncertainties mainly affect the performance evaluation results and further lead to misjudgement by decision-makers. The impacts cannot be ignored and should be addressed effectively.

2.3 Existing solutions to measurement uncertainties and their limitations

Measurement uncertainty is a challenging issue and urgent to be solved for improving the energy efficiency and reliability of HVAC systems. A straightforward way to reduce measurement uncertainties is to calibrate the measuring instruments regularly. It is recommended to calibrate the sensors/meters installed in HVAC systems annually (ASHRAE, 2014), but on-site calibration is constrained by site conditions and costs. Many sensors are never calibrated in their life cycles and always work in unhealthy conditions.

Therefore, some existing studies make efforts to reduce/eliminate the impacts of measurement uncertainties on HVAC systems through indirect ways, including control optimization, sensor fault detection, virtual sensor calibration, etc. They are validated and perform well in their respective field.

2.3.1 Control optimization

As mentioned before, the control systems of HVAC systems are seriously affected by measurement uncertainties. In order to reduce/eliminate the effects, many advanced methods/techniques are used to optimize the conventional control strategies of HVAC systems or used to develop new control strategies for replacing the convention control strategies.

Data fusion is a technique that integrates the data and knowledge from several sources (Castanedo, 2013). It has been successfully used in correcting the cooling load measurements for chiller sequencing control. For example, the fusion of available redundant measurements (Huang et al., 2011) and the fusion of direct and indirect cooling load measurements (Huang et al., 2008; Huang et al., 2009; Sun et al., 2013), are able to reduce the measurement uncertainties and enhance the reliability of the total cooling load-based chiller sequencing controls, the outliers, noises, and biases of measurements are processed effectively.

The control strategies that are insensitive to a certain level of measurement uncertainties/errors are a kind of fault-tolerant control strategies, which are often developed to deal with the measurement uncertainty in HVAC systems. Zhuang and Wang (2020) proposed a risk-based online robust optimal control strategy for cleanroom air conditioning systems, where the component performance degradation and measurement uncertainties are considered. Compared with the convention control strategies, up to 20% of energy saving was achieved. Zhuang et al. (2020) developed probabilistic simplified physical cooling load and capacity models to deal with measurement uncertainties and optimize the chiller sequencing control. Based on the optimal control strategy, the chiller energy efficiency was enhanced, and the indoor thermal comfort was ensured. Yang et al. (2014) used a final correcting factor in a fault-tolerant control strategy to correct the faulty measurements in air conditioning systems. The sensors with fixed bias faults and drifting bias faults can be detected, and the negative effect on the controller can be avoided by using the corrected measurements. Liao et al. (2018) made use of the complementarity of different load indicators to improve the robustness of chiller sequencing control under different levels of uncertainties. The proposed methods performed well even when the uncertainties were significant.

These studies mentioned above have proved that the measurement uncertainties in HVAC systems can be addressed by optimizing the control methods involved, which makes the control systems can tolerate a certain level of measurement uncertainties and improves their robustness. However, an optimal control strategy is generally specially designed for a specific system. Many issues should be considered when optimizing the existing control systems, such as the system types, structures and configurations, sensor networks, and control requirements. The developed optimal control strategy only applies to the specific HVAC system. Its flexibility and generalization ability are very poor. Therefore, control optimization methods are not the best choice to deal with the measurement uncertainties in HVAC systems.

2.3.2 Sensor fault detection

Sensor fault detection methods provide an indirect means to address measurement uncertainties. Its basic idea is shown in Figure 2.1. The health conditions of the sensors installed in HVAC systems can be detected effectively using fault detection methods. The sensors with significant uncertainties are also sensitive to fault detection. If no faulty sensor is found, things are as usual. If one or more faulty sensors are found, the maintenance measures, such as field calibration, repair, or replacement of the faulty sensors, should be taken.

Online sensor fault detection can be achieved, which means that the sensor faults can be detected in time. The extra measures taken can avoid the usage of faulty sensors and ensure that the expected performance of the sensors used can be achieved. Generally, the measurement uncertainties of healthy sensors meet their accuracy classes and are acceptable in engineering practice. Therefore, the measurement uncertainties of sensors can be addressed indirectly using fault detection methods.
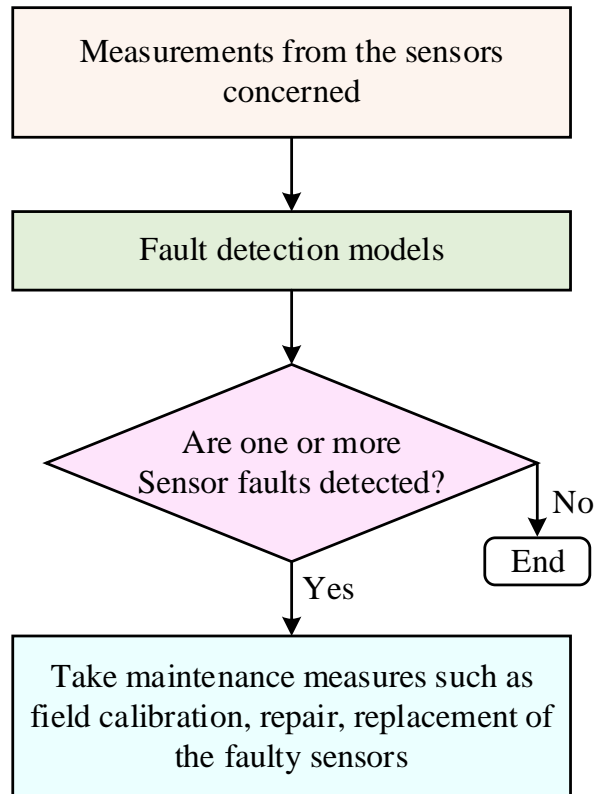
Figure 2.1 Basic idea of using sensor fault detection methods to address measurement

uncertainties

In recent decades, with the rapid development of machine learning techniques, many data-driven sensor fault detection methods are proposed for HVAC systems. Both unsupervised and supervised data mining algorithms, such as principal component analysis (PCA) and neural network (NN), are often used to develop sensor fault detection models. Table 2.2 presents some of the studies on sensor fault detection for HVAC systems. As can be seen from Table 2.2, fault detection for the sensors in HVAC systems (including chiller, air handling unit, variable refrigerant flow, variable air volume, etc) is conducted systematically. The faults of temperature sensors attract the most attention, and those of flow meters and pressure sensors take second place. Bias and drift faults are the two most common sensor faults. Accordingly, many existing studies focused on detecting them, especially the bias fault. In addition, some attention is also paid to the sensor faults of precision degradation and complete failure.

Table 2.2 Overview of studies on sensor fault detection for HVAC systems

Authors (Year)	System/component	Sensor	Method	Fault type
Gao et al. (2022)	Chiller	Temperature sensors and pressure sensors	Deep recurrent canonical correlation analysis and k-nearest neighbour	Drift
Yan et al. (2022)	Air handling unit	Temperature sensors and flow meters	Boltzmann machine	Bias and drift
Luo and Fong (2020)	Chiller	Temperature sensor	Pattern recognition	Bias, drift, precision degradation
Ng et al. (2020)	Chiller	Temperature sensors and flow meters	Bayesian	Bias
Li and Hu (2019); Mao et al. (2018)	Chiller	Temperature sensors, pressure sensors and power meter	PCA and empirical mode decomposition	Bias
Guo et al. (2017)	Variable refrigerant flow	Temperature sensors and pressure sensors	PCA and Satizky-Golay	Bias
Yan et al. (2016)	Air handling unit	Temperature sensors and flow meters	Cluster analysis	Bias
Li et al. (2016)	Chiller	Temperature sensors, flow meters, and power meter	Support vector data description	Bias, drift, precision degradation, complete failure

Xiao et al. (2014)	Variable air volume terminals	Temperature sensor and flow meter	Diagnostic Bayesian network	Bias and complete failure
Du et al. (2014)	Air handling unit	Temperature sensors	NN	Bias, drift, complete failure
Zhu et al. (2012)	Air handling unit	Temperature sensors, flow meters, and pressure sensor	NN, wavelet, and fractal	Bias and drift
Yang et al. (2011)	Air handling unit	Temperature sensor	Fractal correlation dimension	Bias and drift
Chen and Lan (2010)	Building heating/cooling billing system	Temperature sensor, flow meter, differential pressure sensor	PCA	Bias, drift, complete failure
Wang et al. (2010)	Cooling tower, chiller, pumps, heat exchangers	Temperature sensors and flow meters	PCA	Bias
Fan et al. (2010)	Air handling unit	Temperature sensors	Back-propagation neural network, wavelet analysis	Bias and drift

The expected performance of the sensors used in HVAC systems can be achieved and maintained through sensor fault detection, which solves the measurement uncertainties indirectly. On the other hand, it may result in high maintenance costs and low reliability. False alarms and missed faults are inevitable when using sensor fault detection models. The extra measures (field calibration, repair, or replacement) must be taken once the faults (including false alarms) are detected. The costs of processing false alarms are wasted but

unavoidable. For the missed faults, they affect the reliability of sensor fault detection. If the faults are not detected in time, they may cause negative impacts on the system involved. Therefore, measurement uncertainties of sensors in HVAC systems cannot be solved fundamentally using sensor fault detection methods.

2.3.3 Virtual sensor calibration

Virtual in-situ calibration (VIC) is a direct method to solve measurement uncertainties of sensors in HVAC systems, it is proposed by Yu and Li (2015) and extended by Yoon and Yu (2017). The basic idea of VIC is to minimize the difference between the measurements and their benchmarks. It is formulated by Eq. (2.1), the distance function (d_x) consists of a sensor calibration term and a model calibration term, where Y_b and Y_c are the benchmark and corrected measurement of the corresponding sensor, respectively, Y_{bo} is the benchmark output of the system model, Y_R is the reliable output of the system model and can be observed, I is the number of sensors involved, and J is the number of system model outputs.

$$d_x = \underbrace{\sum_{i=1}^{I}\left(Y_{b,i} - Y_{c,i}\right)^2}_{\text{Sensor calibration term}} + \underbrace{\sum_{j=1}^{J}\left(Y_{bo,j} - Y_{R,j}\right)^2}_{\text{Model calibration term}} \tag{2.1}$$

The corrected measurements are obtained by a correction function with unknown parameters to be estimated. The benchmark outputs (Y_{bo}) are the system model outputs corresponding to the corrected measurements, and the model can be a statistical model or a deterministic (mathematical) model (Yoon and Yu, 2017).

The effectiveness of VIC methods in sensor calibration of HVAC systems has been validated systematically. The study by Wang et al. (2021) shows that the systematic and random errors of the sensors concerned were reduced by approximately 95% and 60% on average, respectively, after calibration using the VIC method. Zhao et al. (2022)

calibrated the temperature and humidity sensors and a flow meter for an air handling unit using the VIC method and Gaussian mixture model, results show that the accuracy of all sensors concerned was improved by 75% after calibration. Yoon (2020) used VIC methods coupled with Bayesian inference and autoencoder to calibrate the supply air temperature sensor and mass flow meter for an air handling unit, the impacts of the systematic errors of the sensors concerned on the system energy performance were removed. Choi and Yoon (2020) proposed a virtual sensor-assisted in-situ sensor calibration strategy to calibrate simultaneous sensor errors, including the systematic errors of supply air mass flow meter, mixed air temperature sensor and supply air temperature sensor in an air handling unit. The use of virtual sensors makes the calibration error reduce from 72.7% to 5.2%.

Though the sensor errors can be calibrated directly using VIC methods, there are challenges to using them in engineering practice. The benchmarks and reliable outputs (i.e., Y_b and Y_R in Eq. (2.1)) are difficult to obtain. It usually uses the available system models to establish them (Yoon and Yu, 2018) and sometimes even requires redundancy of sensors for measuring them. Nonetheless, if the benchmarks and reliable data are available, it becomes meaningless to calibrate corresponding sensors. In addition, the VIC methods show a good performance in calibrating the systematic errors of the sensors concerned, but their performance is possibly unsatisfactory in calibrating the random errors of the sensors. The measurement uncertainties of sensors are not solved completely by VIC methods.

2.4 Inverse uncertainty quantification for building energy systems

Inverse uncertainty quantification is a method to estimate unknown parameters of a model based on observation data (Tian et al., 2018). Its mathematical formulation is presented

in Eq. (2.2). Where, E is the observation data, x is the known parameters/inputs of the model, θ is the unknown parameters to be estimated in the model, λ is the model error, ε is the random error of observation data, $f(x,\theta)$ is the model outputs with the inputs x and θ.

$$E = f\left(x,\theta\right) + \lambda + \varepsilon \tag{2.2}$$

Inverse uncertainty quantification for building energy systems is also called model calibration. Bayesian inference is the most commonly used model calibration method. Figure 2.2 shows the flow chart of inverse uncertainty quantification for building energy systems using Bayesian inference. The building energy model can be established by the simulation tools, such as EnergyPlus (Julia et al., 2017) and TRNSYS (Rysanek et al., 2019). The surrogate model can be used to reduce the computational loads and improve the calibration accuracy, it is generally established using the Gaussian process (GP) (Heo et al., 2012) or multiple linear regression (MLR) (Tian et al., 2016). Sensitivity analysis aims to select the most sensitive/important parameters and calibrate them, it can be achieved using the methods of Morris (Booth and Choudhary, 2013), Sobol (Zhu et al., 2020) and so on. In Bayesian modelling, a prior distribution should be assigned to each unknown parameter concerned according to expert knowledge. The posterior distributions of the unknown parameters concerned are inferred based on the model and observation data according to Bayes' theorem.
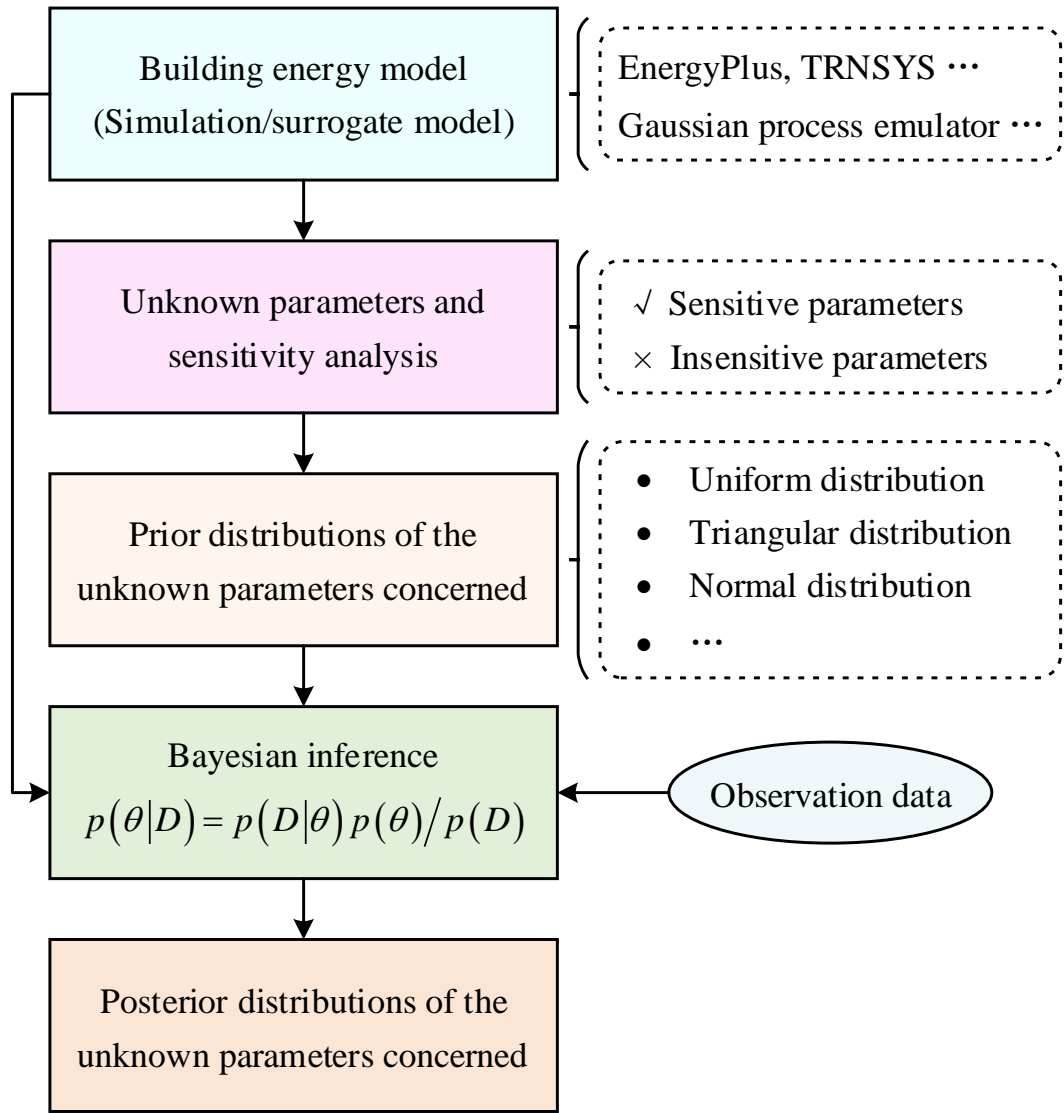
Figure 2.2 Flow chart of inverse uncertainty quantification for building energy systems

Bayesian model calibration generally aims to calibrate the unknown parameters in building energy models and is used for the retrofit analysis of existing buildings and energy consumption prediction of building stock (Hou et al., 2021). Booth et al. (2012) calibrated housing stock models considering different sources of uncertainties, and the average percentage error of daily energy consumption prediction is reduced from 17.6% to 0.5%. Heo et al. (2015) calibrated the normative energy model of an office building and estimated the energy-saving potential of four different energy efficiency measures, which found that model calibration can reduce the uncertainty in model predictions and support retrofit decision-making under uncertainty. Kang and Krarti (2016) used a

Gaussian process emulator to develop a surrogate model for a building energy model and expedited the parameter identification process, the effectiveness and robustness of the developed approach are validated in an office building.

Apart from the studies mentioned above, Table 2.3 presents a series of related studies published in recent years. The observation data, emulators/surrogates, sensitivity analysis methods and simulation tools used in these studies are listed. Energy consumption is the main source of observation data, the Gaussian process is the most commonly used emulator, and EnergyPlus is frequently used to develop the building energy models.

Table 2.3 Recent studies on building energy model calibration

Authors (Year)	Observation data	Emulator/ Surrogate	Sensitive analysis	Simulation tool
Risch et al. (2021)	Hourly heat demand	GP	Morris	TEASER
Yi and Park (2021)	Monthly electric energy uses	ANN[*]	-	EnergyPlus
Yi et al. (2019)	Annual gas and electricity energy use	ANN	-	EnergyPlus
Chen et al. (2019)	Monthly heat demand	GP	-	IES-VE[*]
Chong and Menberg (2018)	Monthly electricity energy consumption	GP	Morris	EnergyPlus
Lim and Zhai (2018)	Monthly electricity and gas energy consumption	MLR	Sensitivity value index	EnergyPlus
Chong et al. (2017)	Hourly energy consumption	GP	Morris	EnergyPlus TRNSYS
Li et al. (2016)	Daily consumption and monthly peak demand of chilled water	GP, MLR	Lasso	EnergyPlus

[*]ANN: Artificial neural network. IES-VE: Integrated Environmental Solutions Virtual Environment.

Both the continuous and discrete parameters in building energy models can be calibrated using Bayesian inference. Table 2.4 summarizes the parameters in building energy models that are frequently investigated in the literature. There are four groups of parameters, including the physical properties, HVAC systems, internal loads and system controls. The column 'Rating' in Table 2.4 shows the calibration frequencies of the corresponding parameters in the literature.

Table 2.4 Parameters in building energy models that need to be calibrated

Group	Parameter	Unit	Rating
Physical property	Wall, roof, and window U-values	$W/(m^2 \cdot K)$	★★★★★
	Infiltration rate (air changes per hour)	1/h	★★★★
	Thermal conductivity	$W/(m \cdot K)$	★
	Thermal resistance	K/W	★
	Solar heat gain coefficient	-	★★
	Window-to-wall ratio	-	★★★
	Daylight percentage	%	★★
HVAC system	Cooling/heating capacity	kW	★
	Coefficient of performance	-	★★★
	Fan efficiency	-	★★
	Cooling/heating coil efficiency	-	★★
	Ventilation rate	m^3/h	★★
Internal load	Equipment power density	W/m^2	★★★★★
	Lighting power density	W/m^2	★★★★★
	Occupant density	m^2/Person	★★★★★
System control	Cooling/heating temperature setpoint	°C	★★★
	Supply air temperature setpoint	°C	★
	Chilled water supply temperature setpoint	°C	★

As can be seen from Table 2.4, most of the studies focused on calibrating the U-values of building envelop and the internal loads derived from the equipment, lighting and occupants. These parameters generally have a high ranking in the sensitivity analysis and have a significant influence on the building energy models.

Bayesian inference-based model calibration method can directly quantify the uncertainties of unknown parameters in building energy models. It has been used for the retrofit analysis of existing buildings and energy consumption prediction of building stock. Bayesian inference shows a strong ability in uncertainty quantification. It is promising to quantify measurement uncertainties in HVAC systems using Bayesian inference.

2.5 Summary

This chapter provides a comprehensive literature review on the uncertainty analysis of HVAC systems. The impacts of measurement uncertainties on HVAC systems are analysed and the existing solutions to measurement uncertainties in the literature are summarised. In addition, Bayesian inference-based inverse uncertainty quantification method is also presented. According to the above review, the research gaps are summarised as follows.

i. Most of the existing solutions adopt indirect methods to deal with measurement uncertainties in HVAC systems. Though they performed well in their respective application scenarios, their flexibility and generalization ability are poor. An effective and direct measurement uncertainty quantification method is urgently needed for HVAC systems.

ii. Bayesian inference has a strong ability in uncertainty quantification of parameters in building energy models, but it is rarely used to quantify measurement uncertainties

in HVAC systems in the literature. It is worthy of study and the effectiveness of measurement uncertainty quantification using Bayesian inference needs to be verified.

iii. Online correction of the measurements with significant/unacceptable uncertainties is of vital importance to improve the energy efficiency and reliability of HVAC systems, extend the service life of the measuring instruments used and reduce the system maintenance costs. It can be achieved after the measurement uncertainties are quantified.

CHAPTER 3   MEASUREMENT UNCERTAINTY

QUANTIFICATION FRAMEWORK

This study proposes to quantify measurement uncertainties directly using Bayesian inference and Markov chain Monte Carlo sampling methods. The organization of this chapter is as follows. Section 3.1 introduces the characteristics of measurement uncertainties. Section 3.2 presents the measurement uncertainty quantification methods adopted in this study, i.e., Bayesian inference and Markov chain Monte Carlo sampling methods. Then a general framework for quantifying measurement uncertainties is proposed in Section 3.3, it is the foundation of this study. The measurement uncertainty quantification methods proposed in Chapters 4 and 6 are developed based on this framework. Section 3.4 presents the diagnostic methods for convergence of Bayesian models and the performance evaluation index for measurement uncertainty quantification methods. Section 3.5 is a summary of this chapter.

3.1 Characteristics of measurement uncertainty

Measurement uncertainties exist inherently regardless of the measuring instruments used. Generally, the measured value ($\tilde{\theta}$) of a variable can be divided into two parts: the true value (θ) and an uncertain term (u_θ), as shown in Eq. (3.1). The true value can never be determined exactly. In this study, the uncertain term represents measurement uncertainty and can be considered to follow a normal distribution with mean μ_θ and standard deviation (*sd*) σ_θ, as shown in Eq. (3.2). Its mean represents the systematic uncertainty (bias) of the measurement, and its standard deviation reflects the random uncertainty (noise) of the measurement. According to the characteristics of a normal distribution, the actual measured value of the variable also follows a normal distribution with mean

$(\theta + \mu_\theta)$ and standard deviation σ_θ, as shown in Eq. (3.3). The relationship between the true value and the measured value is shown in Figure 3.1. The measured value is not a constant, but the distribution parameters (i.e., mean μ_θ and standard deviation σ_θ) are fixed and need to be quantified.

$$\tilde{\theta} = \theta + u_\theta \tag{3.1}$$

$$u_\theta \sim N\left(\mu_\theta, \; \sigma_\theta^2\right) \tag{3.2}$$

$$\tilde{\theta} \sim N\left(\theta + \mu_\theta, \sigma_\theta^2\right) \tag{3.3}$$
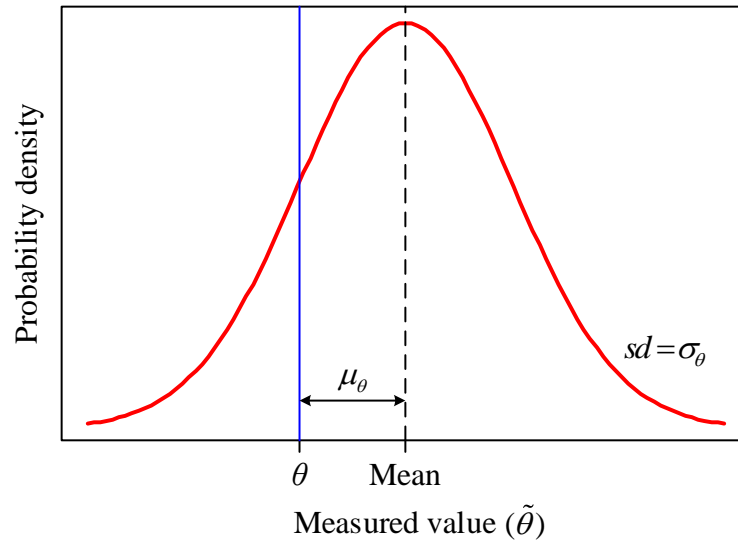
Figure 3.1 Probability distribution of a measured value

For building central cooling and air conditioning systems, the measuring instruments (Temperature sensors, flow meters and power meters, etc.) inevitably have uncertainties. The magnitudes of uncertainties are related to the types, principles, etc of the measuring instruments. Generally, they can meet the requirements of measurement accuracy and can achieve the expected performance after initial commissioning. In this study, the measurement uncertainties that meet the accuracy classes of the measuring instruments are thought to be acceptable in engineering practice. However, performance degradation of measuring instruments cannot be avoided due to long-time service, poor working

environments, improper maintenance, etc. The uncertainties certainly will increase with the performance degradations of measuring instruments and further influence the system operation.

3.2 Uncertainty quantification methods adopted

Bayesian inference is a popular and powerful uncertainty analysis method. It is often used in combination with the Markov chain Monte Carlo sampling method for solving problems with high computational costs or without analytical solutions. Both methods are also used in this study, and this section will introduce them in detail.

3.2.1 Bayesian inference

Bayesian inference utilizes prior distribution and likelihood function to compute the posterior distribution according to Bayes' theorem. The mathematical formulation of Bayes' theorem is stated as Eq. (3.4),

$$P(\theta \mid E) = \frac{P(E \mid \theta) \cdot P(\theta)}{P(E)} \propto P(E \mid \theta) \cdot P(\theta) \tag{3.4}$$

where, θ represents the unknown parameters to be estimated, E is the observational data, $P(\theta|E)$ is the posterior probability, $P(E|\theta)$ is the likelihood function, $P(\theta)$ is the prior probability, and $P(E)$ is the marginal likelihood. The posterior probability is proportional to the prior probability multiplied by the likelihood function. The prior probability is the inherent likeliness and reflects the beliefs about θ without considering the observational data, while the posterior probability signifies the beliefs about θ considering observational data. The posterior probability is calculated using the likelihood function and observational data according to Bayes' theorem, and it is mainly affected by the prior probability and the likelihood function.

3.2.2 Markov chain Monte Carlo sampling methods

The Monte Carlo method can achieve the propagation of distributions and is effective to explore the distributions of unknown uncertainties (ISO/IEC Guide 98-3/Suppl.1, 2008). This study adopts the Markov chain Monte Carlo sampling methods to realize Bayesian inference and quantify the measurement uncertainties. The MCMC sampling methods are commonly used to compute the posterior distribution in Bayesian analysis, they can draw samples from high-dimensional posterior distributions (Tian et al., 2016). Although there are many kinds of MCMC algorithms, most of them are plagued by random walk behaviour and are sensitive to correlated parameters. The Hamiltonian Monte Carlo (HMC) method is one of the most popular MCMC algorithms and can avoid the above issues by taking a series of steps based on first-order gradient information (Chong and Menberg, 2018). However, the performance of HMC is heavily dependent on two main parameters: the leapfrog step size and the number of leapfrog steps per iteration (Chong et al., 2017). To solve this problem, an extension of the HMC algorithm is proposed, namely No-U-Turn Sampler (NUTS) (Hoffman and Gelman, 2014). NUTS can search for the number of leapfrog steps automatically using a recursive algorithm and can adapt the leapfrog step size using a primal-dual averaging scheme. NUTS not only does not require user intervention or costly tuning runs, but also performs at least as well as the HMC method. Therefore, this study uses the NUTS method to generate samples for computing the posterior distributions of unknown parameters in Bayesian inference.

3.3 Measurement uncertainty quantification framework proposed in this thesis

The main objective of this study is to quantify the measurement uncertainties of sensors/meters used in building central cooling and air conditioning systems. Figure 3.2

shows the proposed measurement uncertainty quantification framework, it consists of 7 steps. The details are as follows.

(1) The first step is to select and classify the variables (sensors/meters). Generally, many variables are measured using corresponding sensors/meters for system monitoring and real-time online control. The model will be very complex and redundant if all the variables are used. The selection can be conducted based on the relevance, importance, sensibility, availability, etc of available variables. It sometimes also needs to consider the availability of the constraint models developed in Step 2 (especially for the physical models) when selecting the variables. The selected variables should further be divided into two categories: the target variables $\{\tilde{\theta}_1, \tilde{\theta}_2, ..., \tilde{\theta}_n\}$ and the auxiliary variables $\{y, x_1, x_2, ..., x_m\}$. The target variables are those with significant uncertainties and need to be quantified. In this study, a target variable will be represented by a sign with an accent '~', and it also represents the measured value of the target variable. The auxiliary variables are those with acceptable uncertainties (the uncertainties that meet the accuracy classes of the measuring instruments are acceptable) and do not need to be quantified. The factors, such as the rates of performance degradations and difficulty levels of on-site calibration of the measuring instruments involved, should be considered in classifying the variables.

(2) The second step is to select and develop constraint models. There are two kinds of constraint models: the physical models and the data-driven models. Both models are to find the mapping relationships between the input (y) and outputs (θ, x). The physical model is stated as Eq. (3.5) and the data-driven model is stated as Eq. (3.6). The only difference between them is that the data-driven model is always accompanied by an error term (e). The error term follows a normal distribution with

the mean value of 0, and its standard deviation δ needs to be determined when developing the model. The model residuals are the observations of model errors. Therefore, the standard deviation of the model residuals can be used to represent the standard deviation of the error term.

$$y = f\left(\theta_1, \theta_2, ..., \theta_n, x_1, x_2, ..., x_m\right) \tag{3.5}$$

$$y = f\left(\theta_1, \theta_2, ..., \theta_n, x_1, x_2, ..., x_m\right) + e, \quad e \sim N\left(0, \delta^2\right) \tag{3.6}$$

The selection of constraint models highly depends on the selected variables. The development of physical models is based on the real physical relationships between the selected variables. The physical models cannot be developed if one or more variables involved are unavailable. On the other hand, data-driven models can be developed flexibly regardless of whether there are physical relationships between the selected variables. The data-driven models can be used in a wider range of applications than the physical models.

(3) The third step is to develop the measurement uncertainty models based on the characteristics of measurement uncertainties presented in Section 3.1, as shown in Eq. (3.7). The measured value of a target variable ($\tilde{\theta}_i$) follows a normal distribution. Its mean is the sum of the true value (θ_i) and the systematic uncertainty (μ_i), and its standard deviation (σ_i) is consistent with the standard deviation of random uncertainty.

$$\tilde{\theta}_i \sim N\left(\theta_i + \mu_i, \sigma_i^2\right), \quad i = 1, 2, ..., n \tag{3.7}$$

(4) The fourth step is to assign prior distributions to the unknown parameters to be quantified, including both the systematic and random uncertainties of each target variable, i.e., $\{\mu_i, \sigma_i\}, i = 1, 2, ..., n$. Prior distributions are important for solving Bayesian models, they may affect the speed of convergence. If the prior distribution

is inappropriate, it may need to take more iterations to converge, which lead to an increase in calculation load.

In general, the prior distributions can be derived from expert knowledge, experiments, surveys, technical reports, and industrial standards, among other sources (Heo et al., 2012; Tian et al., 2018). The commonly used prior distributions include the uniform distributions, triangular distributions, and normal distributions, etc.

(5) The fifth step is to generate samples from distributions using Markov chain Monte Carlo sampling methods.

(6) The sixth step is to update the prior distributions of the unknown parameters to be quantified according to Bayes' theorem, as shown in Eq. (3.8). The true value, systematic and random uncertainties of each target variable are unknown. They are quantified by many times of iterations. Steps 5 and 6 will be repeated until the pre-set number of iterations is finished.

$$p\left(\left(\mu,\sigma,\theta\right)\middle|\left(y,x,\tilde{\theta}\right)\right)=\frac{p\left(\left(y,x,\tilde{\theta}\right)\middle|\left(\mu,\sigma,\theta\right)\right)\cdot p\left(\mu,\sigma,\theta\right)}{p\left(y,x,\tilde{\theta}\right)} \qquad (3.8)$$

(7) The seventh step is to construct the posterior distributions of the systematic and random uncertainties of each target variable using the samples generated in Step 5.

1. Selection and classification of variables (sensors/meters)

- Target variables (sensors/meters) $\{\tilde{\theta}_1, \tilde{\theta}_2, ..., \tilde{\theta}_n\}$
- Auxiliary variables (sensors/meters) $\{y, x_1, x_2, ..., x_m\}$

2. Selection and development of constraint models

- Physical models $y = f\left(\theta_1, \theta_2, ..., \theta_n, x_1, x_2, ..., x_m\right)$
- Data-driven models $y = f\left(\theta_1, \theta_2, ..., \theta_n, x_1, x_2, ..., x_m\right) + e, \quad e \sim N\left(0, \delta^2\right)$

3. Development of measurement uncertainty models

- Target variables $\tilde{\theta}_i \sim N\left(\theta_i + \mu_i, \sigma_i^2\right), \quad i = 1, 2, ..., n$

4. Assignment of prior distributions

- Unknown parameters to be quantified $\{\mu_i, \sigma_i\}, \quad i = 1, 2, ..., n$

5. Sampling from distributions

- Markov chain Monte Carlo sampling methods

6. Update of prior distributions

- Bayes' theorem $p\left((\mu, \sigma, \theta)\middle|(y, x, \tilde{\theta})\right) = \dfrac{p\left((y, x, \tilde{\theta})\middle|(\mu, \sigma, \theta)\right) \cdot p(\mu, \sigma, \theta)}{p\left(y, x, \tilde{\theta}\right)}$

7. Construction of posterior distributions

- Unknown parameters to be quantified $\{\mu_i, \sigma_i\}, \quad i = 1, 2, ..., n$

Figure 3.2 Proposed measurement uncertainty quantification framework

3.4 Convergence diagnostics and evaluation index

This study adopts *Stan* to develop Bayesian MCMC models and test the proposed measurement uncertainty quantification methods. *Stan* is a powerful and popular statistical programming language, which is perfect for coding Bayesian MCMC models (Carpenter et al., 2017).

Three key parameters should be set in programming Bayesian MCMC models: the number of Markov chains (N_{chain}), the number of iterations per chain (N_{iter}) and the number of warmup iterations per chain (K). The number of Markov chains will be set to 4 in this study, and the generated samples from different Markov chains will be used to diagnose convergence, they should converge to a same or similar value. The convergence is highly dependent on the number of iterations per chain. The more iterations, the more likely to converge, but the higher the calculation costs. An appropriate number of iterations can not only ensure convergence but also minimize the calculation costs. It will be set flexibly for the cases in this study. The warmup iterations are the first K iterations ($K < N_{iter}$) in each chain, and the rest ($N_{iter} - K$) are called post-warmup iterations. The samples generated in warmup and post-warmup iterations are called warmup and post-warmup samples, respectively. In order to improve the reliability of measurement uncertainty quantification, only the post-warmup samples will be used to construct the posterior distributions of unknown parameters to be estimated, the warmup samples will be discarded. In this study, the number of warmup iterations per chain will be set to half the number of iterations per chain (i.e., $K = N_{iter}/2$).

It generally needs to iterate many times for convergence. The potential scale reduction factor ($\hat{R}$) is often used to diagnose convergence in Bayesian inference (Gelman and Rubin, 1992). It is the weighted average of within-chain sample variance and cross-chain

sample variance. If the chains have converged, the potential scale reduction factor will be very close to 1. A rough convergence criterion is that the potential scale reduction factor is no more than 1.1. This study will use a much tighter threshold to diagnose convergence for exploring the posterior distributions effectively, i.e., it converges when $\hat{R} \leq 1.01$ (Vehtari et al., 2021).

Apart from the potential scale reduction factor, the trace plots and autocorrelations of the post-warmup samples can also be sued to diagnose convergence (Annis et al., 2017). The trace plots show the sampling path of each chain visually and the convergence can be evaluated directly by comparing the sampling paths of different chains. If the samples from different chains are mixed well and the samples are difficult to be distinguished between individual chains, the convergence is achieved. The autocorrelations can reflect the reliability of the samples generated by MCMC algorithms. In MCMC sampling, the current sample is only dependent on the previous sample, the correlation between non-adjacent samples should be small. Therefore, the convergence criterion can be that the autocorrelations decrease very quickly with the increase of lag. In addition, a *thinning* technology can be used to reduce the chain length and autocorrelations (Annis et al., 2017). It is achieved by saving every k^{th} sample from the chain and discarding the rest. Finally, the number of samples used for constructing the posterior distributions (N_{sam}) can be calculated by Eq. (3.9).

$$N_{sam} = N_{chain} \times \frac{N_{iter} - K}{k} \tag{3.9}$$

The performance of the proposed measurement uncertainty quantification methods will be evaluated using the 95% and/or 99% Bayesian credible interval (BCI), posterior means and relative errors (RE). The posterior distributions of the unknown parameters to be estimated can be obtained directly by the proposed methods. The posterior means of the

parameters can be regarded as the estimated values of the parameters. Therefore, the relative error in quantifying a parameter (θ) can be defined by Eq. (3.10). Where, $\bar{\theta}$ is the posterior mean, and θ is the actual value of this parameter.

$$RE(\theta) = \frac{\left|\bar{\theta} - \theta\right|}{\theta} \times 100\% \tag{3.10}$$

3.5 Summary

This chapter introduces the characteristics of measurement uncertainties and the quantification methods adopted in this study. A framework for quantifying measurement uncertainties is presented in detail. Based on this framework, two different measurement uncertainty quantification methods will be proposed, and they are presented in Chapters 4 and 6, respectively. The convergence diagnostics methods, and the performance evaluation index of the measurement uncertainty quantification methods are also presented. They will be used in the following chapters.

CHAPTER 4   PHYSICAL MODEL-BASED

MEASUREMENT UNCERTAINTY QUANTIFICATION

METHOD AND ITS VALIDATION

This chapter presents a physical model-based measurement uncertainty quantification method for multiple water-cooled chiller systems. It is systematically validated using a site test case and four simulation test cases. The site test case is conducted on a water-cooled chiller equipped in the Hong Kong International Commerce Centre (ICC), and the simulation test cases are conducted on a virtual platform. This chapter is organized as follows. The system concerned and the metering arrangement are presented in Section 4.1. The physical model-based measurement uncertainty quantification method is developed in Section 4.2. Section 4.3 introduces the test and validation arrangements for the proposed method. Section 4.4 presents the test results and evaluates the performance of the proposed method on measurement uncertainty quantification. The conclusions are made in Section 4.5.

4.1 Description of the system concerned and metering arrangements

Multiple water-cooled chiller systems are widely used in largescale commercial buildings due to their high energy efficiency and flexibility (Yu and Chan, 2007). A multiple water-cooled chiller system typically consists of a chilled water system and a cooling water system, as shown in Figure 4.1. The chilled water loop connects the chillers with the building. The cooling water loop connects the chillers with the cooling towers. Each chiller is interlocked with a constant-speed chilled water pump on the water return side and a constant-speed cooling water pump on the water inlet side. A number of temperature

sensors, chilled water flow meters (CHWFM), cooling water flow meters (CWFM), power meters, etc., are installed in the system for system monitoring and online real-time control. For each chiller, the power consumption ($P_{CH,i}$), chilled water supply temperature ($T_{chws,i}$) and return temperature ($T_{chwr,i}$), chilled water volume flow rate ($q_{chw,i}$), cooling water inlet temperature ($T_{cwin,i}$) and outlet temperature ($T_{cwout,i}$), and cooling water volume flow rate ($q_{cw,i}$) are measured. On the main pipe, the main chilled water supply temperature (T_{chws}) and return temperature (T_{chwr}), main chilled water volume flow rate (q_{chw}), main cooling water inlet temperature (T_{cwin}) and outlet temperature (T_{cwout}), and main cooling water volume flow rate (q_{cw}) are also measured.
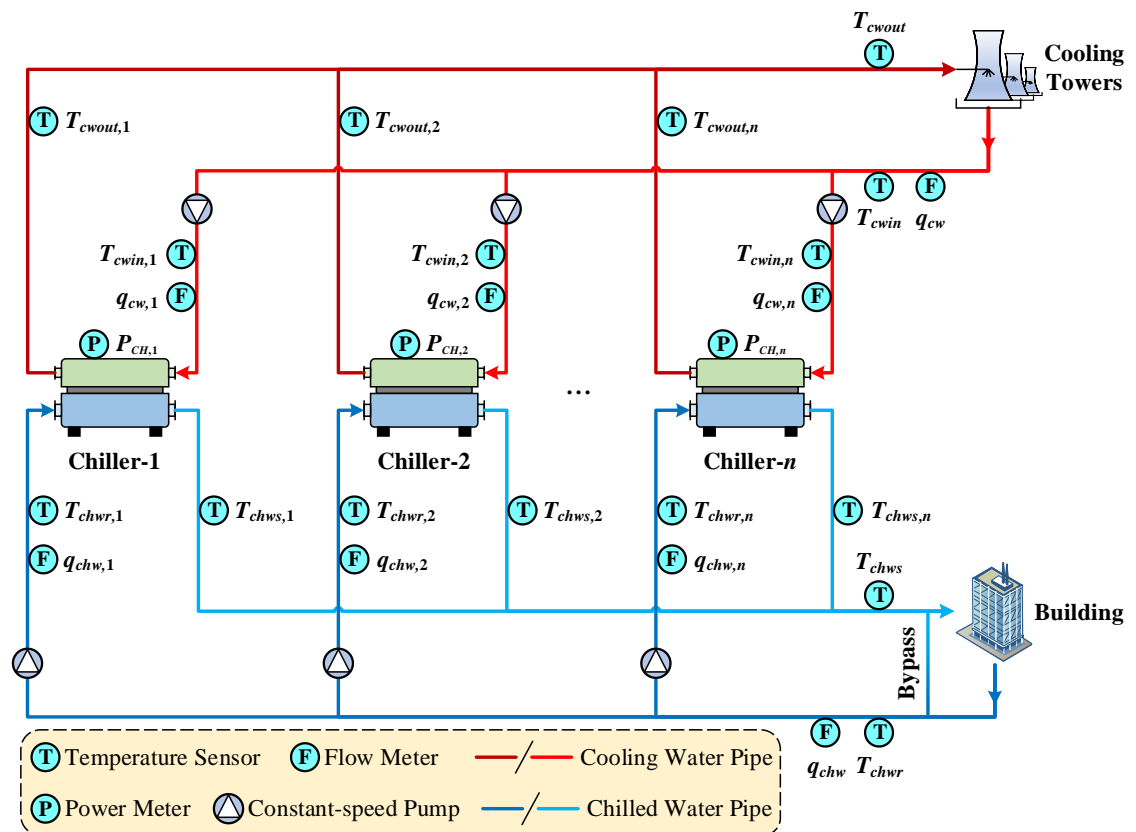
Figure 4.1 Schematic of a multiple water-cooled chiller system and metering arrangement

As mentioned above, power meters, temperature sensors and water flow meters are installed in chiller systems. The uncertainties of these measuring instruments may reduce

the reliability of the control that they participate in, such as the chiller sequencing controls. In consideration of the availability of the constraint models, the variables, including the power consumption, the chilled water flow rate, supply and return temperatures, the cooling water flow rate, inlet and outlet temperatures, are available and can be used to develop physical models for measurement uncertainty quantification. These variables should be divided into the target variables and the auxiliary variables, which will be based on the features and working conditions, etc of the measuring instruments used.

For the flow meters, the site constraints and unfavourable working environment probably lead to performance degradation and make them more likely to suffer significant measurement uncertainties. In addition, field calibrations of flow meters are both complex and costly, and are even not practically possible (ASHRAE, 2014). In fact, regular field calibration of flow meters is not compulsory in Hong Kong and is even not conducted. Online calibration of flow meters is cost-effective and could benefit the reliable operation of HVAC systems and energy savings. For the temperature sensors, the on-site calibration, repair, or replacement of temperature sensors are relatively easier to be implemented. The costs of such efforts are much lower than that of the flow meters. Besides, many sensor fault detection methods have been developed in recent decades and the abnormality of sensors can be detected automatically by these methods (Zhang et al., 2021). With the help of fault detection methods for chilled water supply and return temperature sensors, such as (Mao et al., 2018), the temperature sensors can be calibrated in time once an abnormality is found. Accordingly, it is somehow practical to maintain the accuracy of temperature sensors within an acceptable level. Therefore, it could be an easier solution and practical choice to reduce the measurement uncertainties of temperature sensors through on-site calibration and regular maintenance due to the technical feasibility, lower cost and easier implementation. Their uncertainties can be maintained at an acceptable

level. For power meters, they are often of high accuracy and easier to calibrate, and they are less likely to suffer significant performance degradation. Therefore, the uncertainties of flow meters must be considered, but the uncertainties of power meters and temperature sensors are acceptable and can be ignored. Accordingly, the target variables are the chilled water and cooling water flow rates, and the auxiliary variables are the power consumption, chilled water supply and return temperatures, cooling water inlet and outlet temperatures.

4.2 Development of a physical model-based measurement uncertainty quantification method

This section introduces the procedures and details of developing the physical model-based measurement uncertainty quantification method. It aims to quantify the uncertainties of water flow measurements in multiple water-cooled chiller systems with the auxiliaries of power and temperature measurements.

4.2.1 Outline of the proposed method

Uncertainty affects the measurement quality, accuracy and reliability of decisions made based on the measurements. Quantification of measurement uncertainty is therefore an essential means to ensure or improve the accuracy and reliability of decisions. Figure 4.2 shows the basic procedures of the proposed physical model-based measurement uncertainty quantification method. A key feature is that the measurements are the only inputs needed. The number of chains is set to 4, and the number of iterations per chain can be set properly based on the convergence criteria presented in Section 3.4. The assignments of the prior distributions for the uncertain parameters (i.e., the systematic and random uncertainties of each flow meter involved) are presented in Section 4.2.2. The Markov chain Monte Carlo sampling method is used to generate samples from distributions under physical constraints, including the energy and mass balance models.

The details about the constraint models are presented in Section 4.2.3. During the iterative process, prior distributions are updated continually, and the posterior distributions are calculated using the generated samples and the measurement uncertainty models (i.e., likelihoods in Bayesian models, which are presented in Section 4.2.4) according to Bayes' theorem. The posterior distributions of uncertain parameters are the outputs of the measurement uncertainty quantification method and show the possible distributions of these unknown parameters.
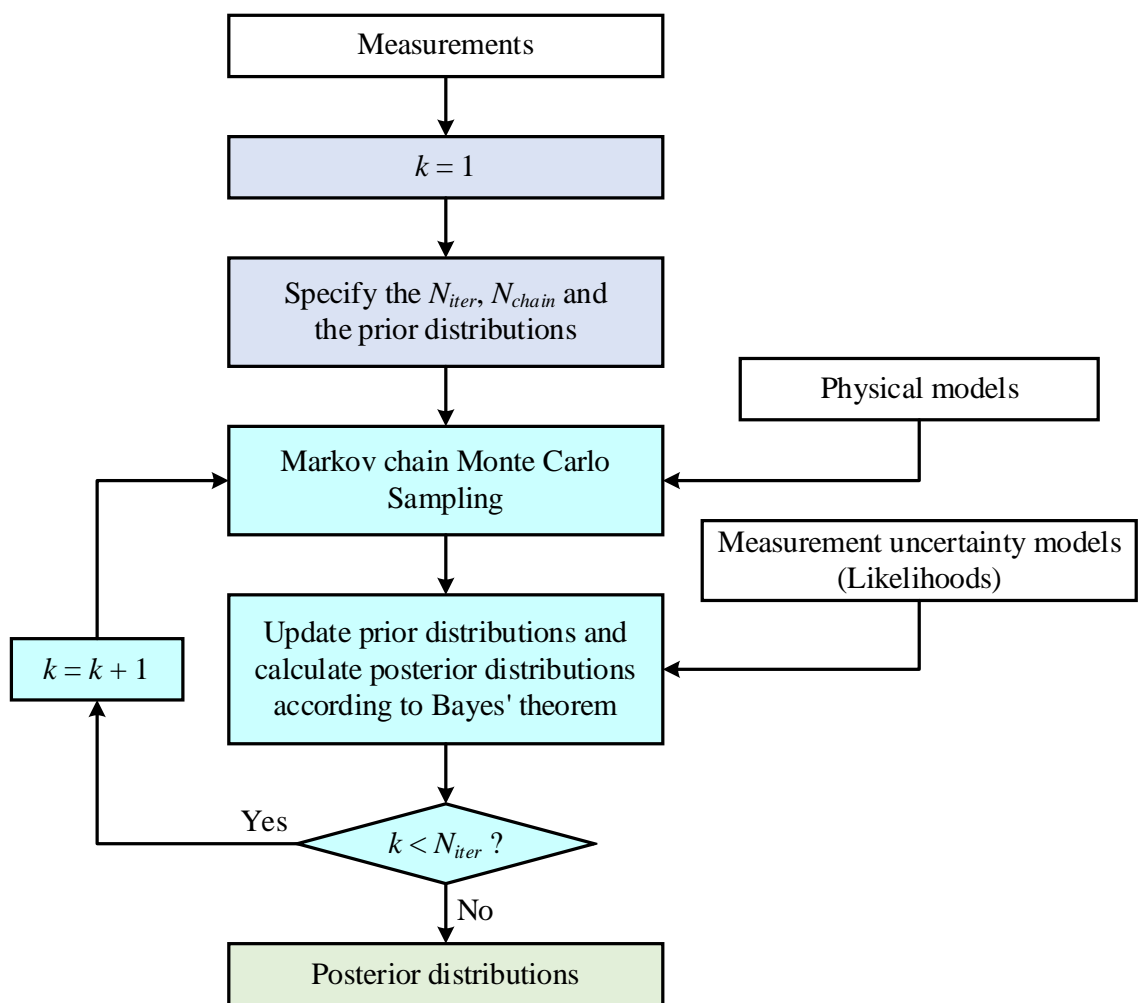
Figure 4.2 Basic procedures of physical model-based measurement uncertainty quantification method

4.2.2 Assignment of prior distributions

In order to estimate the unknown variables and measurement uncertainties, prior distributions must be assigned to each of them. The unknown variables include the true water flow rates, while the measurement uncertainties include the systematic uncertainty and random uncertainty of each flow meter. A normal distribution is chosen as the prior distribution of systematic uncertainty. Its mean is set to 0 because the systematic uncertainty can be positive or negative. Its standard deviation is determined through the hypothesis that the probability of the systematic uncertainty being less than 10% of the rated flow rate (q_r) is 95%, as shown in Figure 4.3. Therefore, the prior distributions of the systematic uncertainties can be determined once the rated flow rates of the corresponding water pumps are determined.
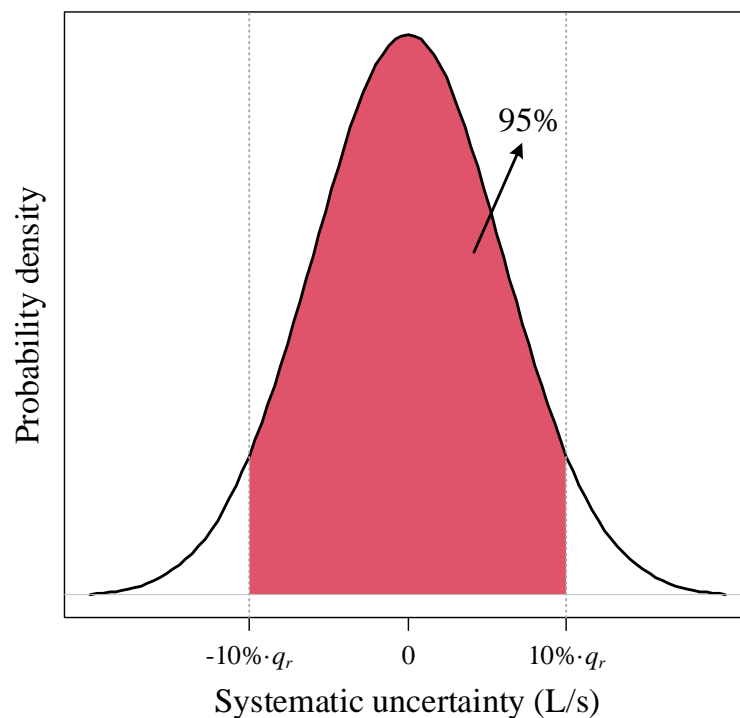
Figure 4.3 Prior distribution of systematic uncertainty

The random uncertainty of each flow meter is not fixed but can be represented by its standard deviation. As it is well known that the standard deviation must be greater than

0, the chi-square distribution with 3 degrees of freedom ($\chi^2(3)$) is assigned to be the prior distributions of random uncertainty of each flow meter, as shown in Figure 4.4.
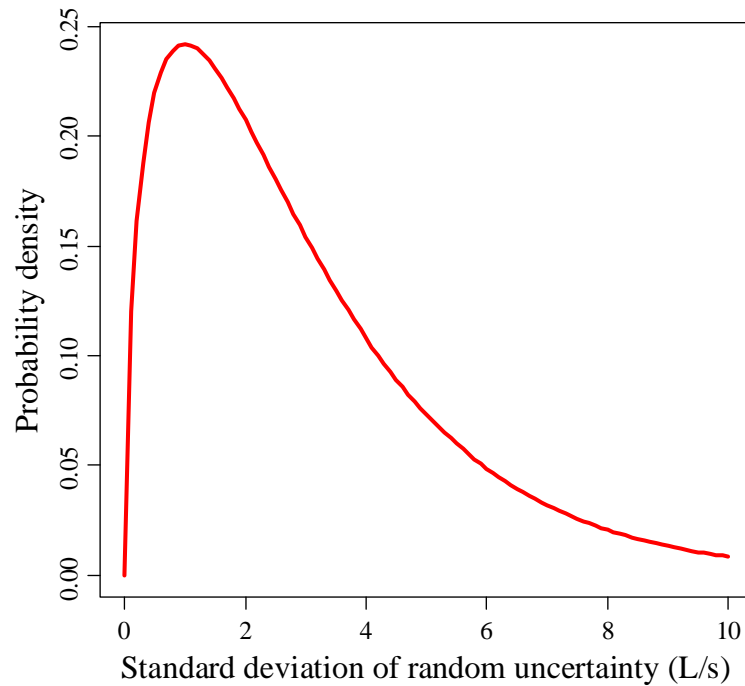
Figure 4.4 Prior distribution of random uncertainty

In order to quantify the measurement uncertainties of flow meters more accurately, further information about the true water flow rates is considered. Because both chilled water and cooling water are driven by constant-speed pumps, their flow rates may follow normal distributions as shown in Eq. (4.1) and (4.2). However, the mean values and standard deviations (ω) of these distributions are unknown. In principle, the water flow rate can be determined by the pump head according to the characteristic curve of the pump concerned. The pump head can be measured on-site. The flow rate corresponding to the measured pump head on the characteristic curve of the pump is then the reference value of the true water flow rate (denoted by q_{ref}). In reality, the mean of the true water flow rate may deviate from q_{ref}, due to the actual pressure heads as well as other factors. The prior distributions of the means of the chilled water flow rates ($\bar{q}_{chw,i}$) and cooling water flow rates ($\bar{q}_{cw,i}$) can be assigned by referring to the assignment of the prior distribution of

43

systematic uncertainty. It is assumed that the probability that the mean deviates from q_{ref} by less than 3% is 95%, as shown in Figure 4.5.

$$q_{chw,i} \sim N\left(\bar{q}_{chw,i}, \omega_{chw,i}^2\right), \quad i = 1, 2, ..., n \tag{4.1}$$

$$q_{cw,i} \sim N\left(\bar{q}_{cw,i}, \omega_{cw,i}^2\right), \quad i = 1, 2, ..., n \tag{4.2}$$
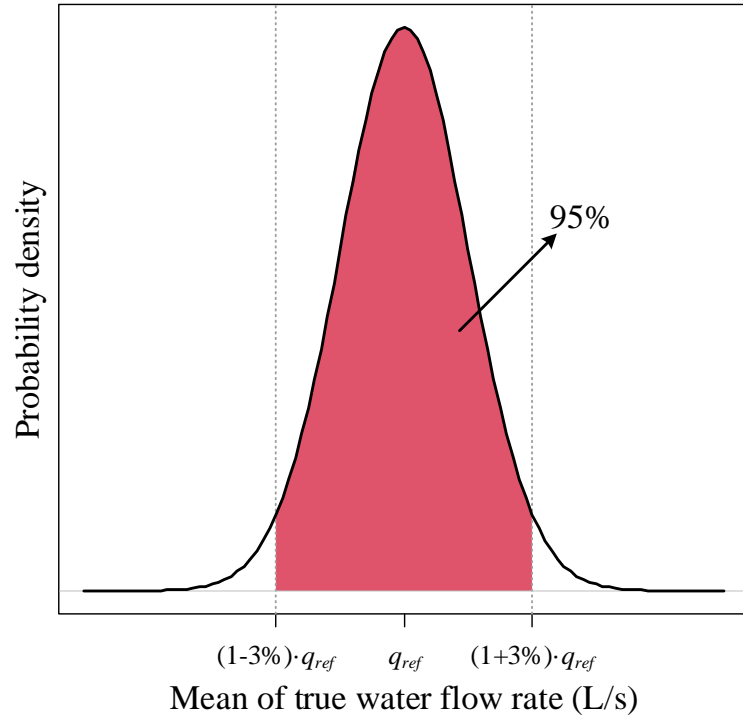
Figure 4.5 Prior distribution of the mean of true water flow rate

4.2.3 Energy and mass balance models

In principle, there are certain numerical relationships between these target and auxiliary variables, as they should obey basic rules such as energy and mass balance. Figure 4.6 shows the principle of a water-cooled chiller (Chiller-*i*). The heat is transferred from the chilled water to the cooling water indirectly by a vapor compression refrigeration cycle, as shown in Figure 4.6 (a). As a medium of heat transfer, the refrigerant absorbs the heat of chilled water and discharges the heat to cooling water. The refrigerant goes through a compression process (1→2), a condensation process (2→3→4), a throttling process

(4→5) and an evaporation process (5→1) to complete a cycle. The state of the refrigerant during the cycle can be presented in the pressure-enthalpy (*p-h*) and temperature-entropy (*T-s*) diagrams, as shown in Figure 4.6 (b) and (c). According to the law of energy balance, the input power of the compressor ($P_{CH,i}$) plus the heat absorption of the evaporator ($Q_{in,i}$) equals the heat rejection of the condenser ($Q_{out,i}$), as shown in Eq. (4.3). Where, *c* is the specific heat capacity of water ($kJ/(kg \cdot °C)$), and ρ is the density of water (kg/m^3).
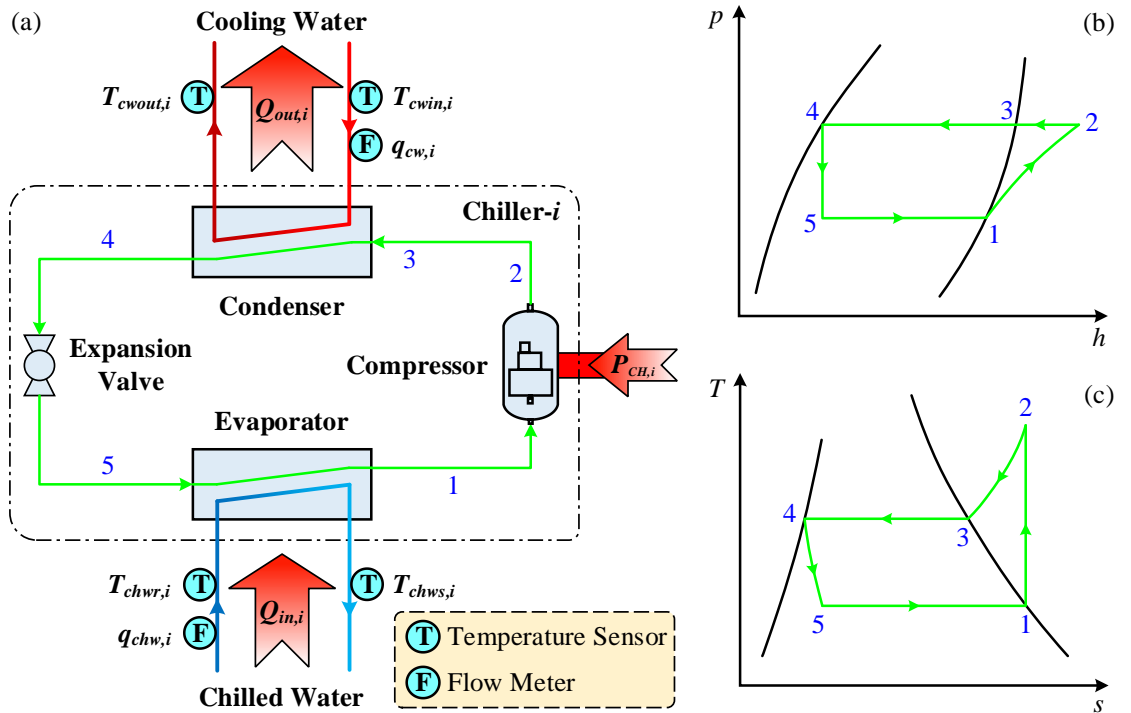
Figure 4.6 Principle of a water-cooled chiller (Chiller-*i*): (a) Schematic diagram, (b) *p-h* diagram, (c) *T-s* diagram

$$\begin{cases} P_{CH,i} + Q_{in,i} = Q_{out,i} \\ Q_{in,i} = c \cdot \rho \cdot q_{chw,i} \cdot \left(T_{chwr,i} - T_{chws,i} \right), \qquad i = 1, 2, ..., n \\ Q_{out,i} = c \cdot \rho \cdot q_{cw,i} \cdot \left(T_{cwout,i} - T_{cwin,i} \right) \end{cases} \qquad (4.3)$$

In addition, in a multiple water-cooled chiller system, the chilled water from each chiller mixes into the main supply pipe, which should also satisfy the law of energy and mass balance, as shown in Eqs. (4.4) and (4.5). Similarly, the mixing of cooling water from

each chiller should satisfy Eqs. (4.6) and (4.7). These equations are used to constrain the MCMC sampling in this study.

$$T_{chws} \cdot q_{chw} = T_{chws,1} \cdot q_{chw,1} + T_{chws,2} \cdot q_{chw,2} + \cdots + T_{chws,n} \cdot q_{chw,n} \qquad (4.4)$$

$$q_{chw} = q_{chw,1} + q_{chw,2} + \cdots + q_{chw,n} \qquad (4.5)$$

$$T_{cwout} \cdot q_{cw} = T_{cwout,1} \cdot q_{cw,1} + T_{cwout,2} \cdot q_{cw,2} + \cdots + T_{cwout,n} \cdot q_{cw,n} \qquad (4.6)$$

$$q_{cw} = q_{cw,1} + q_{cw,2} + \cdots + q_{cw,n} \qquad (4.7)$$

4.2.4 Measurement uncertainty models

According to the characteristics of measurement uncertainty mentioned in Section 3.1, the measured flow rates follow normal distributions as shown in Eqs. (4.8), (4.9), (4.10) and (4.11) respectively. In these equations, only the measured water flow rate ($\tilde{q}$) is available. The true water flow rate (q), mean (μ, systematic uncertainty) and standard deviation (σ, random uncertainty) corresponding to each flow meter are unknown and should be quantified. These measurement uncertainty models are in fact the likelihoods in Bayesian models.

$$\tilde{q}_{chw,i} \sim N\left(q_{chw,i} + \mu_{chwq,i}, \ \sigma^2_{chwq,i}\right), \quad i = 1,2,...,n \qquad (4.8)$$

$$\tilde{q}_{cw,i} \sim N\left(q_{cw,i} + \mu_{cwq,i}, \ \sigma^2_{cwq,i}\right), \quad i = 1,2,...,n \qquad (4.9)$$

$$\tilde{q}_{chw} \sim N\left(q_{chw} + \mu_{chwq}, \ \sigma^2_{chwq}\right) \qquad (4.10)$$

$$\tilde{q}_{cw} \sim N\left(q_{cw} + \mu_{cwq}, \ \sigma^2_{cwq}\right) \qquad (4.11)$$

In the MCMC sampling process, these unknown parameters involved should satisfy the distribution functions above and are constrained by the energy and mass balance models described in Section 4.2.3. When the pre-set/enough iterations are done, these effective

(post-warmup) samples will be used to construct the posterior distributions of the unknown parameters involved and then further analysis can be conducted.

4.3 Test and validation arrangements for the proposed method

The proposed physical model-based measurement uncertainty quantification method is tested using site data. In practical application, the true values of measurements cannot be known exactly, which means that the measurement uncertainty of a meter/sensor cannot be known exactly either. Even though the measurement uncertainty of site data can be quantified by the proposed method, it is very difficult to judge whether the quantified results are correct or not. Hence, four simulation test cases with different levels of measurement uncertainty are conducted to further test and validate the method systematically. Details about the site test case and simulation test cases are introduced in this section.

4.3.1 Site test

This section introduces the configurations of the chiller system used for the site test. And the models, the data used, and the prior distributions of unknown parameters to be quantified, are also presented for quantifying the measurement uncertainties of the water flow meters concerned.

4.3.1.1 Chiller system used for the site test

The chiller system used for the site test is equipped in the International Commerce Centre, which is a super high-rise commercial building in Hong Kong. The system equips six identical water-cooled chillers, and each chiller is interlocked with a constant-speed cooling water pump and a constant-speed primary chilled water pump. The rated cooling capacity of each chiller is 7 230 kW, and the rated flow rates of each cooling water pump

and primary chilled water pump are 410.1 L/s and 345.0 L/s respectively. More details about the chiller system can be found in references (Ma and Wang, 2009, 2011).

The chilled water flow rate and the cooling water flow rate of each chiller are measured on-site, but the main chilled water flow rate and the main cooling water flow rate are not measured in the system. Even so, the proposed physical model-based measurement uncertainty quantification method is also applicable to the case. The measurement uncertainty models are represented by Eqs. (4.8) and (4.9), subject to the physical constraint (i.e. the energy balance model) shown in Eq. (4.3). In this site test, the test results from one of the chillers are selected to demonstrate the use and the performance of the strategy. The data used in this site test was collected on 31 Aug 2020 with a time interval of 5 minutes, and the chiller concerned provided 24-hour service on this day. There are 288 data sets in total.

4.3.1.2 Prior distributions of unknown parameters in the site test

There are 6 unknown parameters to be quantified in this site test, including the systematic uncertainties and the standard deviations of the random uncertainties of chilled water and cooling water flow meters, as well as the means of true chilled water and cooling water flow rates. The prior distributions of these unknown parameters can be assigned according to the rules described in Section 4.2.2, the details are shown in Table 4.1.

Table 4.1 Prior distributions of unknown parameters in the site test

No.	Parameter	Prior distribution
1	Systematic uncertainty of chilled water flow meter	$N(0, 21^2)$
2	Systematic uncertainty of cooling water flow meter	$N(0, 25^2)$
3	Random uncertainty of chilled water flow meter	$\chi^2(3)$
4	Random uncertainty of cooling water flow meter	$\chi^2(3)$
5	Mean of true chilled water flow rate	$N(345, 6.3^2)$
6	Mean of true cooling water flow rate	$N(410.1, 7.5^2)$

4.3.2 Simulation tests

4.3.2.1 Chiller system model used in the simulation tests

A multiple water-cooled chiller system is simulated. The system consists of three identical chillers, three identical chilled water pumps and three identical cooling water pumps. The mathematical model of the chiller is obtained by referring to reference (Kang et al., 2017). The full load coefficient of performance (COP_{FL}) of the chillers with different cooling capacities (C_{rated}) is represented by Eq. (4.12). The ratio (α) of the actual (part-load) COP of the chiller to its full load COP is determined by Eq. (4.13), which is a function of the part load ratio (r_p). The actual COP and the power consumption (P_{CH}) of the chillers can be calculated using Eq. (4.14) and Eq. (4.15), respectively.

$$COP_{FL} = 2.886 \times 10^{-9} \cdot C_{rated}^2 + 0.293 \times 10^{-4} \cdot C_{rated} + 4.711 \tag{4.12}$$

$$\alpha = -0.569 \cdot r_p^3 - 0.258 \cdot r_p^2 + 1.520 \cdot r_p + 0.321 \tag{4.13}$$

$$COP = \alpha \cdot COP_{FL} \tag{4.14}$$

$$P_{CH} = \frac{Q}{COP} \tag{4.15}$$

The rated cooling capacity of each chiller used in the simulation tests is 600 kW. The full load COP is 4.73. The service time of the chillers is between 7:30 and 23:00 during the test period. The cooling load in the test period ranges between 1 200 kW and 1 800 kW as shown in Figure 4.7 (94 points in total), with all three chillers running during the test period. The cooling load is equally distributed to each of the three chillers in the tests, and the rated flow rates of the chilled water pumps and cooling water pumps are 28.6 L/s and 34.7 L/s, respectively. In addition, the measurement uncertainty models are represented by Eqs. (4.8), (4.9), (4.10) and (4.11), subject to physical constraints shown in Eqs. (4.4), (4.5), (4.6) and (4.7), where $n = 3$.
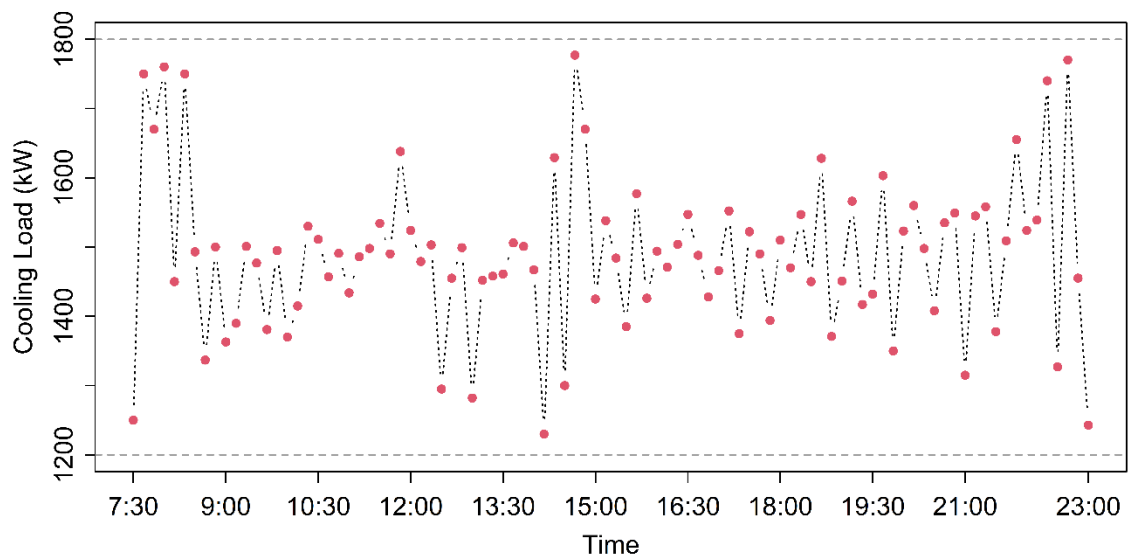
Figure 4.7 Cooling load profile used in the simulation tests

4.3.2.2 Prior distributions of unknown parameters in the simulation tests

There are eight flow meters in total in the chiller system used in the simulation tests, i.e., the chilled water and cooling water flow meters of each chiller and the main chilled water and cooling water flow meters. There are 22 unknown parameters in the simulation tests, including the systematic uncertainties and standard deviations of random uncertainties of

each flow meter, and the means of true chilled water and cooling water flow rates of each chiller. The prior distributions of these unknown parameters are assigned according to the rules described in Section 4.2.2. The details are shown in Table 4.2.

Table 4.2 Prior distributions of unknown parameters in the simulation tests

No.	Parameter	Prior distribution
1-3	Systematic uncertainty of chilled water flow meter 1-3	$N(0, 1.46^2)$
4-6	Systematic uncertainty of cooling water flow meter 1-3	$N(0, 1.79^2)$
7	Systematic uncertainty of main chilled water flow meter	$N(0, 4.38^2)$
8	Systematic uncertainty of main cooling water flow meter	$N(0, 5.37^2)$
9-11	Random uncertainty of chilled water flow meter 1-3	$\chi^2(3)$
12-14	Random uncertainty of cooling water flow meter 1-3	$\chi^2(3)$
15	Random uncertainty of main chilled water flow meter	$\chi^2(3)$
16	Random uncertainty of main cooling water flow meter	$\chi^2(3)$
17-19	Mean of true chilled water flow rate from chiller 1-3	$N(28.6, 0.438^2)$
20-22	Mean of true cooling water flow rate from chiller 1-3	$N(34.7, 0.531^2)$

4.3.2.3 Measurement uncertainty generation

In these simulation tests, chiller plant simulation is conducted without measurement uncertainties. The "actual measurements" are generated by adding uncertainties to the simulation outputs. The simulation outputs are considered to be the true values without measurement uncertainties. The measurement uncertainties of the flow meters are generated according to the characteristics of measurement uncertainty. As mentioned in Section 3.1, the measurement uncertainty of a flow meter follows a normal distribution. Hence, the measurement uncertainty of each flow meter is generated randomly by a given normal distribution, as shown in Eqs. (4.16), (4.17), (4.18) and (4.19).

$$u_{chwq,i} \sim N(\mu_{chwq,i}, \sigma_{chwq,i}^2), \quad i = 1, 2, 3 \tag{4.16}$$

$$u_{cwq,i} \sim N(\mu_{cwq,i}, \sigma_{cwq,i}^2), \quad i = 1, 2, 3 \tag{4.17}$$

$$u_{chwq} \sim N(\mu_{chwq}, \sigma_{chwq}^2) \tag{4.18}$$

$$u_{cwq} \sim N(\mu_{cwq}, \sigma_{cwq}^2) \tag{4.19}$$

Because the sample size is limited and the generation of random numbers is pseudo-random, the generated measurement uncertainties may not follow the given normal distribution strictly. In addition, there is more than one variable should be considered simultaneously. Therefore, the conditioned Latin hypercube sampling (cLHS) method (Minasny and McBratney, 2010; Minasny and McBratney, 2006) is used to cope with this challenge, as it can generate near-random samples for each variable from a multi-variable distribution. In these simulation tests, the measurement uncertainties of all flow meters are generated according to given normal distributions. 940 000 data sets are generated first, then 94 data sets are sampled from the population.

Table 4.3 lists the pre-set values of these unknown parameters in the simulation tests, including the systematic uncertainties and the standard deviations of the random uncertainties of each flow meter. The levels of measurement uncertainties in the four simulation test cases are different. The systematic uncertainties of the flow meters in Case 1 and Case 4 are about 10% of the rated flow rates of corresponding water pumps, while they are about 5%. in Case 2 and Case 3. In addition, the systematic uncertainties of the flow meters in Case 1 and Case 2 are positive, which tends to result in the measured flow rate being greater than the true flow rate. Conversely, the systematic uncertainties of the flow meters in Case 3 and Case 4 are negative, which tends to result in that the measured

flow rate is less than the true flow rate. The standard deviations of the random uncertainties follow a slowly rising trend in all tests.

Table 4.3 Pre-set values of measurement uncertainties in the simulation tests (Unit: L/s)

Flow meter	Case 1 (10%)	Case 2 (5%)	Case 3 (-5%)	Case 4 (-10%)
Systematic uncertainty				
Main chilled water flow meter	8.50	4.50	-4.50	-8.50
Chilled water flow meter 1	2.50	1.50	-1.50	-2.50
Chilled water flow meter 2	2.75	1.75	-1.75	-2.75
Chilled water flow meter 3	3.00	1.25	-1.25	-3.00
Main cooling water flow meter	10.00	5.00	-5.00	-10.00
Cooling water flow meter 1	3.25	2.00	-2.00	-3.25
Cooling water flow meter 2	3.75	1.50	-1.50	-3.75
Cooling water flow meter 3	3.50	1.75	-1.75	-3.50
Standard deviation of random uncertainty				
Main chilled water flow meter	1.50	1.75	2.00	2.25
Chilled water flow meter 1	1.25	1.00	1.75	1.50
Chilled water flow meter 2	0.75	1.50	1.25	2.00
Chilled water flow meter 3	1.00	1.25	1.50	1.75
Main cooling water flow meter	1.75	2.00	2.25	2.50
Cooling water flow meter 1	1.00	1.75	1.50	2.00
Cooling water flow meter 2	1.25	1.50	2.00	1.75
Cooling water flow meter 3	1.50	1.25	1.75	2.25

4.4 Performance evaluation of the proposed method on flow measurement uncertainty quantification

The proposed method is validated by using it to quantify the measurement uncertainties of flow meters in five different test cases, including a site test case using real site data and four simulation test cases with different levels of measurement uncertainties. The possible distributions (i.e., posterior distributions) of measurement uncertainties (both systematic and random uncertainties) are obtained. In order to systematically analyse and evaluate the results, 95% and/or 99% Bayesian credible intervals and the posterior means of the parameters to be quantified are also presented. Moreover, the site test case iterates 500 000 times per chain and each simulation test case iterate 2 000 times per chain for convergence.

4.4.1 Site test

The measurement uncertainties of both chilled water and cooling water flow meters can be quantified successfully. It does 500 000 iterations in total, but 250 000 "warmup" samples are discarded. In addition, the *thinning* technique is used to reduce the autocorrelations and chain length in this test case. It saves every 250th sample from the Markov chain and the rest are discarded. Figure 4.8 shows the traces and autocorrelations of the post-warmup MCMC samples in this test case. As can be seen from Figure 4.8, the Markov chains of random uncertainties are well convergent and their autocorrelations decay fast. Although the Markov chains of systematic uncertainties do not converge as well as the random uncertainties, they are also acceptable. These post-warmup MCMC samples can be used to construct the posterior distributions of the unknown parameters involved.

Figure 4.8 Traces and autocorrelations of post-warmup MCMC samples in site test case

Table 4.4 shows the quantified measurement uncertainties in the site test case. It can be observed that both the systematic uncertainty and the random uncertainty of the cooling water flow meter are larger than that of the chilled water flow meter. The posterior mean of the systematic uncertainty of the chilled water flow meter is 4.17% of the rated flow rate of the chilled water pump, while the posterior mean of the systematic uncertainty of the cooling water flow meter is 11.99% of the rated flow rate of the cooling water pump.

Table 4.4 Quantified measurement uncertainties in the site test case

Flow meter	95% credible interval (L/s)	Posterior mean (L/s)	Percentage
Systematic uncertainty			
Chilled water flow meter	[5.53, 23.18]	14.39	4.17%
Cooling water flow meter	[41.16, 57.30]	49.18	11.99%
Standard deviation of random uncertainty			
Chilled water flow meter	[2.56, 4.00]	3.34	-
Cooling water flow meter	[16.00, 18.81]	17.34	-

The ranges of the 95% Bayesian credible intervals are relatively narrow. They are 17.65 L/s and 16.14 L/s for the systematic uncertainties of the chilled water and cooling water flow meters respectively. The corresponding random uncertainties are 1.44 L/s and 2.81 L/s for the chilled water and cooling water flow meters respectively, which are rather small. In statistics, a narrow credible interval can generally provide more information about the population parameter. Therefore, the above results seem to be reliable. According to the specifications of the flow meters used, the accuracy of the insertion flow meters is about 2% (ASHRAE, 2014), and the actual site installation and aging may also affect the accuracy of flow measurements. Hence, a systematic uncertainty of 4.17% is quite acceptable for chilled water flow meters in practical buildings. Concerning the cooling water flow meter, a systematic uncertainty of 11.99% is obviously beyond normal deviations caused by meter accuracy and installation, giving it a high probability of being in an unhealthy condition. These results may also reflect errors from other sensors, like the power meter and temperature sensors.

It is hard to fully confirm whether the quantified results are correct because the measurement errors and uncertainties of the two flow meters cannot be known exactly. On-site verification of the flow meters at such a range of flow measurement deviation is very difficult due to the limitations of site conditions. In fact, the true flow rate cannot be obtained no matter how accurate the measuring instruments used are. Therefore, simulation tests are a simpler and more direct means to further test and validate the method.

4.4.2 Simulation test 1: High level of positive uncertainty

Figure 4.9 and Figure 4.10 show the traces and autocorrelations of post-warmup MCMC samples in this simulation test case respectively. 1000 warmup samples are discarded. As can be seen from the figures, the Markov chains of each parameter are well converged and the autocorrelations of MCMC samples are reduced rapidly. These post-warmup MCMC samples can be used to construct the posterior distributions of the unknown parameters involved.

Figure 4.9 Traces of post-warmup MCMC samples in Simulation test case 1

Figure 4.10 Autocorrelations of post-warmup MCMC samples in Simulation test case 1

Table 4.5 shows the quantified measurement uncertainties in Simulation test case 1, where the systematic uncertainties of the water flow meters are set to around 10% of the rated flow rates of the corresponding pumps. The 95% Bayesian credible intervals and the posterior means are presented. The pre-set values of the measurement uncertainties (both the systematic uncertainties and the standard deviations of random uncertainties) of the flow meters are also listed in the table for comparison. As shown in Table 4.5, the pre-set values fall within the 95% Bayesian credible intervals, and the posterior means are very close to the corresponding pre-set values. Particularly for the systematic uncertainties of the main chilled water and cooling water flow meters, their posterior means are almost the same as their pre-set values.

Table 4.5 Quantified measurement uncertainties in Simulation test case 1

Flow meter	Pre-set value (L/s)	95% credible interval (L/s)	Posterior mean (L/s)	Relative error (%)	Relative systematic uncertainty (%)
Systematic uncertainty					
Main CHWFM	8.50	[7.40, 9.68]	8.52	0.24	0.02
CHWFM-1	2.50	[1.95, 3.32]	2.63	5.20	0.45
CHWFM-2	2.75	[2.11, 3.41]	2.77	0.73	0.07
CHWFM-3	3.00	[2.15, 3.48]	2.84	5.30	0.56
Main CWFM	10.00	[8.77, 11.17]	9.99	0.10	0.01
CWFM-1	3.25	[2.73, 4.06]	3.38	4.00	0.37
CWFM-2	3.75	[3.15, 4.54]	3.85	2.67	0.29
CWFM-3	3.50	[2.86, 4.32]	3.62	3.43	0.35
Standard deviation of random uncertainty					
Main CHWFM	1.50	[1.27, 1.83]	1.53	2.00	-
CHWFM-1	1.25	[1.03, 1.44]	1.22	2.40	-
CHWFM-2	0.75	[0.55, 0.91]	0.72	4.00	-
CHWFM-3	1.00	[0.85, 1.23]	1.03	3.00	-
Main CWFM	1.75	[1.53, 2.16]	1.80	2.86	-
CWFM-1	1.00	[0.73, 1.10]	0.90	10.00	-
CWFM-2	1.25	[1.08, 1.52]	1.28	2.40	-
CWFM-3	1.50	[1.38, 1.89]	1.62	8.00	-

The relative error and the "relative systematic uncertainty" are also presented in Table 4.5. The relative error has been defined in Section 3.4. Similarly, the relative systematic uncertainty is defined as the absolute error of the uncertainty estimation (i.e., the difference between the pre-set value of the uncertain parameter and the posterior mean) divided by the design flow rate associated with the flow meter concerned or the rated flow rate of the corresponding water pump. It can be observed that the maximum relative errors are 5.30% and 10.00% for the quantified systematic uncertainties and quantified random

uncertainties respectively, indicating reasonably good accuracy. In addition, the relative systematic uncertainties are very small, ranging between 0.01% and 0.56%. This method can therefore be used to validate flow meters and improve measurement accuracy effectively. In fact, relative systematic uncertainty may be a better index to evaluate the quantified results in practical application, since the actual systematic uncertainties (pre-set values) are unknown. As can be seen from the test results, the measurement uncertainties of flow meters can be quantified successfully with high accuracy in this simulation test case.

4.4.3 Simulation test 2: Medium level of positive uncertainty

Figure 4.11 and Figure 4.12 show the traces and autocorrelations of post-warmup MCMC samples in this simulation test case respectively. It can be observed that the Markov chains of each parameter are well converged and the autocorrelations of MCMC samples are reduced rapidly. These post-warmup MCMC samples can be used to construct the posterior distributions of the unknown parameters involved.

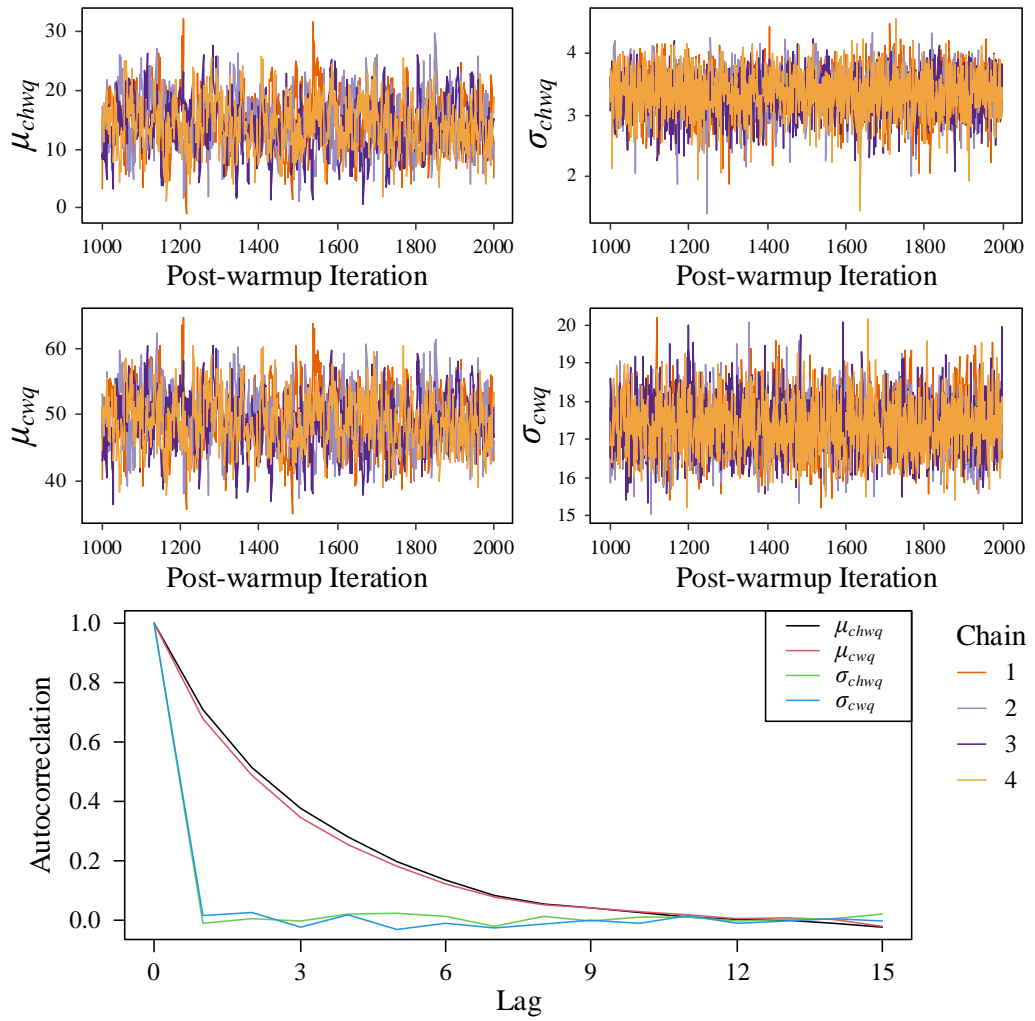Figure 4.11 Traces of post-warmup MCMC samples in Simulation test case 2
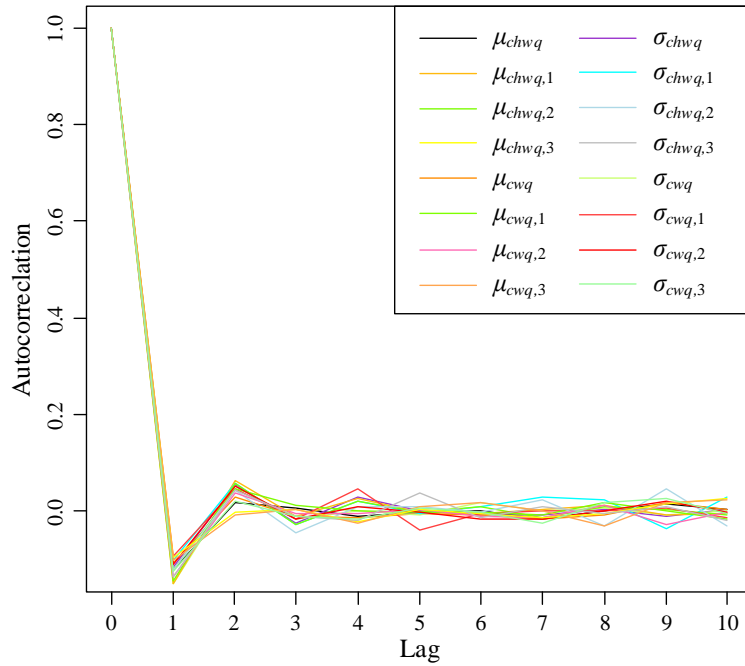
Figure 4.12 Autocorrelations of post-warmup MCMC samples in Simulation test case 2

Table 4.6 shows the quantified measurement uncertainties in Simulation test case 2, where the systematic uncertainties of the water flow meters are set to around 5% of the rated flow rates of the corresponding pumps. It can be observed that the pre-set values fall within the 95% Bayesian credible intervals, and since the posterior means are close to the pre-set values, the measurement uncertainties in this test case have been quantified successfully. For the quantified systematic uncertainties in this test case, the relative errors are larger than that in Simulation test case 1, as the maximum relative error is 20.00%. The relative systematic uncertainties are still small (0.31-0.87%). The proposed method can still be used to validate flow meters and improve measurement accuracy. For the quantified random uncertainties in this test case, the relative errors are small, with a maximum value of 12.80%. Therefore, the method performs better in quantifying random uncertainties than systematic uncertainties in this simulation test case.

Table 4.6 Quantified measurement uncertainties in Simulation test case 2

Flow meter	Pre-set value (L/s)	95% credible interval (L/s)	Posterior mean (L/s)	Relative error (%)	Relative systematic uncertainty (%)
Systematic uncertainty					
Main CHWFM	4.50	[3.89, 6.11]	5.02	11.55	0.61
CHWFM-1	1.50	[0.90, 2.26]	1.59	6.00	0.31
CHWFM-2	1.75	[1.25, 2.66]	1.94	10.86	0.66
CHWFM-3	1.25	[0.84, 2.16]	1.50	20.00	0.87
Main CWFM	5.00	[4.29, 6.63]	5.48	9.60	0.46
CWFM-1	2.00	[1.14, 2.60]	1.89	5.50	0.32
CWFM-2	1.50	[0.94, 2.41]	1.68	12.00	0.52
CWFM-3	1.75	[1.29, 2.67]	1.98	13.14	0.66
Standard deviation of random uncertainty					
Main CHWFM	1.75	[1.52, 2.18]	1.83	4.57	-
CHWFM-1	1.00	[0.70, 1.09]	0.89	11.00	-
CHWFM-2	1.50	[1.25, 1.76]	1.48	1.33	-
CHWFM-3	1.25	[1.08, 1.52]	1.29	3.20	-
Main CWFM	2.00	[1.64, 2.33]	1.96	2.00	-
CWFM-1	1.75	[1.49, 2.04]	1.75	0.00	-
CWFM-2	1.50	[1.34, 1.84]	1.58	5.33	-
CWFM-3	1.25	[1.19, 1.67]	1.41	12.80	-

4.4.4 Simulation test 3: Medium level of negative uncertainty

Figure 4.13 and Figure 4.14 show the traces and autocorrelations of post-warmup MCMC samples in this simulation test case respectively. It can be observed that the Markov chains of each parameter are well converged and the autocorrelations of MCMC samples are reduced rapidly. These post-warmup MCMC samples can be used to construct the posterior distributions of the unknown parameters involved.
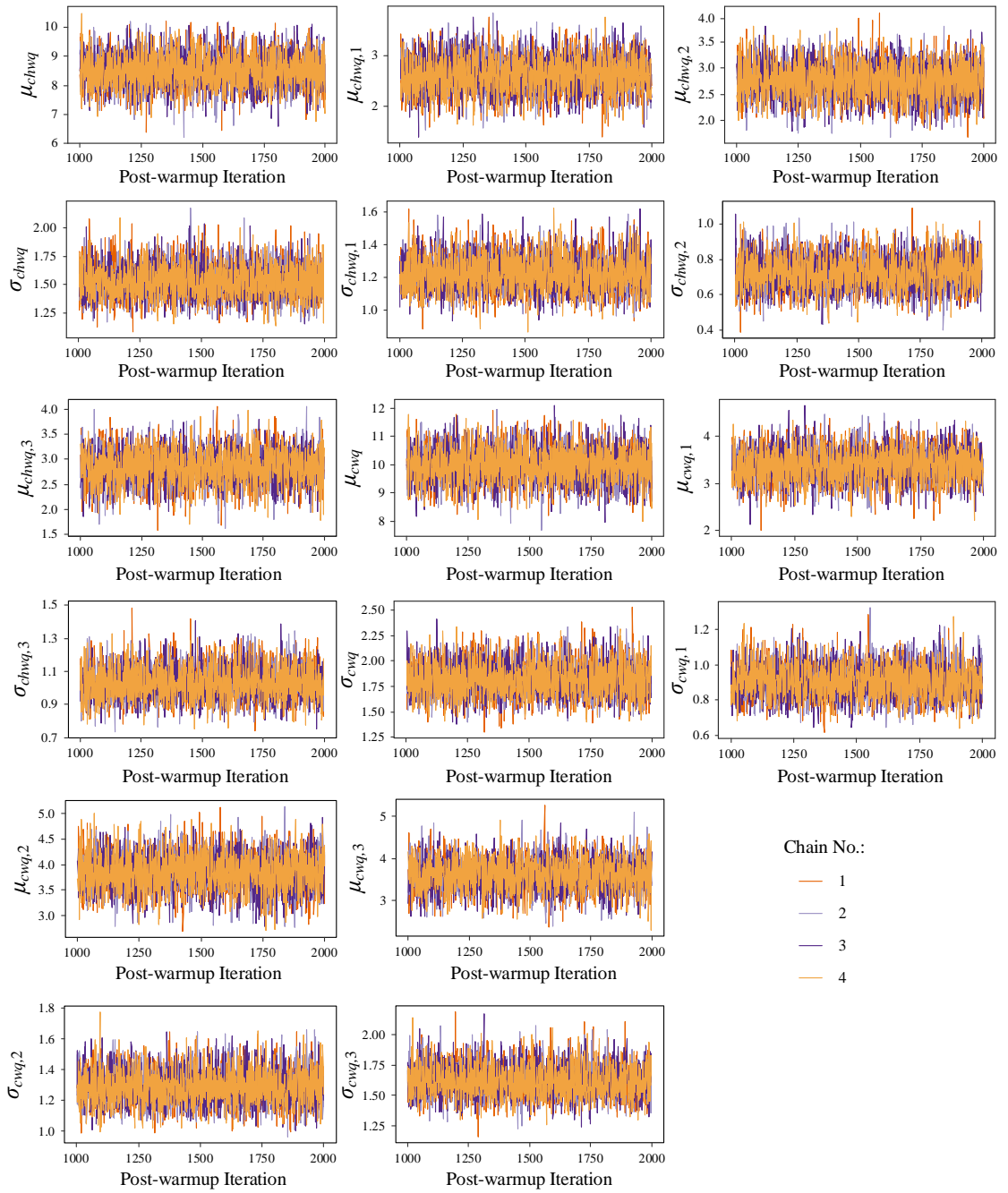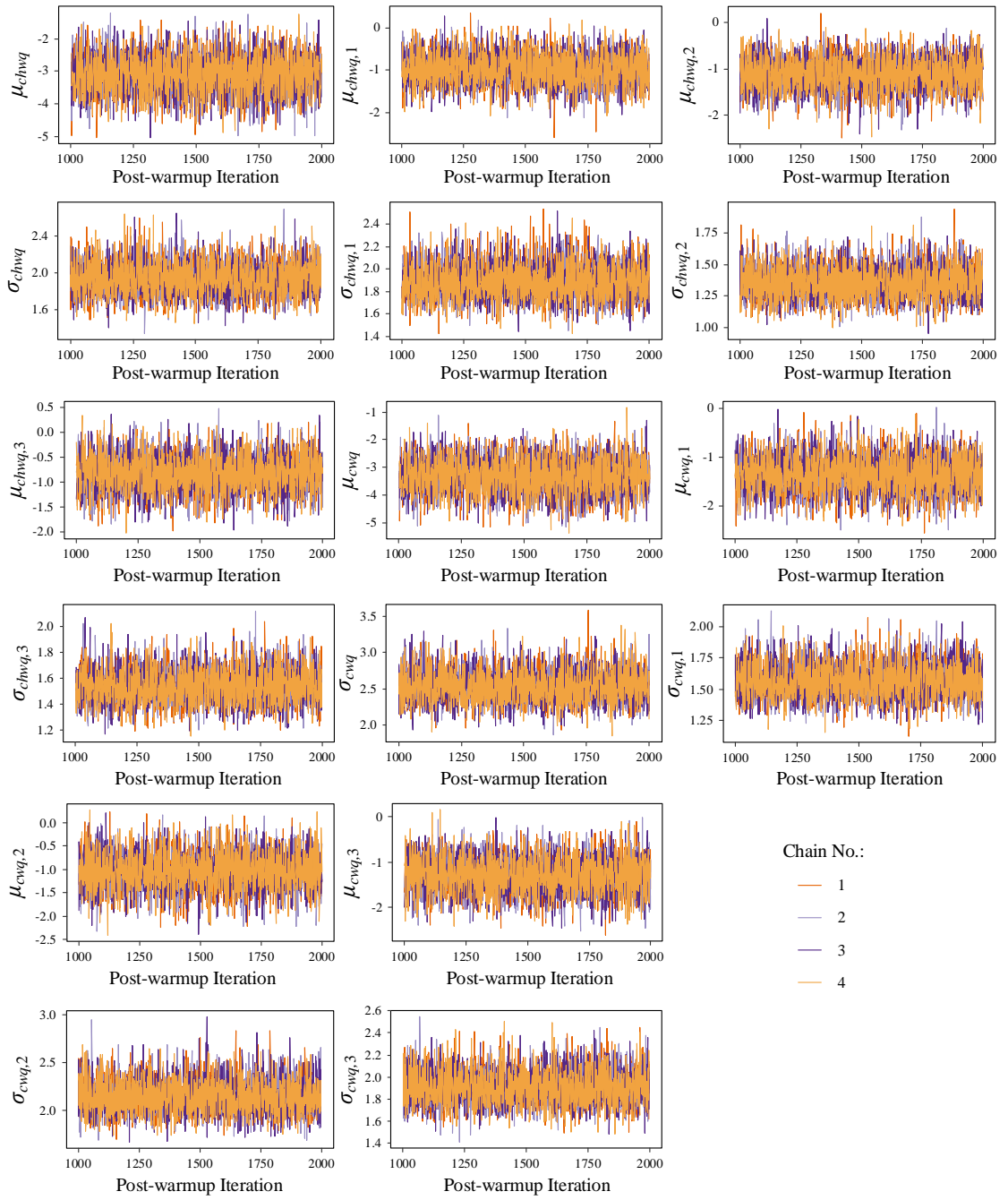
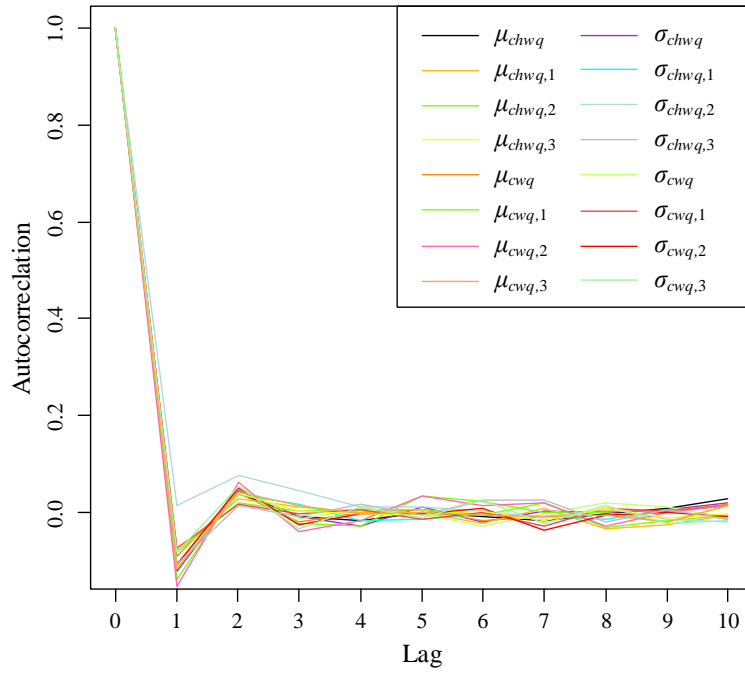Figure 4.13 Traces of post-warmup MCMC samples in Simulation test case 3
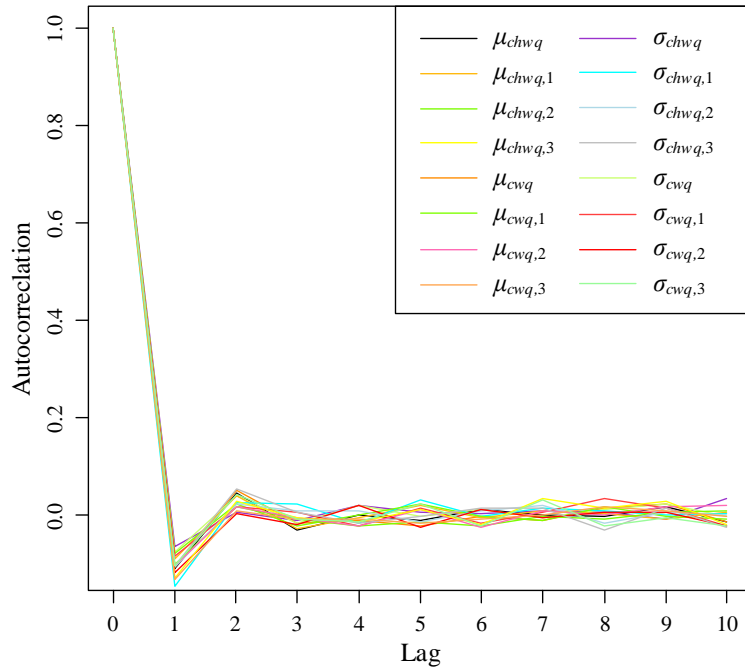
Figure 4.14 Autocorrelations of post-warmup MCMC samples in Simulation test case 3

Table 4.7 shows the quantified measurement uncertainties in Simulation test case 3, where the systematic uncertainties of the water flow meters are set to be around -5% of the rated flow rate of corresponding pumps. For the quantified systematic uncertainties of the main chilled water and cooling water flow meters, the pre-set values do not fall within the 95% Bayesian credible intervals, and so the 99% Bayesian credible intervals are also presented. It can be observed that the pre-set values are very close to the lower limits of the 99% Bayesian credible intervals. The differences between the pre-set values and the posterior means are significant. For the quantified systematic uncertainties of the other flow meters in this test case, the pre-set values are close to the lower limits of the 95% Bayesian credible intervals, and the differences between the pre-set values and the posterior means are also relatively significant. The relative errors in this test case are more significant than that in Simulation test case 1 and Simulation test case 2, with the maximum error being 38.57%. The relative systematic uncertainties are still within a relatively small range (1.33-2.24%). The results show that the method is still effective for validating flow meters and improving measurement accuracy, and it can also provide

66

valuable and meaningful information in practical application. For the quantified random uncertainties of the flow meters in this test case, the pre-set values fall within the 95% Bayesian credible intervals, and the posterior means are very close to the pre-set values. The maximum relative error is 12.44% and the relative errors are within an acceptable range. The random uncertainties of flow meters in this test case are quantified with satisfactory accuracy. The method performs better in quantifying random uncertainties compared with systematic uncertainties in this test case.

Table 4.7 Quantified measurement uncertainties in Simulation test case 3

Flow meter	Pre-set value (L/s)	95% credible interval (L/s)	99% credible interval* (L/s)	Posterior mean (L/s)	Relative error (%)	Relative systematic uncertainty (%)
Systematic uncertainty						
Main CHWFM	-4.50	[-4.27, -1.97]	[-4.60, -1.61]	-3.11	30.89	1.62
CHWFM-1	-1.50	[-1.71, -0.25]	-	-0.98	34.67	1.82
CHWFM-2	-1.75	[-1.78, -0.45]	-	-1.11	36.57	2.24
CHWFM-3	-1.25	[-1.56, -0.11]	-	-0.83	33.60	1.47
Main CWFM	-5.00	[-4.54, -2.09]	[-4.94, -1.74]	-3.31	33.80	1.62
CWFM-1	-2.00	[-2.08, -0.63]	-	-1.34	33.00	1.90
CWFM-2	-1.50	[-1.83, -0.26]	-	-1.04	30.67	1.33
CWFM-3	-1.75	[-2.06, -0.54]	-	-1.28	26.86	1.35
Standard deviation of random uncertainty						
Main CHWFM	2.00	[1.61, 2.30]	-	1.93	3.50	-
CHWFM-1	1.75	[1.62, 2.22]	-	1.89	8.00	-
CHWFM-2	1.25	[1.13, 1.62]	-	1.35	8.00	-
CHWFM-3	1.50	[1.30, 1.82]	-	1.54	2.67	-
Main CWFM	2.25	[2.14, 2.98]	-	2.53	12.44	-
CWFM-1	1.50	[1.32, 1.86]	-	1.57	4.67	-
CWFM-2	2.00	[1.83, 2.52]	-	2.14	7.00	-
CWFM-3	1.75	[1.63, 2.23]	-	1.91	9.14	-

4.4.5 Simulation test 4: High level of negative uncertainty

Figure 4.15 and Figure 4.16 show the traces and autocorrelations of post-warmup MCMC samples in this simulation test case respectively. It can be observed that the Markov chains of each parameter are well converged and the autocorrelations of MCMC samples are reduced rapidly. These post-warmup MCMC samples can be used to construct the posterior distributions of the unknown parameters involved.
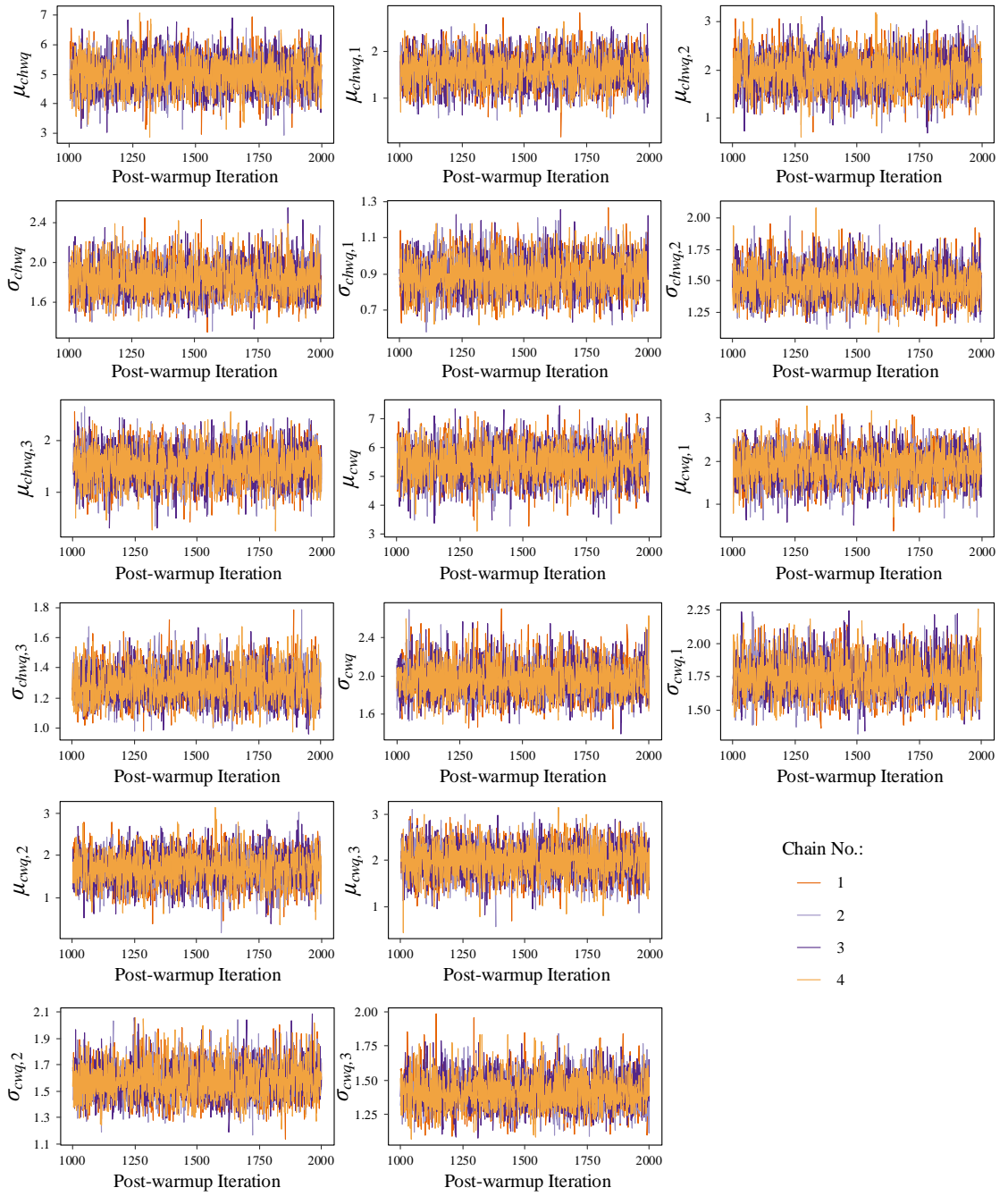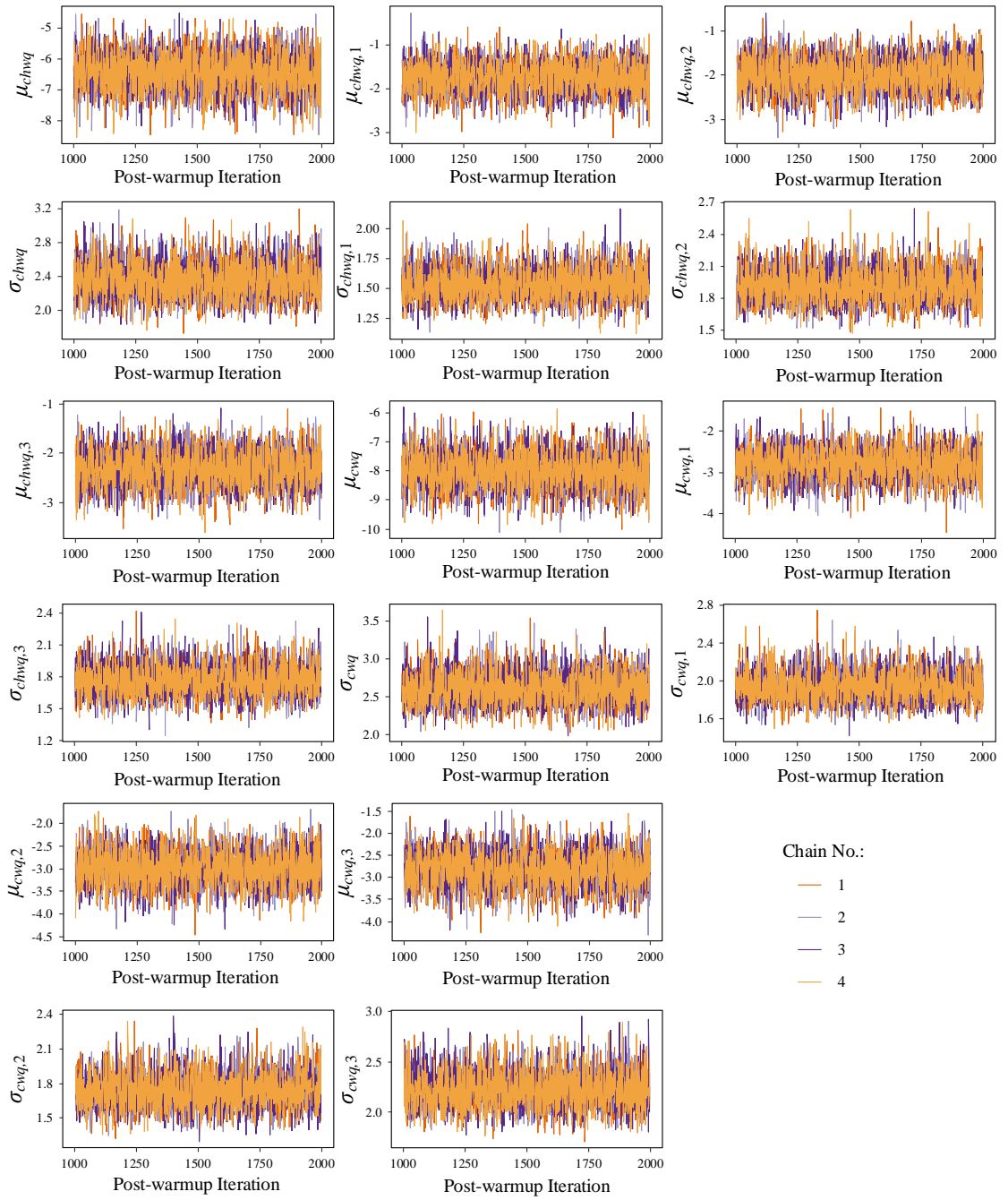
Figure 4.15 Traces of post-warmup MCMC samples in Simulation test case 4
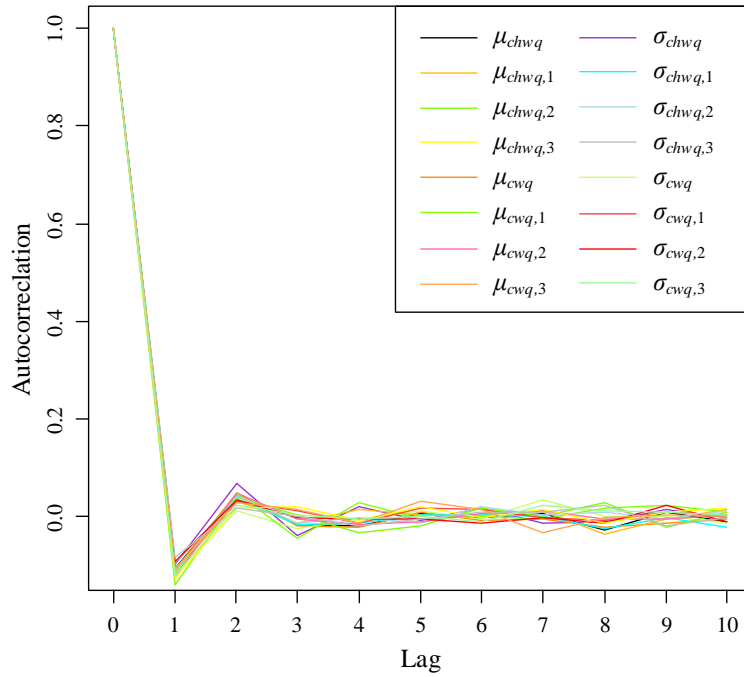
Figure 4.16 Autocorrelations of post-warmup MCMC samples in Simulation test case 4

Table 4.8 shows the quantified measurement uncertainties in Simulation test case 4, where the systematic uncertainties of the water flow meters are set to around -10% of the rated flow rate of the corresponding pumps. Both the 95% and 99% Bayesian credible intervals of the quantified systematic uncertainties in this test case are presented. Besides the main chilled water and cooling water flow meters, the pre-set values of the quantified systematic uncertainties fall within the 99% Bayesian credible intervals. The differences between the pre-set values and the posterior means are significant, leading to large relative errors with a maximum value of 30.40%. The relative systematic uncertainties range between 1.27% and 2.66%. Similar to the previous simulation test cases, the method can provide valuable and meaningful information in applications. For the quantified random uncertainties in this test case, the pre-set values fall within the 95% Bayesian credible intervals, and the posterior means are very close to the pre-set values. The maximum relative error is 4.50% and the relative errors are within an acceptable range. The method also performs better in quantifying random uncertainties than systematic uncertainties in this simulation test case.

70

Table 4.8 Quantified measurement uncertainties in Simulation test case 4

Flow meter	Pre-set value (L/s)	95% credible interval (L/s)	99% credible interval (L/s)	Posterior mean (L/s)	Relative error (%)	Relative systematic uncertainty (%)
			Systematic uncertainty			
Main CHWFM	-8.50	[-7.64, -5.25]	[-8.16, -4.80]	-6.44	24.24	2.40
CHWFM-1	-2.50	[-2.44, -1.06]	[-2.68, -0.85]	-1.74	30.40	2.66
CHWFM-2	-2.75	[-2.74, -1.26]	[-2.98, -1.06]	-1.99	27.64	2.66
CHWFM-3	-3.00	[-3.03, -1.57]	[-3.25, -1.40]	-2.30	23.33	2.45
Main CWFM	-10.00	[-9.23, -6.74]	[-9.60, -6.34]	-7.98	20.20	1.94
CWFM-1	-3.25	[-3.56, -2.08]	[-3.80, -1.85]	-2.81	13.54	1.27
CWFM-2	-3.75	[-3.73, -2.23]	[-3.95, -2.01]	-2.99	20.27	2.19
CWFM-3	-3.50	[-3.62, -2.04]	[-3.86, -1.75]	-2.82	19.43	1.96
			Standard deviation of random uncertainty			
Main CHWFM	2.25	[1.98, 2.79]	-	2.35	4.44	-
CHWFM-1	1.50	[1.29, 1.82]	-	1.54	2.67	-
CHWFM-2	2.00	[1.63, 2.25]	-	1.91	4.50	-
CHWFM-3	1.75	[1.49, 2.07]	-	1.77	1.14	-
Main CWFM	2.50	[2.23, 3.07]	-	2.60	4.00	-
CWFM-1	2.00	[1.66, 2.28]	-	1.94	3.00	-
CWFM-2	1.75	[1.46, 2.06]	-	1.73	1.14	-
CWFM-3	2.25	[1.90, 2.61]	-	2.22	1.33	-

4.4.6 Discussion and comparison of the test results

According to the outputs of the four simulation test cases presented in Section 4.4.2-4.4.5, the measurement uncertainties of water flow meters, including both the systematic uncertainties and the random uncertainties, can be quantified effectively by the proposed method. Figure 4.17 summarizes the measurement uncertainty quantification results of

the four simulation test cases. The relative errors and absolute errors of the measurement uncertainty quantification are presented. It can be observed that the errors in quantifying the random uncertainties of flow meters in all test cases are very small, but the errors in quantifying the systematic uncertainties of flow meters vary from case to case. The errors are small for case 1 and case 2, but they are significant for case 3 and case 4.
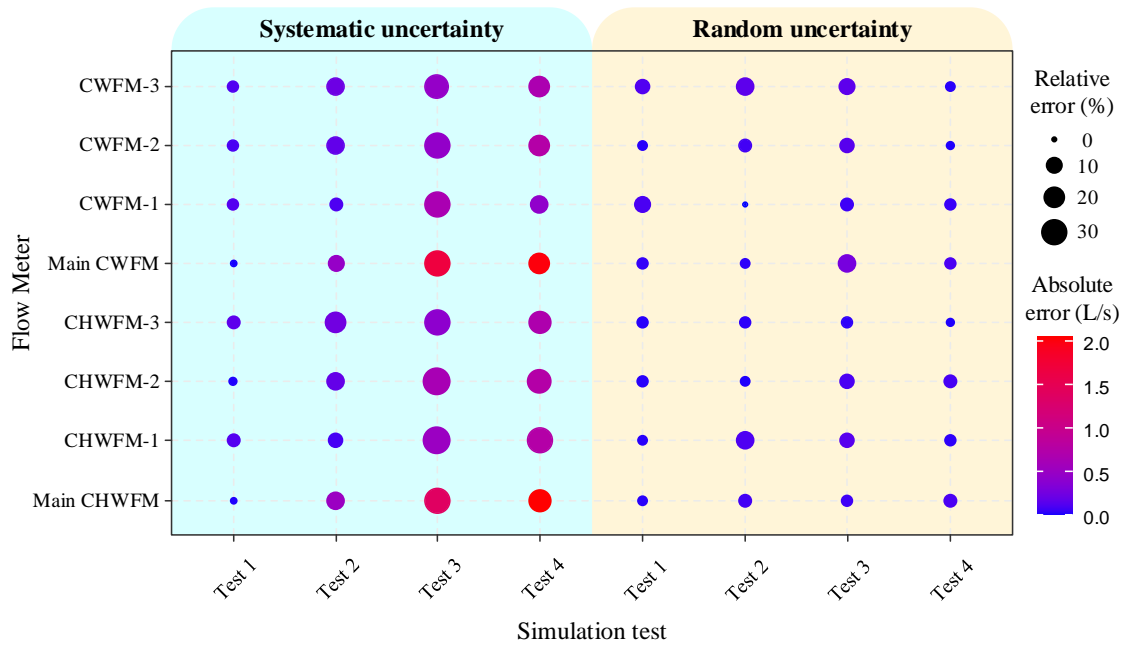
Figure 4.17 Relative errors and absolute errors of measurement uncertainty quantification for simulation test cases

The proposed method performs very well in quantifying systematic uncertainties in Simulation test cases 1 and 2. Although the performance of the method in quantifying systematic uncertainties in Simulation test cases 3 and 4 is not as good as that in Simulation test cases 1 and 2, its performance is still acceptable. The method is still effective for validating flow meters and improving measurement accuracy and can provide valuable and meaningful information in practical applications. In addition, the random uncertainties of the flow meters can be quantified accurately by the method no matter how significant they are. In general, the method performs better in quantifying random uncertainties than systematic uncertainties.

The levels of the quantified measurement uncertainties in the four simulation test cases are consistent with the levels of the pre-set measurement uncertainties. In other words, the levels of the measurement uncertainties of different flow meters can be identified by the method. The information is also meaningful and valuable in practical application. If the identified measurement uncertainties of one or more flow meters are obviously higher than that of other flow meters, more attention should be paid to these flow meters and calibrations on the measurement accuracy of these flow meters are needed or decisions requiring flow rate measurements of high accuracy should be avoided. For example, as presented in Section 4.4.1, the quantified measurement uncertainty of the cooling water flow meter in the site test case is much larger than the typical uncertainty range of flow measurement. If this cooling water flow measurement is used by a critical decision-making strategy, priority should be given to checking/calibrating the flow meter or re-consider the decision-making strategy itself.

As mentioned in Section 3.2, for the Bayesian models, both prior distributions and likelihoods may affect posterior distributions. It is possible to improve the accuracy of the proposed method from these two aspects. The likelihoods are associated with observational data. In principle, the posterior distributions are mainly affected by likelihoods if the quantity of observational data is large enough. However, the computational load will increase significantly if the number of observational data increases. Therefore, the size of the observational data cannot be increased without limit. A trade-off between the quantity of observational data and the computational load should be made. On the other hand, the assignments of the prior distributions of the parameters to be quantified are based on expert judgement. A good prior distribution will be of great help in accurately quantifying the measurement uncertainty. Maximum utilization of

information about the parameters to be quantified should be achieved to obtain the best prior distributions.

The proposed physical model-based measurement uncertainty quantification method is promising to be put into practice. The flow meters can be calibrated at any time by the method. A threshold of acceptable uncertainty can be set for each flow meter. If the quantified uncertainty of a flow meter is greater than the threshold, the operators can conduct an on-site calibration for the flow meter or replace the flow meter directly, and the impacts of the unacceptable uncertainty on system operation can be reduced.

4.5 Summary

This chapter presents the physical model-based measurement uncertainty quantification method. It is validated systematically using a site test case and four simulation test cases with different levels of measurement uncertainties. The test cases are conducted on multiple water-cooled chiller systems. The measurement uncertainties (including the systematic and random uncertainties) of water flow meters are quantified with the auxiliaries of power meters and temperature sensors based on energy and mass balance models. Based on the results of the test cases, the main conclusions can be drawn as follows.

- The physical model-based measurement uncertainty quantification method can effectively quantify the measurement uncertainties (including the systematic and random uncertainties) of chilled water and cooling water flow meters in multiple water-cooled chiller systems.

- The performance of the method in quantifying systematic uncertainties is satisfactory. The method is effective for validating flow meters and improving their measurement

accuracy, and it can provide valuable and meaningful information in practical application.

- The random uncertainties can be quantified accurately by the proposed method no matter how significant they are. The method performs better in quantifying random uncertainties than systematic uncertainties.

- The levels of measurement uncertainties of different flow meters can be identified by the quantification method. It can be used to detect which flow meters need to be calibrated and assess the reliability of flow measurements, particularly concerning critical decision-making.

CHAPTER 5   PROBABILITY-BASED ONLINE ROBUST CHILLER SEQUENCING CONTROL STRATEGY WITH MEASUREMENT UNCERTAINTIES PROCESSED BY PHYSICAL MODEL-BASED METHOD

This chapter presents a probability-based robust sequencing control strategy for multiple water-cooled chiller plants under flow measurement uncertainties. Since Chapter 4 has shown that the physical model-based measurement uncertainty quantification method has good performance. This chapter also uses the method to correct the target measurements online and optimize the conventional total cooling load-based chiller sequencing control strategy. The organization of this chapter is as follows. Section 5.1 introduces the conventional total cooling load-based chiller sequencing control strategy and its drawbacks. Section 5.2 presents the proposed probability-based chiller sequencing control strategy. Section 5.3 presents the online test platform and arrangement for the proposed control strategy. The test results are presented in Section 5.4. Section 5.5 discusses the advantages and application potential of the proposed control strategy. And the conclusions are made in Section 5.6.

5.1 Conventional total cooling load-based chiller sequencing control strategy and its drawbacks

Figure 5.1 shows the schematic diagram of a typical water-cooled chiller plant, where only the primary chilled water distribution loop is presented. Each chiller is interlocked with a constant-speed cooling water pump and a constant-speed chilled water pump. Sensors and meters are installed for system monitoring and real-time online control. And

here only the sensors/meters installed in the main pipe are concerned. The measured variables mainly include the main chilled water volume flow rate (q_{chw}), return temperature (T_{chwr}) and supply temperature (T_{chws}), and the main cooling water volume flow rate (q_{cw}), inlet temperature (T_{cwin}) and outlet temperature (T_{cwout}), and the power consumption of chillers (P_{CH}).
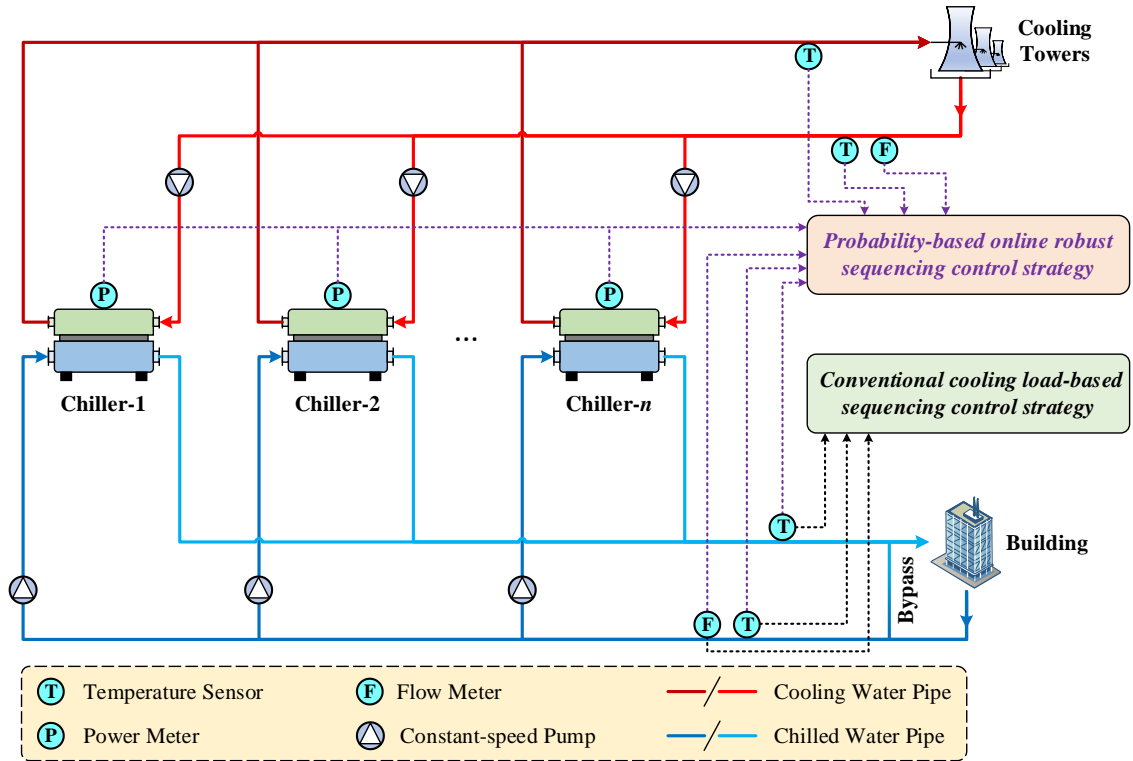
Figure 5.1 Schematic diagram of a typical water-cooled chiller plant

The cooling load-based chiller sequencing control strategy is commonly used to control the staging of chillers. The start and stop of the chillers are controlled according to the instantaneous building load and the chiller capacities. Figure 5.2 shows the conventional cooling load-based chiller sequencing control strategy. For the cooling plants with identical chillers, the thresholds of cooling load for switching on the $(N+1)^{th}$ chiller (Q_{N+1}^{on}) and switching off the Nth chiller (Q_N^{off}) are defined by Eqs. (5.1) and (5.2) respectively. Where C_{rated} is the rated chiller capacity, l is the chiller capacity loss rate, and d is a dead band. The chiller capacity loss is introduced because the actual maximum chiller capacity

deviates from its rated value in different working conditions. The dead band is used to avoid frequent switching of chillers when the cooling load varies around the thresholds. The number of operating chillers at the next time instant (N_{t+1}) can be determined by Eq. (5.3). Where, the subscript "t" represents the sampling time, and Q_t is the instantaneous building load at the current time instant. In this study, the chiller capacity loss rate l is set to 2.50%, and the dead band d is set to 0.10.
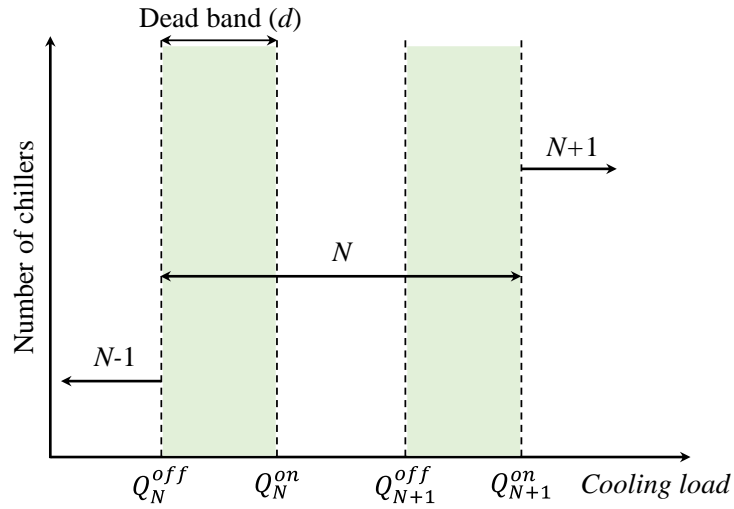
Figure 5.2 Conventional cooling load-based chiller sequencing control strategy

$$Q_{N+1}^{on} = N \cdot (1-l) \cdot C_{rated} \tag{5.1}$$

$$Q_N^{off} = (N-1) \cdot (1-l) \cdot C_{rated} \cdot (1-d) \tag{5.2}$$

$$N_{t+1} = \begin{cases} N_t - 1, & Q_t < Q_N^{off} \\ N_t, & Q_N^{off} \le Q_t \le Q_{N+1}^{on} \\ N_t + 1, & Q_t > Q_{N+1}^{on} \end{cases} \tag{5.3}$$

The instantaneous building load is estimated based on the measured total chilled water flow rate, return and supply temperatures, as shown in Eq. (5.4). c is the specific heat capacity of water (kJ/(kg·°C)). ρ is the density of water (kg/m^3). The unavoidable measurement uncertainties may lead to significant errors in cooling load measurements, and further affect the performance of the cooling load-based chiller sequencing control.

According to the previous analysis (in Section 4.1) about the measuring instruments used in chiller systems, only the measurement uncertainties of water flow meters are considered here as well, while the measurement uncertainties of power meters and temperature sensors are deemed to be acceptable and not considered.

$$\tilde{Q}_t = c\rho \cdot \tilde{q}_{chw,t} \cdot \left(T_{chwr,t} - T_{chws,t}\right) \tag{5.4}$$

The real-time measured chilled water flow rate ($\tilde{q}_{chw,t}$) and cooling water flow rate ($\tilde{q}_{cw,t}$) are denoted by Eq. (5.5) and Eq. (5.6), respectively. The measured water flow rate ($\tilde{q}_t$) equals the true water flow rate (q_t) plus the measurement uncertainty (u). The measurement uncertainty includes the systematic uncertainty (μ) and the random uncertainty (σ) of the corresponding flow meter.

$$\tilde{q}_{chw,t} = q_{chw,t} + u_{chwq}, \qquad u_{chwq} \sim N\left(\mu_{chwq}, \sigma^2_{chwq}\right) \tag{5.5}$$

$$\tilde{q}_{cw,t} = q_{cw,t} + u_{cwq}, \qquad u_{cwq} \sim N\left(\mu_{cwq}, \sigma^2_{cwq}\right) \tag{5.6}$$

The performance of the conventional cooling load-based chiller sequencing control strategy heavily depends on the accuracy of chilled water flow measurements. In order to reduce the impacts of flow measurement uncertainties on direct cooling load measurements, a probability-based online robust chiller sequencing control strategy is proposed. In addition to the chilled water flow rate, supply and return temperatures, the proposed control strategy also uses the cooling water flow rate, inlet and outlet temperatures, and the total power consumption of chillers, as shown in Figure 5.1. The details of the proposed control strategy and its validation will be presented in the following sections.

5.2 The proposed probability-based online robust chiller sequencing control strategy

This section presents the probability-based online robust chiller sequencing control strategy in detail, including the outline of the control strategy, the uncertainty processing model used for quantifying the flow measurement uncertainties, the analysis of cooling load distributions, and the online decision-making scheme and risk assessment for the control strategy.

5.2.1 Outline of the probability-based online robust chiller sequencing control strategy

In the proposed online robust probability-based chiller sequencing control strategy, the chiller staging is determined according to the probability distributions of cooling loads. Figure 5.3 shows the outline of the proposed control strategy. The real-time measurements, including the power consumption, chilled water flow rate, supply and return temperatures, cooling water flow rate, inlet and outlet temperatures, are input into an uncertainty processing model for handling the uncertainties in flow measurements. The model is developed based on an energy balance model and the characteristics of flow measurement uncertainty using Bayesian inference and Markov chain Monte Carlo sampling methods. Then the probability distribution (posterior distribution) of the main chilled water flow rate can be constructed using the effective samples generated by the uncertainty processing model. Accordingly, the probability distribution of the cooling load can further be determined, which is the corrected cooling load. Based on the distribution function, the probabilities of the cooling load distribution in different ranges can be obtained according to the empirical cumulative distribution function (ECDF). Finally, the control decision is made, and the risk is assessed according to the probabilities.

The details about the proposed probability-based online robust chiller sequencing control strategy are illustrated in Sections 5.2.2-5.2.4.
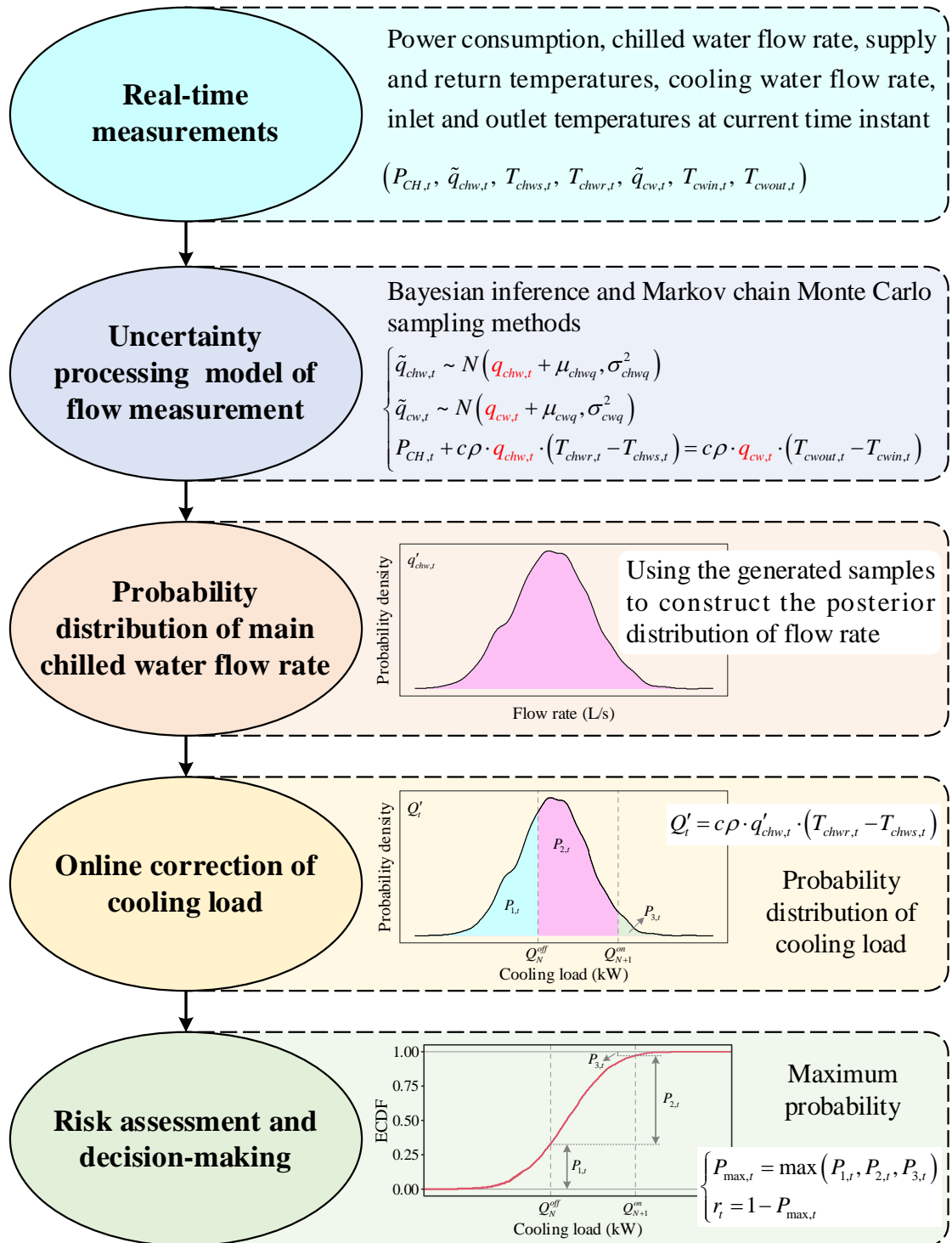
Figure 5.3 Outline of the probability-based online robust chiller sequencing control strategy

5.2.2 Uncertainty processing model of flow measurements

The measured chilled water and cooling water flow rates follow the normal distributions as shown in Eq. (5.7) and Eq. (5.8), respectively. These two distribution functions are the likelihoods in Bayesian models. The uncertainties in flow measurements could be determined by the proposed physical model-based measurement uncertainty quantification method based on historical system operating data. In the uncertainty processing model, only the actual chilled water flow rate ($q_{chw,t}$) and cooling water flow rate ($q_{cw,t}$) are unknown and need to be quantified. The energy balance model, as shown in Eq. (5.9), is used to constrain the MCMC sampling. The generated samples by MCMC should satisfy this equation.

$$\tilde{q}_{chw,t} \sim N\left(q_{chw,t} + \mu_{chwq}, \sigma^2_{chwq}\right) \tag{5.7}$$

$$\tilde{q}_{cw,t} \sim N\left(q_{cw,t} + \mu_{cwq}, \sigma^2_{cwq}\right) \tag{5.8}$$

$$P_{CH,t} + c\rho \cdot q_{chw,t} \cdot \left(T_{chwr,t} - T_{chws,t}\right) = c\rho \cdot q_{cw,t} \cdot \left(T_{cwout,t} - T_{cwin,t}\right) \tag{5.9}$$

The developed uncertainty processing model of flow measurements can be updated regularly by operating data to adapt to system changes. Though the posterior distributions of both chilled water and cooling water flow rates can be obtained simultaneously, this study only needs the chilled water flow rate for calculating the cooling load.

5.2.3 Probability distribution of cooling load and analysis

The posterior distribution of the main chilled water flow rate ($q'_{chw,t}$) is obtained by the uncertainty processing model, a sketch map of the distribution is shown in Figure 5.4. The cooling load (Q'_t) is calculated by Eq. (5.10). The probability distribution of cooling load is then obtained, and a sketch map is shown in Figure 5.5. The cooling load

distribution form is the same as the total chilled water flow rate distribution form because the measurement uncertainties of temperature sensors are not considered.

$$Q'_t = c\rho \cdot q'_{chw,t} \cdot \left(T_{chwr,t} - T_{chws,t}\right)$$ (5.10)
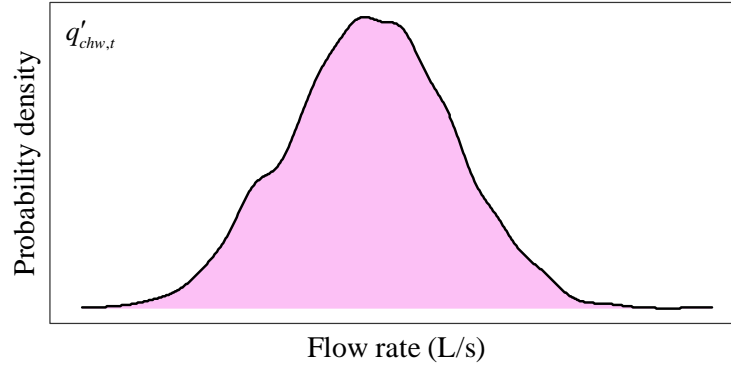
Figure 5.4 Sketch map of the posterior distribution of the main chilled water flow rate
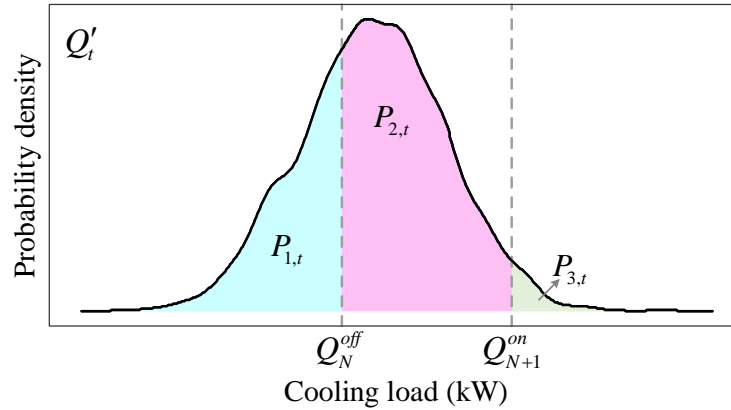
Figure 5.5 Sketch map of the probability distribution of cooling load

As shown in Figure 5.5, the probability density curve (or the area under the curve) is divided into three parts by the thresholds Q_N^{off} and Q_{N+1}^{on} (the thresholds are consistent with the thresholds in conventional chiller sequencing control strategy), the area of each part represents the probability that the cooling load is within the corresponding range. These probabilities are calculated by the empirical cumulative distribution function (ECDF), as shown in Eq. (5.11). Figure 5.6 shows the sketch map of the ECDF curve.

$$\begin{cases} P_{1,t} = P\left(Q_t' < Q_N^{off}\right) = \mathrm{ECDF}_t\left(Q_N^{off}\right) \\ P_{2,t} = P\left(Q_N^{off} \le Q_t' \le Q_{N+1}^{on}\right) = \mathrm{ECDF}_t\left(Q_{N+1}^{on}\right) - \mathrm{ECDF}_t\left(Q_N^{off}\right) \\ P_{3,t} = P\left(Q_t' > Q_{N+1}^{on}\right) = 1 - \mathrm{ECDF}_t\left(Q_{N+1}^{on}\right) \end{cases} \tag{5.11}$$
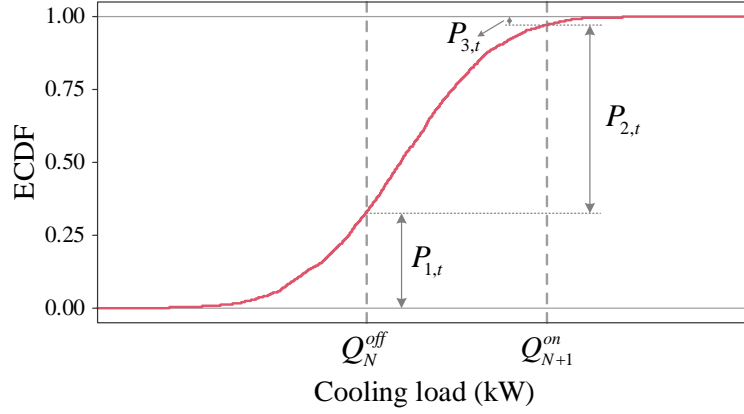
Figure 5.6 Sketch map of the ECDF curve of cooling load

The probabilities, $P_{1,t}$, $P_{2,t}$ and $P_{3,t}$, are the core of the proposed control strategy and will be used for online decision-making and risk assessment. Details of their usages are presented in Section 5.2.4.

5.2.4 Online decision-making scheme and risk assessment

Figure 5.7 shows the decision-making scheme of the probability-based online robust sequencing control strategy for the cooling plants with identical chillers. The number of operating chillers at the next time instant (N_{t+1}) is determined by comparing the magnitudes of the probabilities (i.e. $P_{1,t}$, $P_{2,t}$ and $P_{3,t}$), as shown in Eq. (5.12). If $P_{1,t}$ is the maximum probability ($P_{\max,t}$), one of the operating chillers should be switched off; If $P_{2,t}$ is the maximum probability, the current chiller running status should be kept; If $P_{3,t}$ is the maximum probability, one of the idling chillers should be switched on.
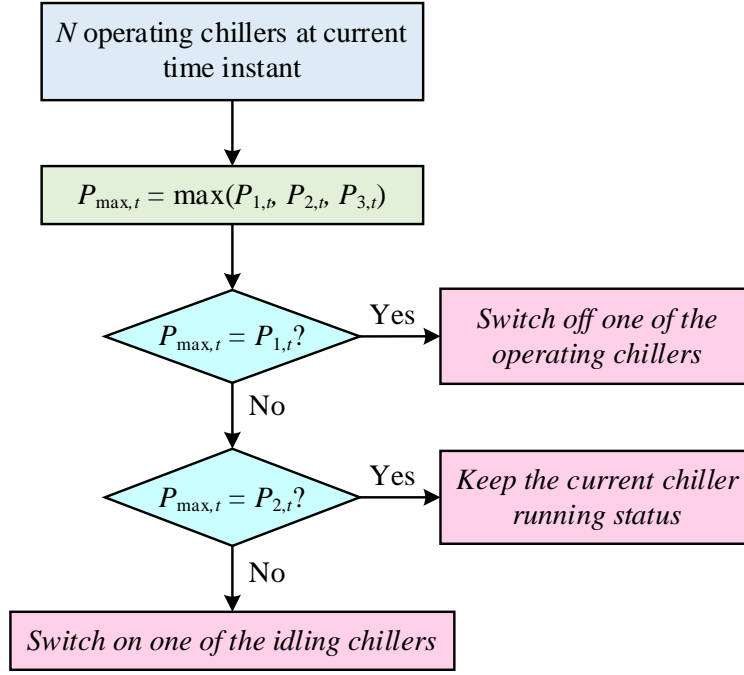
Figure 5.7 Online decision-making scheme of the proposed control strategy

$$N_{t+1} = \begin{cases} N_t - 1, & P_{\max,t} = P_{1,t} \\ N_t, & P_{\max,t} = P_{2,t} \\ N_t + 1, & P_{\max,t} = P_{3,t} \end{cases} \tag{5.12}$$

The risk (r_t) is defined as the probability of an incorrect decision made by the proposed control strategy, as shown in Eq. (5.13). According to its definition, the risk reaches its minimum value of 0 when one of the probabilities is equal to 1 and its maximum value of 0.67 when the three probabilities are equal $(P_{1,t} = P_{2,t} = P_{3,t} \approx 0.33)$. Hence, the risk would range from 0 to 0.67. The risks are used to evaluate the reliabilities of decisions made by the proposed control strategy under low-quality and uncertain measurements. The lower the risk, the higher the reliability. A risk boundary (r_b) is set for distinguishing between the high-risk control decisions and the low-risk control decisions. If the risk of a control decision is higher than the risk boundary, the control decision needs to be double-checked by operators for the sake of reliable operation. In this study, the risk boundary is set to 0.30.

$$r_t = 1 - \max\left(P_{1,t}, P_{2,t}, P_{3,t}\right) \tag{5.13}$$

5.3 Test platform and validation arrangements for the proposed sequencing control strategy

The online robust probabilistic chiller sequencing control strategy has been tested on a dynamic virtual platform built based on the chiller plant serving a real high-rise building.

5.3.1 Description of the chiller plant used in the tests

The studied chiller plant has been mentioned previously in Chapter 4. It serves a super high-rise commercial building (i.e., ICC) in Hong Kong, where cooling is demanded throughout the year. Table 5.1 presents the specifications of the main equipment in the chiller plant. The central cooling system consists of six identical chillers with a rated coefficient of performance (COP) of 5.37. Each chiller is interlocked with a constant-speed cooling water pump and a constant-speed primary chilled water pump. The chillers produce supply chilled water with a temperature setpoint of 5.5 °C. And the heat is rejected by 11 cooling towers with a total capacity of 51 709 kW.

Table 5.1 Specifications of the main equipment in the chiller plant

No.	Equipment	Number	Rated capacity (kW)	Flow rate (L/s)	Power (kW)
1	Chiller	6	7 230	-	1 346
2	Cooling tower A	6	5 234	-	152
3	Cooling tower B	5	4 061	-	120
4	Chilled water pump	6	-	345.0	126
5	Cooling water pump	6	-	410.1	202

Figure 5.8 shows the weekly cooling load profile used for testing the proposed control strategy. The data is extracted from the building management system (BMS) directly, and it is regarded as the actual cooling load (i.e., without measurement uncertainties). The cooling is required all day, and the chiller plant needs to provide 24-hour service.
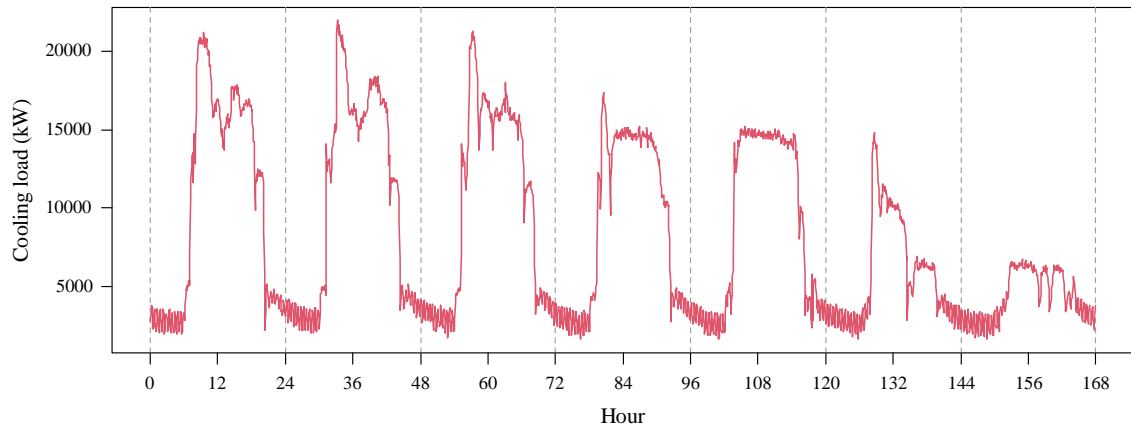
Figure 5.8 Weekly cooling load profile used for testing the proposed control strategy

5.3.2 TRNSYS-Python co-simulation test platform

A TRNSYS-Python co-simulation test platform is used to validate the effectiveness of the proposed control strategy. The transient system (TRNSYS) simulation tool is designed for simulating the dynamic behaviour of thermal energy systems. The studied chiller plant can be well modelled in TRNSYS. Python is a popular programming language with powerful computational capabilities. The uncertainty processing model of flow measurements and the online robust probabilistic chiller sequencing controller can be programmed easily in Python. TRNSYS provides a user-friendly component (Type 169) to communicate with Python, which makes TRNSYS play well with Python. As shown in Figure 5.9, the measurements from the chiller plant model are firstly processed by the uncertainty processing model. Then the online robust probabilistic sequencing controller makes decisions, and the control signals are sent back to the chiller plant platform. As an external input, the measurement uncertainties of chilled water and cooling

87

water flow rates are input to the chiller plant model directly to obtain the measurements. In order to avoid frequent switching of chillers and reduce computational load, the time interval of decision-making in the controller is set as 5 minutes.
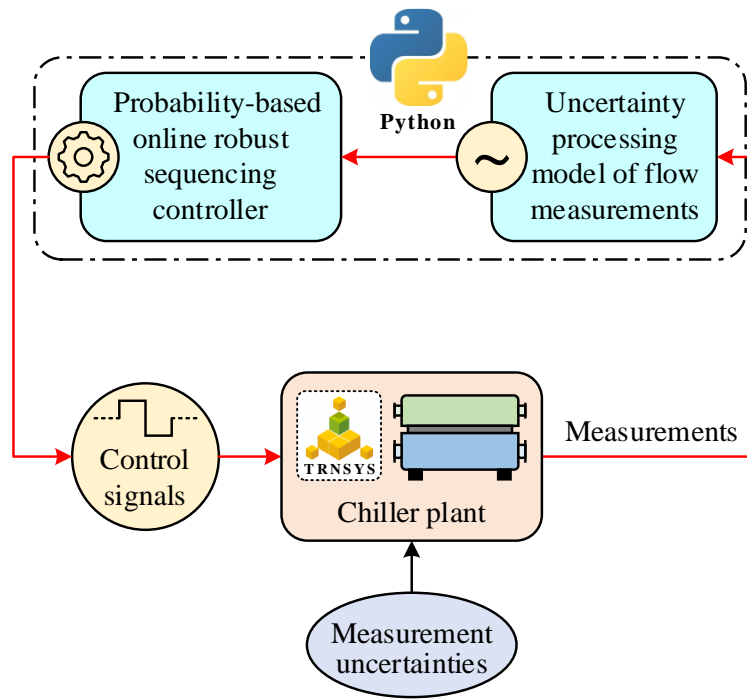
Figure 5.9 TRNSYS-Python co-simulation test platform

5.3.3 Arrangement of online validation tests

The proposed control strategy is systematically validated by two test cases with different measurement uncertainties, as shown in Table 5.2. In case 1, the systematic uncertainties are positive, and the measured water flow rates tend to be greater than the actual water flow rates. In case 2, the systematic uncertainties are negative, and the measured water flow rates tend to be less than the actual water flow rates. In addition, the systematic uncertainty of the chilled water flow meter (30.0 L/s) in both test cases is 8.70% of the rated flow rate of the chilled water pump. Such a level of measurement uncertainty may affect the chiller sequencing control significantly and cannot be ignored. The flow measurement uncertainty is generated according to the normal distributions in Table 5.2.

The measured water flow rates are obtained by adding the generated uncertainties to the actual water flow rates (TRNSYS outputs).

Table 5.2 Measurement uncertainty of flow meters in each case (Unit: L/s)

No.	Chilled water flow meter	Cooling water flow meter
Case 1	$\sim N(30.0,\ 8.0^2)$	$\sim N(40.0,\ 10.0^2)$
Case 2	$\sim N(-30.0,\ 8.0^2)$	$\sim N(-40.0,\ 10.0^2)$

5.4 Performance evaluation of the probability-based chiller sequencing control strategy

The errors of cooling loads and the chiller plant performance are used to evaluate the proposed probability-based online robust chiller sequencing control strategy. The risks in the decision-making processes are used to evaluate the reliability of the proposed control strategy.

5.4.1 Validation test 1: Measured cooling loads > Actual cooling loads

5.4.1.1 Comparison between quantification errors and measurement errors of cooling loads in test case 1

The chilled water flow rates are quantified by the uncertainty processing model, and the distributions of cooling loads are then obtained. The means and 95% Bayesian credible intervals are used to show the quantified cooling loads, as shown in Figure 5.10. The results of cooling load quantification were evaluated by comparing the measurement errors and the quantification errors of cooling loads. The measured cooling loads ($\tilde{Q}_t$) and the means of the quantified cooling loads ($\bar{Q}'_t$) can be calculated by Eq. (5.14). The measurement error ($\tilde{e}_t$) is defined as the difference between the measured cooling load

and the actual cooling load, and the quantification error (e_t') is defined as the difference between the mean and the actual cooling load, as shown in Eq. (5.15), where Q_t is the actual cooling loads. Figure 5.11 shows the distributions of the measurement errors and the quantification errors of cooling loads. It can be observed that the measurement errors of cooling loads were much more significant than the quantification errors, and they were distributed in a wide range (0 - 900 kW). The quantification errors of cooling loads were concentrated in an acceptable narrow range of around 0 kW. The root-mean-square error (RMSE) of the measured ($\tilde{E}_{RMS}$) and quantified (E_{RMS}') cooling loads can be calculated by Eq. (5.16), where n_s is the total number of samples. They were 416.14 kW and 84.42 kW respectively in this test case. Compared with the measured cooling loads, the RMSE of the quantified cooling loads was reduced remarkably by 79.71%. The uncertainty processing model of the proposed control strategy was effective in solving the positive measurement uncertainties of flow meters and reducing the errors of cooling loads. Because the conventional control strategy uses the measured cooling loads directly, the measurement errors may lead to significant faults in decision-making. In the proposed control strategy, the quantified cooling loads are used. The faults in decision-making can be reduced as the quantification errors are small.
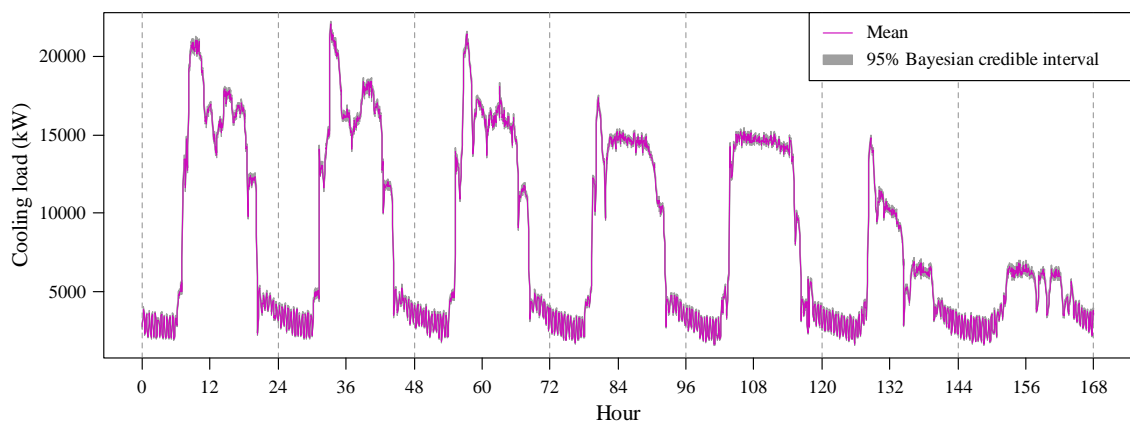
Figure 5.10 Quantified cooling loads of Case 1 using the proposed control strategy

$$\begin{cases} \tilde{Q}_t = c\rho \cdot \tilde{q}_{chw,t} \cdot \left(T_{chwr,t} - T_{chws,t} \right) \\ \bar{Q}'_t = c\rho \cdot \vec{q}'_{chw,t} \cdot \left(T_{chwr,t} - T_{chws,t} \right) \end{cases} \tag{5.14}$$

$$\begin{cases} \tilde{e}_t = \tilde{Q}_t - Q_t \\ e'_t = \bar{Q}'_t - Q_t \end{cases} \tag{5.15}$$

$$\begin{cases} \tilde{E}_{RMS} = \sqrt{\dfrac{1}{n_s} \sum_t \left(\tilde{Q}_t - Q_t \right)^2} \\ E'_{RMS} = \sqrt{\dfrac{1}{n_s} \sum_t \left(\bar{Q}'_t - Q_t \right)^2} \end{cases} \tag{5.16}$$

Figure 5.11 Error distributions of measured and quantified cooling loads in Case 1

5.4.1.2 Evaluation of chiller operation performance in test case 1

A practical chiller sequencing control strategy should always avoid unnecessary switching on/off of chillers as far as possible. Frequent switching of chillers affects the lifespan of the chiller plant and may increase maintenance costs. Figure 5.12 presents the comparison of operating chiller numbers when the conventional and the proposed control strategies are used in Case 1. Due to the positive measurement uncertainties, the cooling loads were over-estimated. The chillers tended to be switched on in advance and switched

off with a delay when the conventional control strategy was used. And the operating chiller number varied frequently, especially in the last two days. However, the frequent switching of chillers was avoided using the proposed control strategy. The total switching number of chillers is calculated and presented in Table 5.3. It had been reduced by 35.71% compared with that when the conventional control strategy was used.
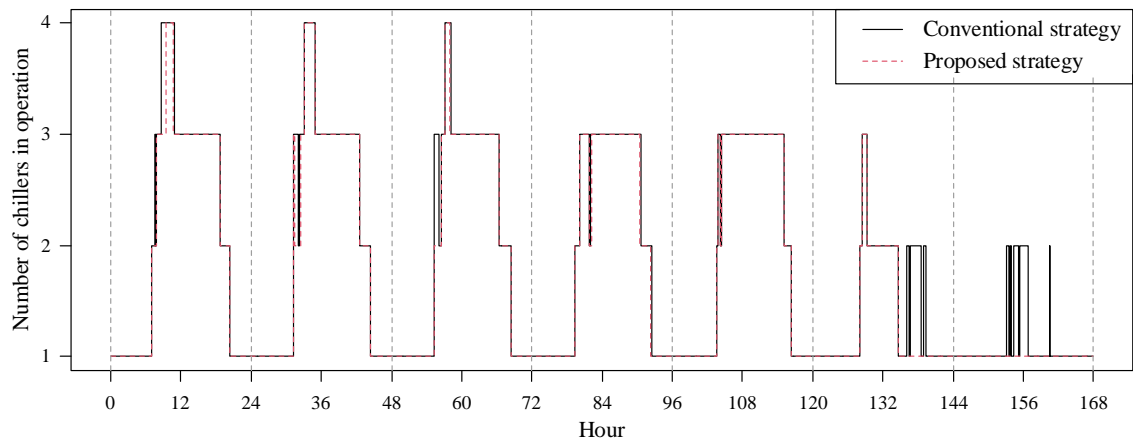
Figure 5.12 Number of chillers in operation during the test period in case 1

In order to further evaluate the operating performance of the chiller plant under the conventional and proposed control strategies, the total energy consumption and the cumulative unmet cooling load of the chiller plant are also calculated and presented in Table 5.3. Table 5.3 also shows the increments/reduction of the three indexes under the proposed control strategy relative to the conventional control strategy. The chiller plant cannot provide adequate cooling to users if the total cooling capacities of the chillers in operation do not meet the cooling loads. Such a situation leads to an increase in the supply chilled water temperature and poor indoor thermal comfort. It cannot be avoided as a time interval is generally set for decision-making and make the control strategy does not make decisions in real time. The cumulative unmet cooling load of the chiller plant ($Q_{unmet,cum}$) can be used to assess the impacts of the situation and it is defined by Eq. (5.17). It is the integral of the unmet cooling load of chillers (Q_{unmet}) over time. Where T_{set} is the supply

chilled water temperature setpoint. As shown in Table 5.3, compared with the conventional control strategy, the total energy consumption of the chiller plant was reduced by 0.49% and the cumulative unmet cooling load of the chiller plant was increased by 3.14%.

$$Q_{unmet,cum} = \int_{t=0}^{t=168} Q_{unmet,t} dt = \int_{t=0}^{t=168} \left(c\rho \cdot q_{chw,t} \cdot \left(T_{chws,t} - T_{set} \right) \right) dt \qquad (5.17)$$

Table 5.3 Operation performance of chiller plant using the conventional and proposed control strategies

Control strategy	Total switching number		Total energy consumption		Cumulative unmet cooling load	
	-	Reduction (%)	kWh	Reduction (%)	kWh	Increment (%)
Conventional	56	-	380 585	-	3 117	-
Proposed	36	35.71	378 715	0.49	3 215	3.14

In this case, when using the proposed control strategy, the overall performance of the chiller plant is satisfactory. The proposed control strategy could significantly reduce the number of unnecessary chiller switching. The total energy consumption had also been reduced slightly. The drawback was that the cumulative unmet cooling load was increased a little (3.14%). But the compromise between the significant decrease in total chiller switching number and the slight increase in cumulative unmet cooling load was perfectly acceptable. To conclude, the proposed control strategy can tolerate the positive measurement uncertainties.

5.4.1.3 Risk assessment of decision-making in test case 1

Figure 5.13 shows the quantified risks of control decision-making in case 1 under the proposed control strategy. It can be observed that the risks of most control decisions were

lower than the risk boundary. The high-risk control decisions only accounted for 0.25% of the total control decisions, 99.75% of control decisions were reliable and did not need to be double-checked by operators.
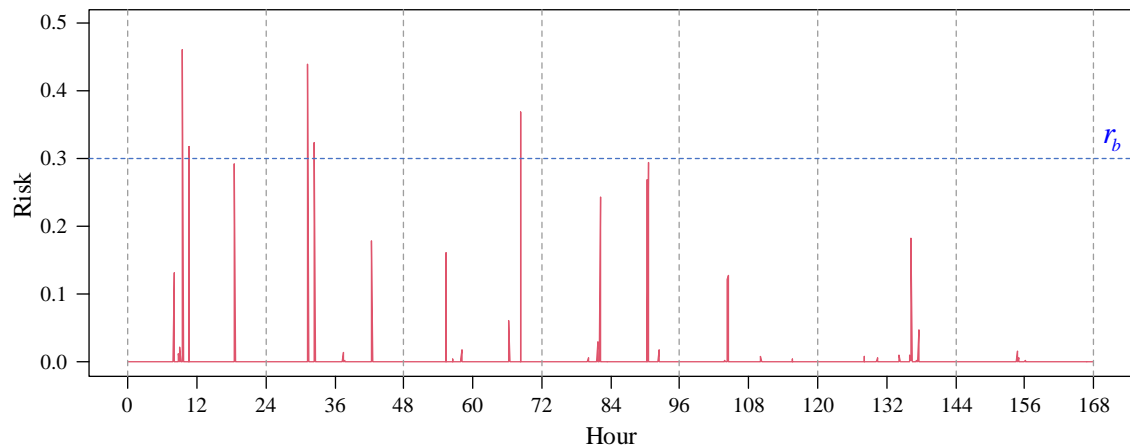
Figure 5.13 Quantified risks of control decision-making in case 1 using the proposed control strategy

5.4.2 Validation test 2: Measured cooling loads < Actual cooling loads

5.4.2.1 Comparison between quantification errors and measurement errors of cooling loads in test case 2

Figure 5.14 shows the quantified cooling loads of case 2. The distributions of measurement errors and quantification errors of cooling loads are presented in Figure 5.15. The measurement errors were distributed in a wide range (-900 – 0 kW), while the quantification errors were concentrated in an acceptable narrow range of around 0 kW. In addition, the RMSEs of the measured and quantified cooling loads were 411.92 kW and 85.09 kW, respectively. The measurement errors were much higher than the quantification errors. The uncertainty processing model of the proposed control strategy was also effective in solving the negative uncertainties in flow measurements, the RMSE of the quantified cooling loads was reduced by 79.34% compared with the measured cooling loads.

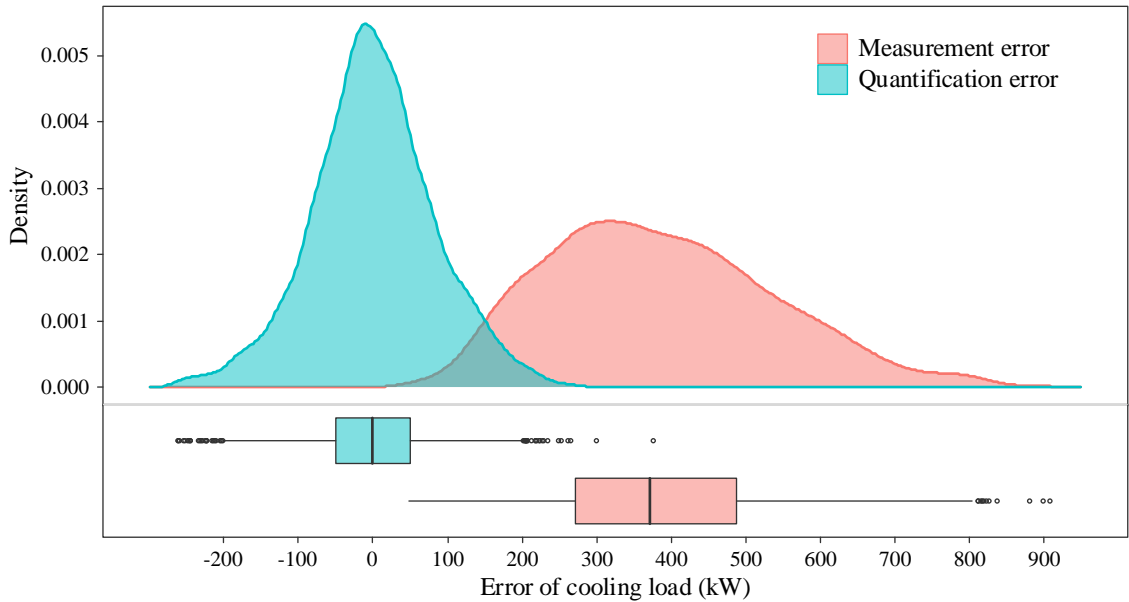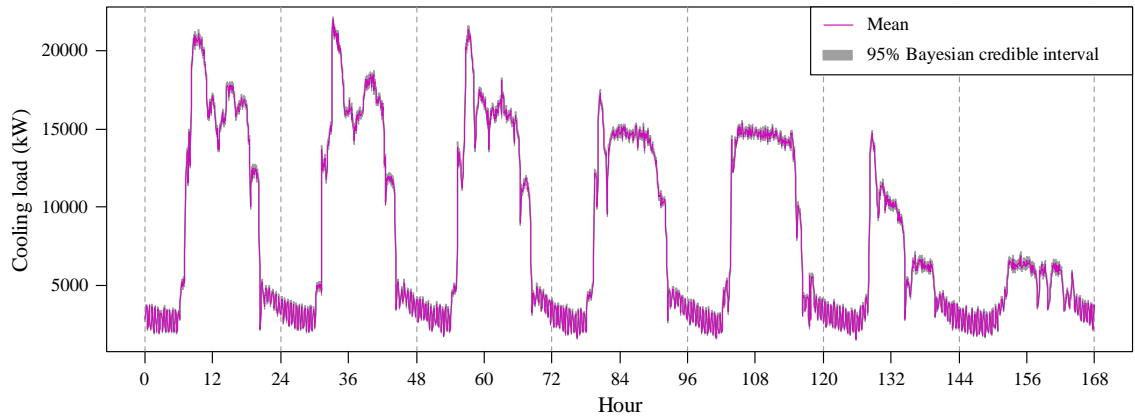Figure 5.14 Quantified cooling loads in case 2 using the proposed control strategy
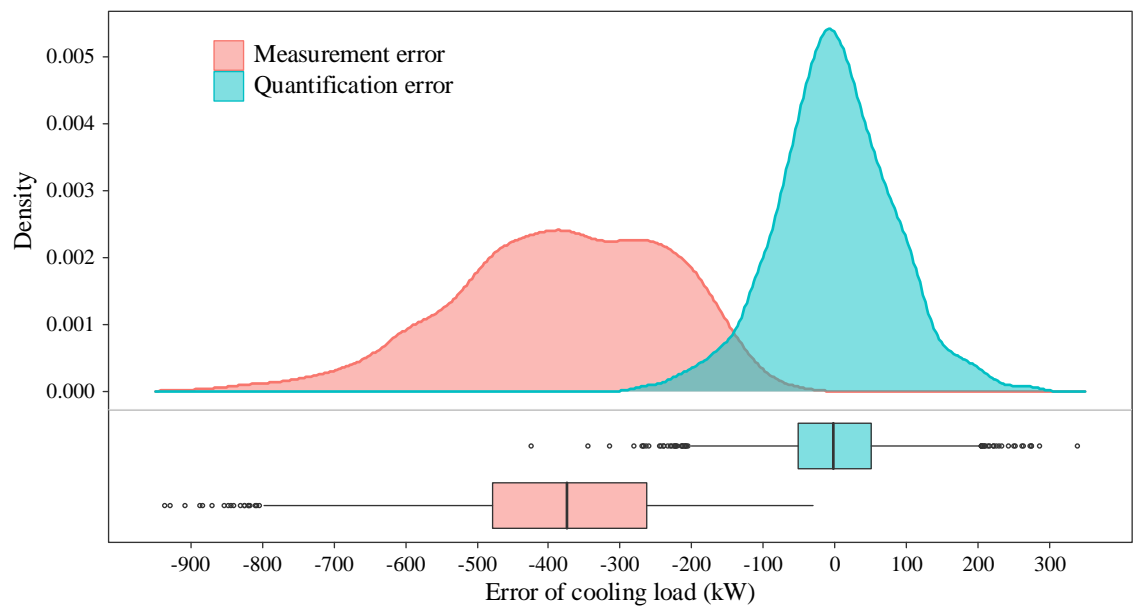
Figure 5.15 Error distributions of measured and quantified cooling loads in case 2

5.4.2.2 Evaluation of chiller operation performance in case 2

Figure 5.16 shows the number of chillers in operation during the test period in case 2 under the conventional and the proposed control strategies. There was a little bit of difference between the variations of the number of chillers in operation under the two control strategies. Due to the existence of negative measurement uncertainties, the cooling loads were under-estimated. The chillers tended to be switched on with a delay and switched off in advance when using the conventional control strategy. The cumulative

95

unmet cooling load would increase, and as a result, the indoor thermal comfort would be compromised.
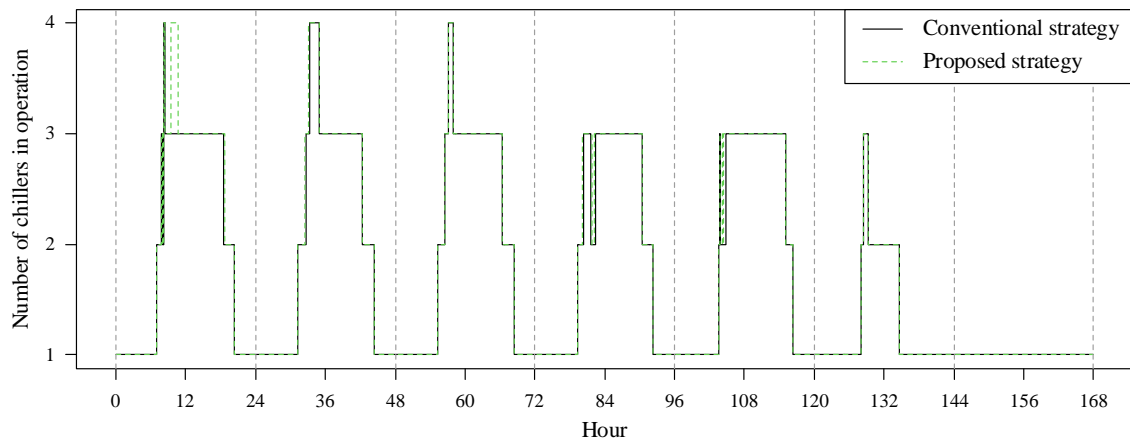
Figure 5.16 Number of chillers in operation during the test period in case 2

Table 5.4 shows the total switching number, the total energy consumption and the cumulative unmet cooling load of the chiller plant when the conventional and the proposed control strategies are used. Their differences are also presented. It can be observed that the cumulative unmet cooling load increased significantly compared with that in case 1. It was consistent with the above analysis. Compared with the conventional control strategy, the total switching number and the total energy consumption of the chiller plant were increased by 5.56% and 0.08%, respectively. The cumulative unmet cooling load was reduced significantly by 31.22%.

Table 5.4 Operation performance of chiller plant using the conventional and proposed control strategies

Control strategy	Total switching number		Total energy consumption		Cumulative unmet cooling load	
	-	Increment (%)	kWh	Increment (%)	kWh	Reduction (%)
Conventional	36	-	378 401	-	6 586	-
Proposed	38	5.56	378 714	0.08	4 530	31.22

In this case, the overall performance of the chiller plant is also satisfactory when the proposed control strategy is used. The proposed control strategy reduced the cumulative unmet cooling load significantly with slight increases in the total chiller switching number and the total energy consumption of the chiller plant. To conclude, the proposed strategy can also tolerate the negative measurement uncertainties.

5.4.2.3 Risk assessment of decision-making in test case 2

The quantified risks of control decision-making in case 2 under the proposed control strategy are shown in Figure 5.17. It can be observed that the risks of most control decisions were lower than the risk boundary. The high-risk control decisions only accounted for 0.30% of the total control decisions, 99.70% of control decisions were reliable and did not need to be double-checked by operators.
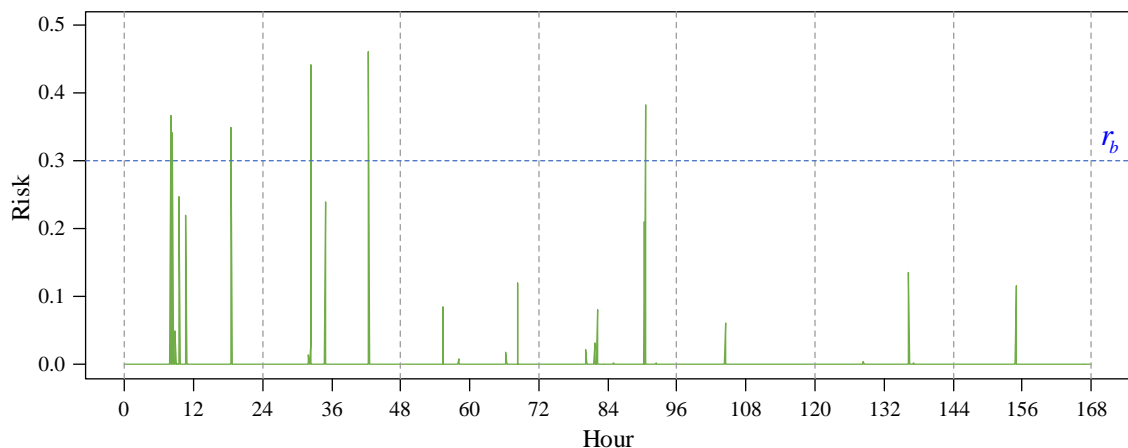
Figure 5.17 Quantified risks of control decision-making in case 2 using the proposed control strategy

5.5 Discussion

According to the test results and analysis presented in Section 5.4, the measurement uncertainties of flow meters show significant impacts on the conventional cooling load-based chiller sequencing control. Using the results of the proposed control strategy as the

benchmark, the positive flow measurement uncertainties led to a significant increase of 55.56% in unnecessary chiller switching, while the negative flow measurement uncertainties led to a significant increase of 45.39% in the cumulative unmet cooling load. Similar results were obtained in the literature. For example, an existing study has reported that a medium level of measurement uncertainties led to a decrease of about 43% in overall chiller switching number and an increase of about 41% in under-cooling percentage when using cooling load-based chiller sequencing control (Liao et al., 2015). Another study found that the total chiller switching number decreased by 23.1%, but the cumulative supply air temperature tracking error increased significantly by 146.8 times (equivalent to an increase in the average tracking error from 0.004 K to 0.630 K), due to measurement uncertainties (Liao et al., 2014). Both above-mentioned studies indicated that cooling load-based chiller sequencing control was affected by measurement uncertainties significantly, which is consistent with the results of this study. But the degrees of influence in these studies were different, which possibly depends on the measurement uncertainty levels and types, cooling load profiles, system specifications, etc.

Validation results showed that the proposed control strategy performed much better than the conventional control strategy. The proposed control strategy could tolerate both the positive and negative flow measurement uncertainties. The root-mean-square error of cooling loads was reduced dramatically by about 79% after being processed by the developed uncertainty processing model of flow measurements. Compared with the conventional control strategy, the total chiller switching number and the cumulative unmet cooling load were reduced by 35.71% and 31.22% respectively. While the total energy consumption in both validation test cases only changed a little (< 0.50%). This is possible because the actual cooling loads (Figure 5.8) did not change no matter if the flow

measurement uncertainties were handled or not. The slight reduction or increment of energy consumption was probably caused by the working time of individual electrical devices (including the chillers, pumps, and cooling towers) and the part load performance of chillers. The literature (Liao et al., 2014) also found that the total energy consumption reduced slightly by 4.12% under measurement uncertainty. Based on the proposed control strategy, the flow meters with significant measurement uncertainties can still be safely used in chiller plants. The service life of flow meters can be extended dramatically, and the operating and maintenance costs can decrease significantly.

For the risk assessment, the risk boundary can be set flexibly according to the actual requirements. The higher the requirement for reliability, the lower the risk boundary should be set. However, if the risk boundary is set too low, the proportion of high-risk control decisions may increase. And the operating cost would increase as the operators need to spend more time double-checking the high-risk control decisions. A trade-off between the reliability level and the operating cost should be made.

The test and validation of the proposed control strategy are based on a cooling plant with identical chillers. The key function of this strategy is to calibrate and correct the measured cooling loads. Therefore, it is also applicable to cooling plants with non-identical chillers using cooling load-based sequencing control. In the case of the non-identical chillers, the control logic and the settings of cooling load thresholds will be slightly different as the priority of chillers should be taken into consideration.

Generally, due to the degradation of sensor performance, its measurement uncertainty may increase over time. The uncertainty processing model in the proposed control strategy should be updated regularly to cope with this problem. The physical model-based measurement uncertainty quantification method proposed in Chapter 4 gives an opportunity to update the uncertainty processing model automatically. In addition, a

simple energy balance model is involved in the development of the uncertainty processing model, similar physical models can be developed easily in HVAC systems. Therefore, it is potential to generalize the proposed control strategy to other HVAC systems with a little modification. The proposed control strategy has high flexibility and strong generalization ability. These advantages of the proposed control strategy make it have wider applicability compared with the existing fault-tolerant control strategies.

The proposed probability-based online robust chiller sequencing control strategy aims to optimize the conventional cooling load-based chiller sequencing control under flow measurement uncertainties. The uncertainties of flow measurements are quantified using Bayesian inference and Markov chain Monte Carlo sampling methods. The measured cooling loads can be calibrated and corrected online. The control decisions are made based on "probability values" of cooling load distribution over a range rather than a specific value. The risks can also be assessed simultaneously. The proposed control strategy is innovative. In addition, both the systematic and random uncertainties of flow meters are considered simultaneously in this strategy. Compared with existing studies which considered random uncertainties only, such as Li et al. (2014); Liao et al. (2014); Liao et al. (2015), this study is more comprehensive and more in line with practical application scenarios.

5.6 Summary

Chiller sequencing control is crucial to the reliable operation of multiple-chiller plants. This chapter proposed a probability-based online robust sequencing control strategy for chiller plants under low-quality and uncertain measurements. The proposed control strategy can tolerate uncertainties in water flow measurements. An uncertainty processing model of flow measurements was developed based on an energy balance model using

Bayesian inference and Markov chain Monte Carlo sampling methods. As the core of the proposed control strategy, the uncertainty processing model of flow measurements can quantify the distributions of chilled water flow rates and obtain the probability distributions of cooling loads. Chiller sequencing control decisions were made based on the probability distributions of the quantified cooling loads. The risks in the decision-making process were also assessed. Based on the validation results, the main conclusions can be drawn as follows:

- The proposed probability-based online robust chiller sequencing control strategy dramatically reduced the major impacts of both positive and negative flow measurement uncertainties on the multiple-chiller plants. Compared with the conventional total cooling load-based chiller sequencing control strategy, the total switching number of chillers was reduced by 35.71% under the positive flow measurement uncertainties, and the cumulative unmet cooling load was reduced by 31.22% under the negative flow measurement uncertainties.

- As the core of the proposed control strategy, the uncertainty processing model of flow measurements could quantify the chilled water flow rates accurately, which led to a significant decrease (about 79%) in the RMSE of cooling loads.

- The risks in the decision-making process could be quantified to evaluate the reliability of the proposed control strategy and the high-risk decisions could be avoided through double-checking by operators.

CHAPTER 6   DATA-DRIVEN MODEL BASED MEASUREMENT UNCERTAINTY QUANTIFICATION METHOD AND ITS VALIDATION

In Chapter 4, it has been shown that the physical model-based measurement uncertainty quantification method performs well, but the method is not applicable for the cases where the physical models cannot be established, or extra costs (e.g., installation of extra sensors) should be paid to establish the physical models. For example, the energy balance model of an air-cooled chiller system cannot be built easily based on existing measurements as the heat rejection of the condenser is very difficult to measure or estimate. This limitation may largely affect the application of the method. Therefore, this chapter develops a data-driven model-based measurement uncertainty quantification method to cope with this challenge. It is validated systematically by quantifying both the systematic and random uncertainties of a chilled water flow meter in an actual air-cooled chiller.

The organization of this chapter is as follows. Section 6.1 introduces the development of the proposed data-driven model-based measurement uncertainty quantification method in detail. Section 6.2 presents the test platform and validation arrangements for the proposed data-driven model-based measurement uncertainty quantification method. Section 6.3 presents the validation results of the proposed method and evaluates its performance in quantifying different levels of flow measurement uncertainties. A discussion of the proposed method is presented in Section 6.4. The conclusions are made in Section 6.5.

6.1 Development of the data-driven model-based measurement uncertainty quantification method

This section presents the development of the proposed data-driven model-based measurement uncertainty quantification method with one target variable (θ) and a series of auxiliary variables (y, x_1, x_2, ..., x_m). The data-driven model development and the measurement uncertainty quantification procedures will be introduced respectively.

6.1.1 Outline of the proposed method

Figure 6.1 shows the outline of the proposed data-driven model-based measurement uncertainty quantification method. It mainly consists of two parts: (a) Data-driven model development, and (b) Measurement uncertainty quantification. For part (a) data-driven model development, the normal operation data (reference data of the target variable) is used and should be pre-processed first. Then the pre-processed data are used to develop the data-driven regression model. Its function form (f ($\cdot$)) and error distribution (δ, standard deviation) need to be determined. For part (b) measurement uncertainty quantification, the actual measurement data also should be pre-processed first. Then the uncertainty of the target variable in the actual measurements is quantified based on the developed regression model using Bayesian inference and Markov chain Monte Carlo sampling methods. Accordingly, the posterior distributions of both the systematic uncertainty (μ) and random uncertainty (σ) of the target variable can be discovered effectively. The data-driven model development and the measurement uncertainty quantification procedures will be presented in detail in Sections 6.1.2 and 6.1.3, respectively.

103

(a) Data-driven model development

Normal operation data
$\left(\theta_{ref}, y, x_1, x_2, ..., x_m\right)$

Data pre-processing

Data-driven regression model development
$\begin{cases} y = f\left(\theta_{ref}, x_1, x_2, ..., x_m\right) + e \\ e \sim N\left(0, \delta^2\right) \end{cases}$

Regression function and error distribution
(*f, e*)

(b) Measurement uncertainty quantification

Actual measurement data
$\left(\tilde{\theta}, y, x_1, x_2, ..., x_m\right)$

Data pre-processing

Well-trained regression model
(*Regression function and error distribution*)

Measurement uncertainty quantification
(*Bayesian inference and Markov chain Monte Carlo*)
$\begin{cases} y \sim N\left(f\left(\theta_{ref}, x_1, x_2, ..., x_m\right), \delta^2\right) \\ \tilde{\theta} \sim N\left(\theta + \mu, \sigma^2\right) \end{cases}$

Posterior distributions
(μ, σ)

Figure 6.1 Outline of the proposed data-driven mode-based measurement uncertainty quantification method

6.1.2 Data-driven model development

The data-driven regression model is the core of the proposed measurement uncertainty quantification method. It is to establish a mapping relationship between the inputs (independent variables) and the output (dependent variable). The regression function of output *y* and inputs $X = |\theta_{ref}, x_1, x_2, ..., x_m|$ (including the target variable (θ_{ref}) and other related/available auxiliary variables) is denoted by Eq. (6.1). The function is always accompanied by an error term (*e*) and it follows a normal distribution with mean 0 and standard deviation δ.

$$y = f\left(X\right) + e = f\left(\theta_{ref}, x_1, x_2, ..., x_m\right) + e, \quad e \sim N\left(0, \delta^2\right) \tag{6.1}$$

To determine the regression function form $f(X)$ and the error distribution, the data-driven regression model should be trained by a series of normal operation data, as shown in Figure 6.1a. Firstly, the raw dataset should be pre-processed. The meaningless samples (a sample is defined as a group of data points collected at the same time) and the samples with missed values should be removed from the training dataset. Then the regression model is developed using the pre-processed data, and the regression function form can be determined. The error distribution can be constructed by the model residuals as the residuals are the observations of the model error.

The developed regression model is a benchmark model. The normal operation data should be collected when the system operates normally with no significant measurement uncertainties due to performance degradation of sensors/meters used. The sensors/meters work at the expected performance. The measurement errors meet the accuracy classes of corresponding sensors/meters, such levels of uncertainties are unavoidable but acceptable in engineering practice. In other words, the normal operation data is the reference data with acceptable measurement uncertainties.

6.1.3 Measurement uncertainty quantification procedures

The proposed method aims to quantify the measurement uncertainty of the target variable in the actual measurement data. According to the description in Section 3.1, the measured value of the target variable ($\tilde{\theta}$) is equal to the reference value (θ_{ref}) plus an uncertain term (u), as shown in Eq. (6.2). The uncertain term follows a normal distribution with mean μ and standard deviation σ. The mean represents the systematic uncertainty, and the standard deviation represents the random uncertainty. According to the characteristics of normal distribution, the measured flow rates would follow the normal distribution with mean ($\theta_{ref} + \mu$) and standard deviation σ, as shown in Eq. (6.3). In the distribution

function (Eq. (6.3)), only the measured value of the target variable is available, the reference value of the target variable, systematic uncertainty and random uncertainty are unknown and should be quantified.

$$\tilde{\theta} = \theta_{ref} + u, \qquad u \sim N\left(\mu, \ \sigma^2\right) \tag{6.2}$$

$$\tilde{\theta} \sim N\left(\theta_{ref} + \mu, \ \sigma^2\right) \tag{6.3}$$

Similarly, the output y of the regression model presented in Section 6.1.2 would follow a normal distribution with mean $f\left(\theta_{ref}, x_1, x_2, \dots, x_m\right)$ and standard deviation δ, as shown in Eq. (6.4). It is worth noting that the target variable in Eq. (6.4) is its reference value rather than its measured value. Its measured value may not satisfy Eq. (6.1) due to measurement uncertainty.

$$y \sim N\left(f\left(\theta_{ref}, \ x_1, \ x_2, \ \dots, \ x_m\right), \ \delta^2\right) \tag{6.4}$$

The measurement uncertainty quantification procedures are presented in Figure 6.1b. Firstly, the actual measurement data (possibly with significant uncertainties relative to the reference data) are pre-processed to remove outliers. Then the measurement uncertainty of the target variable is quantified based on the well-trained regression model (Eq. (6.4)) and the measurement uncertainty model (Eq. (6.3)) using Bayesian inference and Markov chain Monte Carlo sampling methods. The posterior distributions of both systematic and random uncertainties of the target variable can be obtained.

6.2 Test platform and validation arrangements for the proposed method

The proposed data-driven model-based measurement uncertainty quantification method is tested and validated systematically on a real air-cooled chiller system. The

measurement uncertainty of the chilled water flow meter is quantified using the proposed method under the auxiliary measurements of the power meter and temperature sensors.

Figure 6.2 shows the overall validation processes. Firstly, the operation data of an air-cooled chiller is extracted from BMS, and the data is pre-processed and divided into two data subsets. Secondly, one data subset (Dataset-1) is used to develop the benchmark regression model, and the other data subset (Dataset-2) is combined with the pre-set flow measurement uncertainty to generate an uncertain dataset. Thirdly, the flow measurement uncertainty in the uncertainty dataset is quantified using the proposed measurement uncertainty quantification method. Finally, the performance of the proposed method in quantifying flow measurement uncertainties is evaluated by comparing the quantified results with the pre-set values.
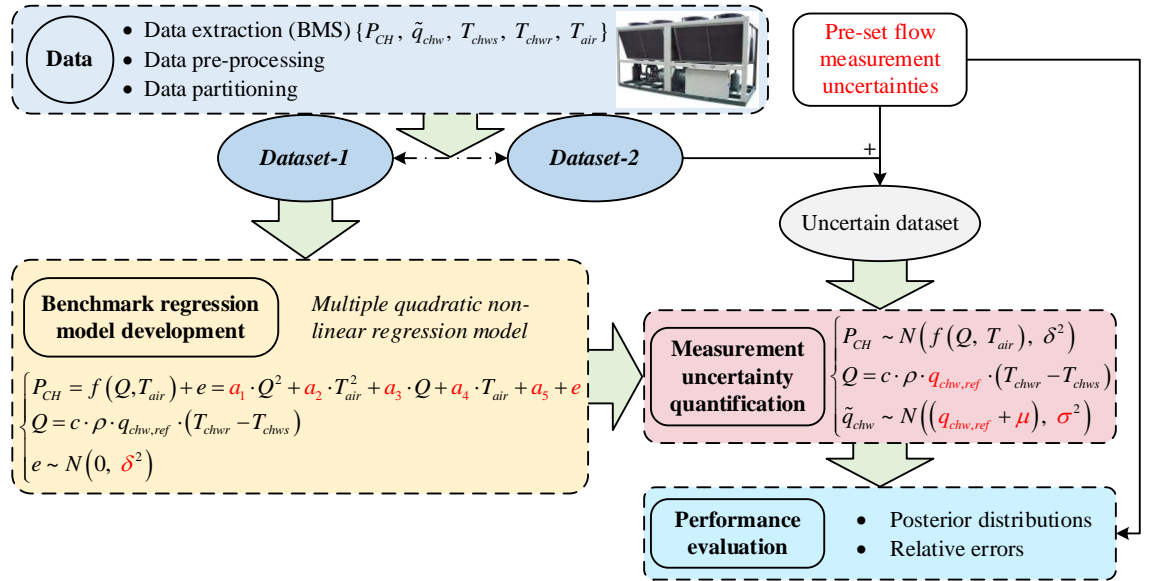
Figure 6.2 The overall validation processes

6.2.1 The air-cooled chiller system used in the tests

The studied air-cooled chiller serves a campus building in Hong Kong. Figure 6.3 shows the air-cooled chiller and its schematic diagram. The power consumption (P_{CH}), chilled water flow rate (q_{chw}), chilled water return temperature (T_{chwr}) and supply temperature

(T_{chws}) are measured for system monitoring and online real-time control. The heat absorption of the evaporator (Q_{in}) and power consumption of the compressor can be obtained easily, but the heat rejection of the condenser (Q_{out}) can hardly be measured directly. It is a typical case where the physical model (energy balance model) is unavailable. But the data-driven model is fully applicable to this case.
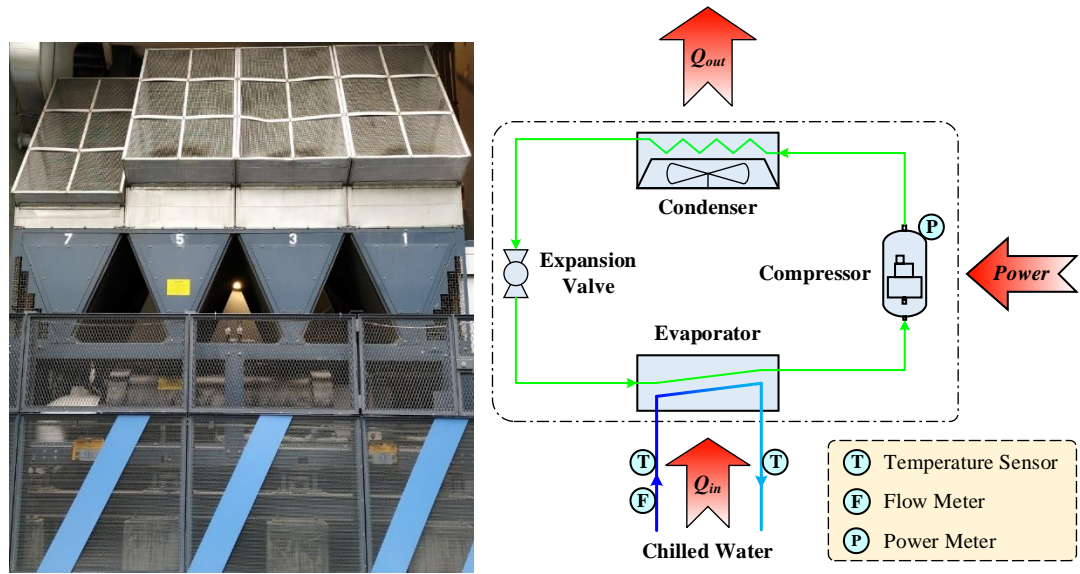
Figure 6.3 The studied air-cooled chiller and its schematic diagram

Table 6.1 shows the specifications and design parameters of the studied chiller. The rated cooling capacity and nominal power input of the chiller are 900.0 kW and 256.4 kW, respectively. And its integrated part load value (IPLV) and coefficient of performance (COP) are 5.80 and 3.51, respectively. The designed inlet and outlet water temperatures are 12.5 °C and 7.0 °C respectively. And the designed chilled water flow rate is 39.0 L/s.

Table 6.1 Specifications and design parameters of the studied air-cooled chiller

No.	Parameter	Unit	Value
1	Rated cooling capacity	kW	900.0
2	Nominal power input	kW	256.4
3	Integrated part load value	-	5.80
4	Coefficient of performance	-	3.51
5	Designed inlet water temperature	°C	12.5
6	Designed outlet water temperature	°C	7.0
7	Designed chilled water flow rate	L/s	39.0

6.2.2 Data description and pre-processing

The data used in this study were collected in 2019. The variables collected include the chiller power, chilled water flow rate, supply and return chilled water temperatures, and ambient air temperature (T_{air}). All variables are recorded every 10 minutes simultaneously. The service time of the chiller is generally from 7:00 AM to 11:00 PM on weekdays. Therefore, the data collected during non-working hours are meaningless and should be removed. In addition, the samples that contain any missing value are also removed. After pre-processing, the dataset contains 2 974 samples in total and is used for modelling and validation.

The 2 974 samples are divided into two subsets randomly, a subset with 1 974 samples (Dataset-1) is used to train the regression model, and a subset with 1 000 samples (Dataset-2) is used to generate uncertain data. More details are presented in the following sections.

6.2.3 Non-linear regression model development

The target variable is the chilled water flow rate, and the auxiliary variables are the power consumption of the chiller, the chilled water supply and return temperatures, and the outdoor air temperature. The method should be validated systematically by quantifying different levels of measurement uncertainties (both systematic and random uncertainties) of the chilled water flow meter.

A multiple quadratic non-linear regression model is developed based on Dataset-1. Eq. (6.5) presents the function form of the regression model. The output (dependent variable) is the power consumption of the chiller, and the inputs (independent variables) include the reference chilled water flow rate, the chilled water return and supply temperatures, and the outdoor air temperature.

$$\begin{cases} P_{CH} = f\left(Q, T_{air}\right) + e = a_1 \cdot Q^2 + a_2 \cdot T_{air}^2 + a_3 \cdot Q + a_4 \cdot T_{air} + a_5 + e \\ Q = c \cdot \rho \cdot q_{chw,ref} \cdot \left(T_{chwr} - T_{chws}\right) \\ e \sim N\left(0, \ \delta^2\right) \end{cases} \tag{6.5}$$

where, $a_{1\text{-}5}$ are the coefficients, c is the specific heat capacity of water (kJ/(kg·°C)), and ρ is the water density (kg/m^3).

The model is trained using Dataset-1. The coefficients and the residual distribution are determined using the ordinary least squares (OLS) method. The sum of the squares of the differences between the observed output and those predicted by the regression function of the inputs should be minimized. Figure 6.4 shows the residual distribution of the predicted power consumption. The normal quantile-quantile (Q-Q) plot of the residuals is also drawn for estimating the similarity between the residual distribution and a theoretical distribution, as shown in Figure 6.5. Most of the points fall on a straight line, but the points at the ends deviate a little from the line, and a thin-tailed distribution is

found. It indicates that the residual distribution approximately fits a normal distribution. Its mean is 0, and its standard deviation (δ) is 11.39. The coefficients, including the residual distribution parameter, are presented in Table 6.2. The coefficient of determination (R^2) of the model is 0.92, indicating that the regression model is not ideal but acceptable.
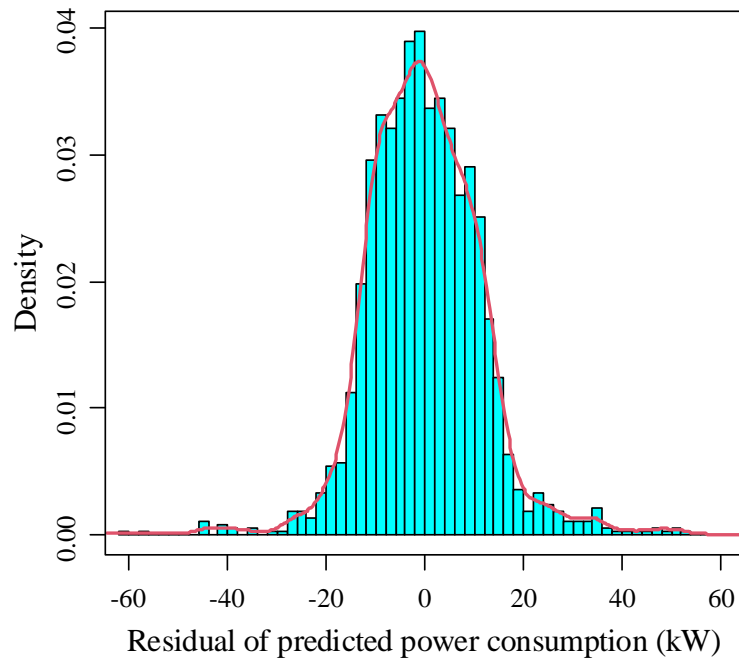
Figure 6.4 Residual distribution of the non-linear regression model
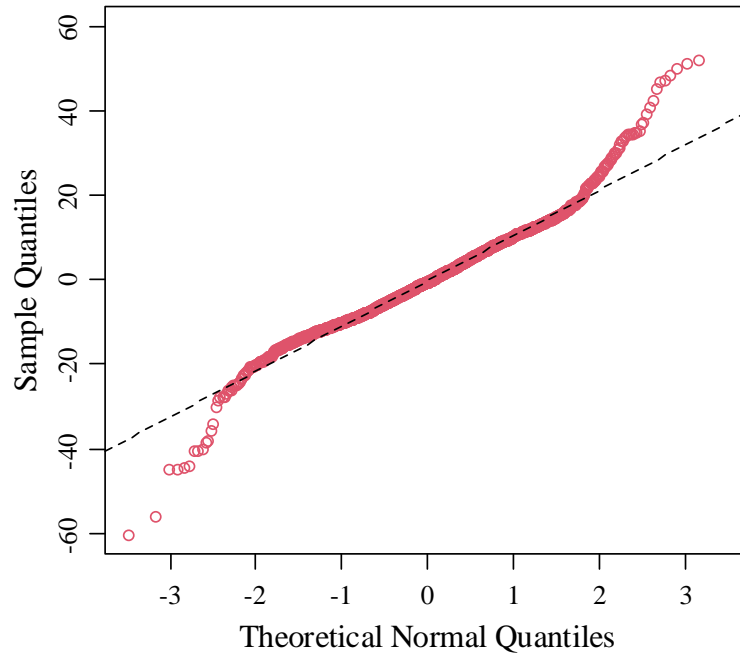
Figure 6.5 Normal quantile-quantile plot for residuals

Table 6.2 Coefficients and residual distribution parameter of the non-linear regression model

Coefficient	a_1	a_2	a_3	a_4	a_5	δ
Value	0.0001582	0.09859	0.1470	-1.313	-16.89	11.39

6.2.4 Measurement uncertainty quantification for chilled water flow meter

In order to evaluate the performance of the proposed data-driven model-based measurement uncertainty quantification method systematically, a new operation dataset with measurement uncertainty is needed. Dataset-2 is used to construct the uncertain dataset. Firstly, the uncertainties of chilled water flow measurements are generated artificially based on a given normal distribution. Then the uncertain dataset is obtained by adding the generated uncertain term to the chilled water flow rates of Dataset-2. The distribution parameters (mean and standard deviation) of the generated uncertainties in the uncertain dataset will be quantified by the proposed method for its validation.

According to the characteristics of normal distribution and the regression model developed in Section 6.2.3, Eq. (6.6) is established. The reference chilled water flow rate ($q_{chw,ref}$) is involved in this equation and it satisfies Eq. (6.7). The two equations are the likelihood functions in Bayesian analysis. The systematic uncertainty (μ) and random uncertainty (σ) are unknown and need to be quantified. Their posterior distributions will be obtained using the proposed method.

$$
\begin{cases}
P_{CH} \sim N\left(\left(0.0001582 \times Q^2 + 0.09859 \times T_{air}^2 + 0.147 \times Q - 1.313 \times T_{air} - 16.89\right),\ 11.39^2\right) \\
Q = c \cdot \rho \cdot q_{chw,ref} \cdot \left(T_{chwr} - T_{chws}\right)
\end{cases}
$$

$$
(6.6)
$$

$$
\tilde{q}_{chw} \sim N\left(\left(q_{chw,ref} + \mu\right),\ \sigma^2\right) \qquad (6.7)
$$

It is of great importance to assign an appropriate prior distribution to each of the parameters to be quantified, i.e., the systematic and random uncertainties of the flow measurements. In this study, the prior distribution of systematic uncertainty is normal and assigned based on a hypothesis. It assumes that the probability of the systematic uncertainty being less than 10% of the designed chilled water flow rate is 95%. As shown in Figure 6.6, the mean and standard deviation of the prior distribution are 0 and 1.99 respectively. The standard deviation of random uncertainty must be non-negative. The half-normal distribution ($\sim |N(0,1)|$) is used as its prior distribution, as shown in Figure 6.7.
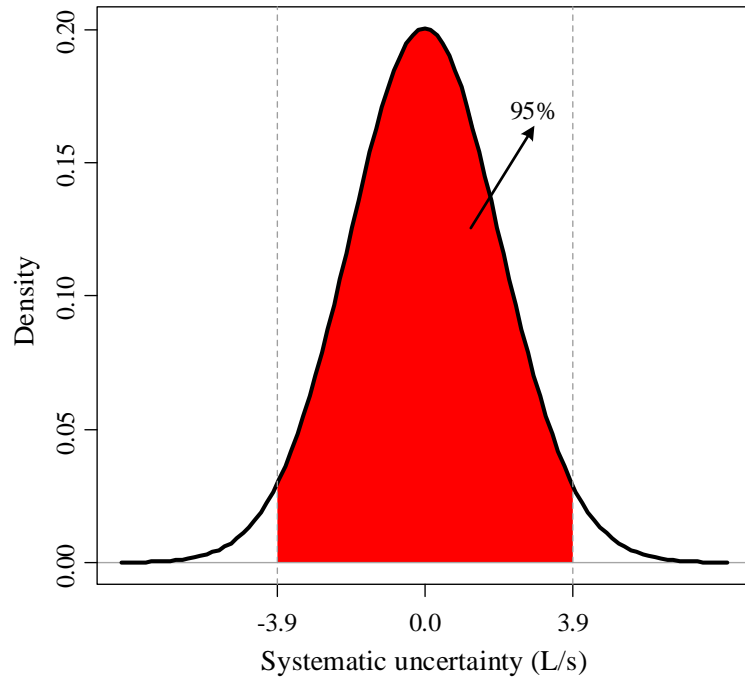
Figure 6.6 Prior distribution of systematic uncertainty
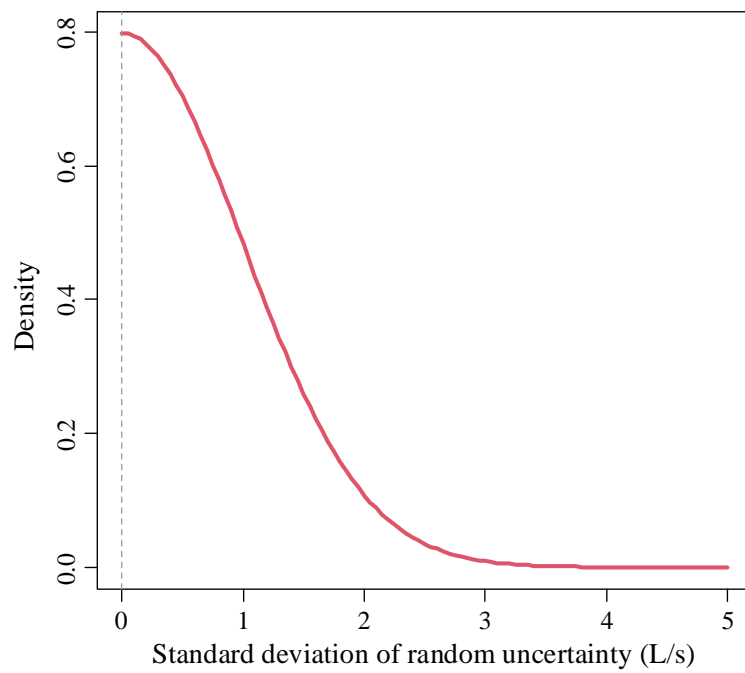
Figure 6.7 Prior distribution of random uncertainty

6.2.5 Uncertainty levels to be quantified

The distribution of flow measurement uncertainty is not immutable. It may change slowly

with sensor performance degradation over time. It is necessary to validate the ability of

the proposed method in quantifying different levels of flow measurement uncertainties. Therefore, four cases with different levels of measurement uncertainties are used to systematically test and validate the proposed method. Table 6.3 shows the detailed pre-set/introduced uncertainties in each case. The measurement uncertainties of the chilled water flow meter are generated randomly based on the given normal distributions in Table 6.3. The uncertain dataset mentioned in Section 6.2.2 is obtained by adding the generated uncertainties to a normal dataset (Dataset-2) and used to test the proposed measurement uncertainty quantification method.

As can be seen from Table 6.3, the systematic uncertainties of Case 1 and Case 2 are positive, and they are negative in Case 3 and Case 4. Case 1 and Case 4 have a high level of uncertainties, their systematic uncertainties are 10.26% of the designed chilled water flow rate. Case 2 and Case 3 have a low level of uncertainties, their systematic uncertainties are 5.13% of the designed chilled water flow rate. For the random uncertainties of these cases, they are gradually increased. These cases cover the common scenarios in practical applications, and they can be used to test and validate the proposed method comprehensively.

Table 6.3 Actual measurement uncertainty of chilled water flow rate in each case

Case No.	Uncertainty level	Systematic uncertainty (L/s)	Random uncertainty (L/s)
Case 1	High	4.0	1.5
Case 2	Low	2.0	2.0
Case 3	Low	−2.0	2.5
Case 4	High	−4.0	3.0

The measurement uncertainties of chilled water flow measurements in each Case are generated randomly based on the given normal distributions in Table 6.3. The uncertain dataset mentioned in Section 6.2.4 is obtained by adding the generated uncertainties to a normal dataset (Dataset-2) and used to test the proposed method.

6.3 Performance evaluation of the proposed method on flow measurement uncertainty quantification

The trace plots, autocorrelations and potential scale reduction factors of the systematic and random uncertainties of flow measurements are presented to diagnose the convergence of the quantification in each case. The posterior distributions of both systematic and random uncertainties are obtained and their posterior means, 95% Bayesian credible intervals and relative errors are provided to evaluate the performance of the proposed strategy in quantifying flow measurement uncertainties.

The number of iterations per chain is set to 4000 for each case, and the *thinning* technique is not used (i.e., $k = 1$).

6.3.1 Systematic uncertainty quantification of flow measurements

6.3.1.1 Convergence diagnostics of systematic uncertainty quantification

Figure 6.8 shows the sampling paths in quantifying the systematic uncertainty of flow measurements in each case. The potential scale reduction factors are also presented in the upper right corner of each sub-figure. As can be seen that the post-warmup samples of systematic uncertainty in each case had strong centralized tendencies. They fluctuated around a certain value, and the samples from different chains could not be distinguished easily. The potential scale reduction factor in each case was equal to 1.00. These all indicated convergence to posterior distributions. In addition, the autocorrelations of post-

warmup samples are used to further diagnose the convergence, as shown in Figure 6.9. The autocorrelations of post-warmup samples in each case were reduced to about 0 rapidly with the increase of lag, which also demonstrated convergence. Therefore, these post-warmup samples were qualified to construct the posterior distributions of the systematic uncertainties of flow measurements in each case.

Figure 6.8 Sampling paths in quantifying the systematic uncertainty of flow measurements in (a) Case 1, (b) Case 2, (c) Case 3 and (d) Case 4

Figure 6.9 Autocorrelations of post-warmup samples in quantifying the systematic

uncertainty of flow measurements in each case

6.3.1.2 Posterior distributions of systematic uncertainties

Figure 6.10 shows the posterior distribution of systematic uncertainty of flow

measurements in each case, which is constructed using the corresponding post-warmup

samples in Figure 6.8. Corresponding to the posterior distributions, the numerical results

are presented in Table 6.4. For the quantified systematic uncertainty of flow

measurements in each case, its posterior mean was very close to its pre-set value (see

Table 6.3). And the 95% Bayesian credible interval was narrow and contained its pre-set

value. In addition, the relative error of the posterior mean relative to its pre-set value was

within 7.5%, which was fully acceptable in engineering practice.

Figure 6.10 Posterior distributions of systematic uncertainty of flow measurements in

(a) Case 1, (b) Case 2, (c) Case 3 and (d) Case 4

Table 6.4 Numerical results of systematic uncertainty quantification

	Posterior mean (L/s)	95% Bayesian credible interval (L/s)	Relative error (%)
Case 1	3.95	[3.69, 4.22]	1.25
Case 2	2.07	[1.79, 2.36]	3.50
Case 3	-1.85	[-2.15, -1.55]	7.50
Case 4	-3.78	[-4.09, -3.46]	5.50

In summary, different levels of systematic uncertainties in flow measurements were

quantified successfully using the proposed method, which indicates that the performance

of the method in quantifying the systematic uncertainties of flow measurements was satisfactory.

6.3.2 Random uncertainty quantification of flow measurements

6.3.2.1. Convergence diagnostics of random uncertainty quantification

Figure 6.11 shows the sampling paths in quantifying the random uncertainty of flow measurements in each case. The potential scale reduction factors are also presented in the upper right corner of each sub-figure. As can be seen from Figure 6.11 that the post-warmup samples of random uncertainty in each case fluctuated around a certain value, they had strong centralized tendencies. Besides, the samples from different chains could not be distinguished easily. The potential scale reduction factor in each case was equal to 1.00. These all indicated convergence to posterior distributions. In addition, the autocorrelations of post-warmup samples are shown in Figure 6.12, which are used to further diagnose the convergence. The autocorrelations of post-warmup samples in each case were reduced to about 0 rapidly with the increase of lag, which also demonstrated convergence. Therefore, these post-warmup samples were qualified to construct the posterior distributions of the random uncertainties of flow measurements in each case.
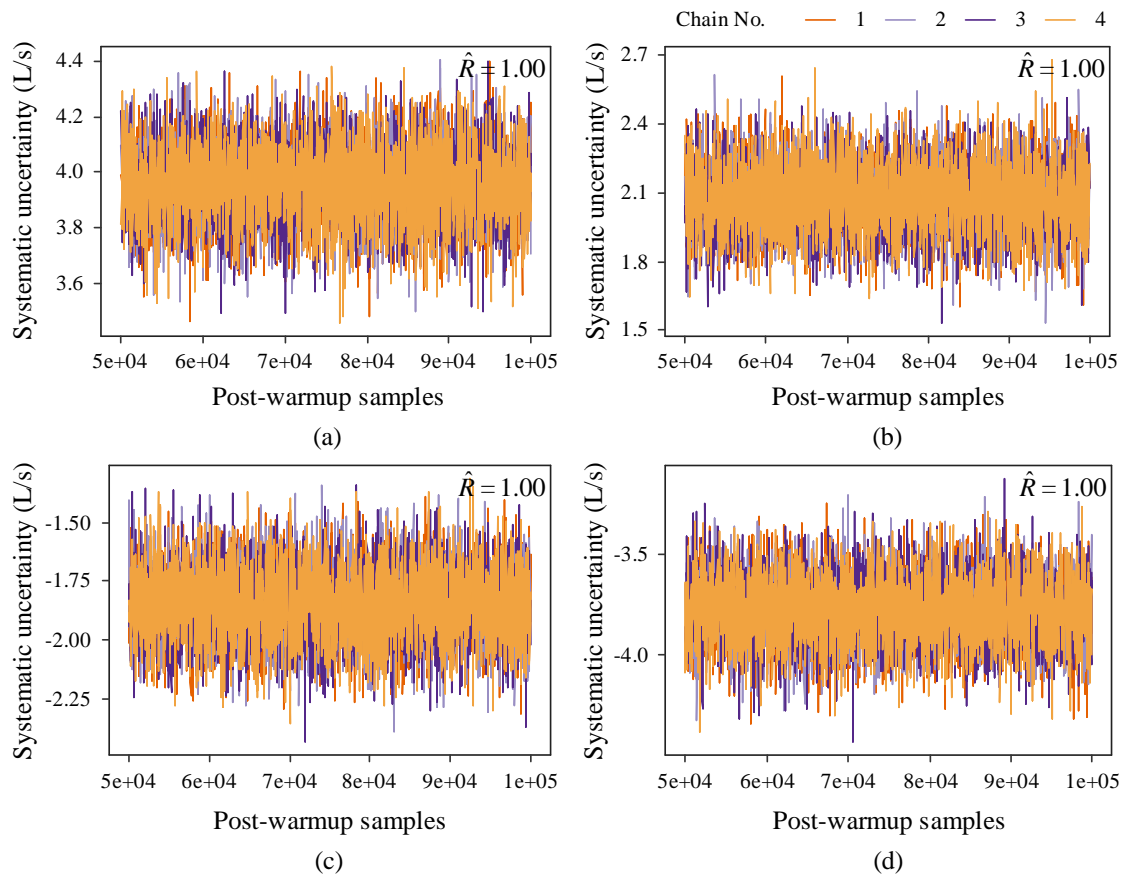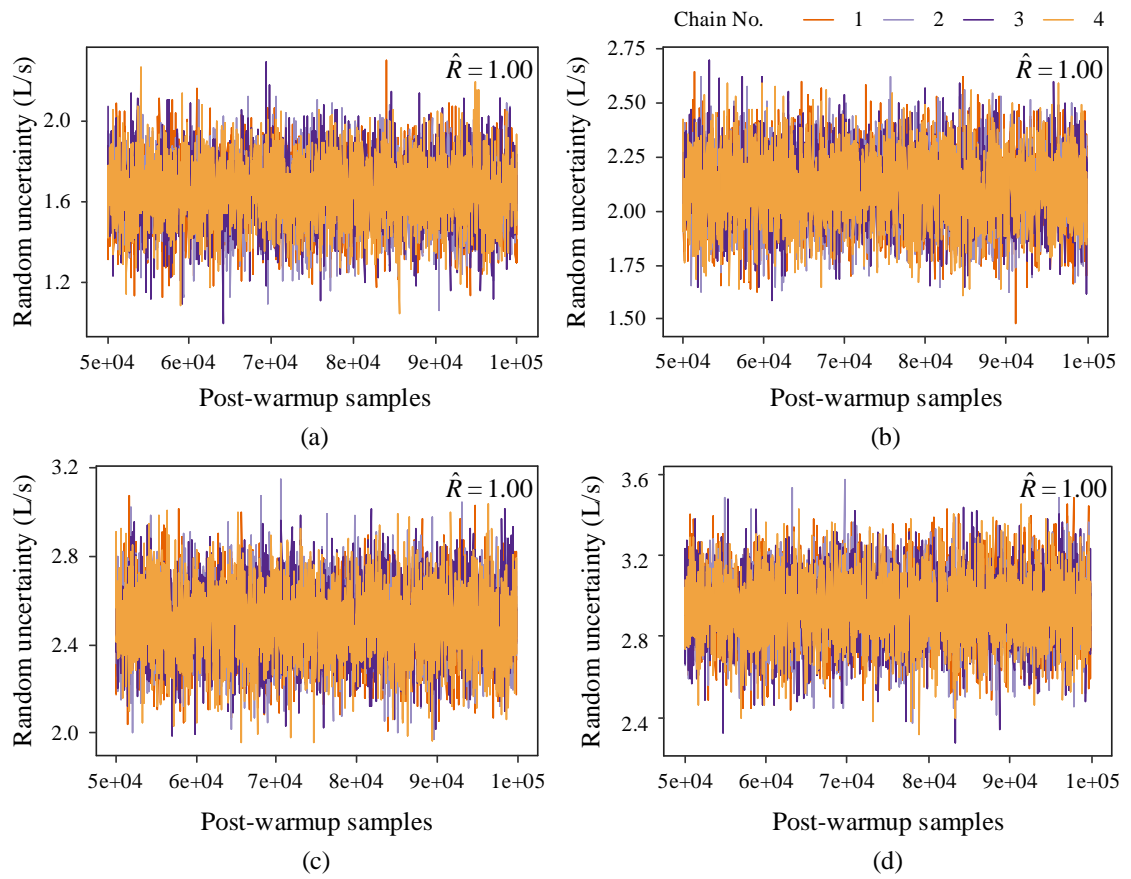
Figure 6.11 Sampling paths in quantifying the random uncertainty of flow

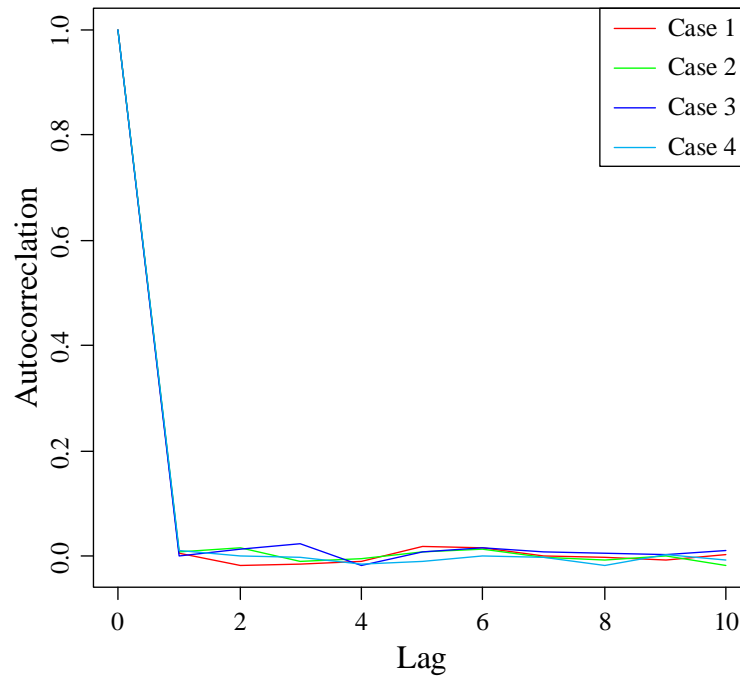measurements in (a) Case 1, (b) Case 2, (c) Case 3 and (d) Case 4
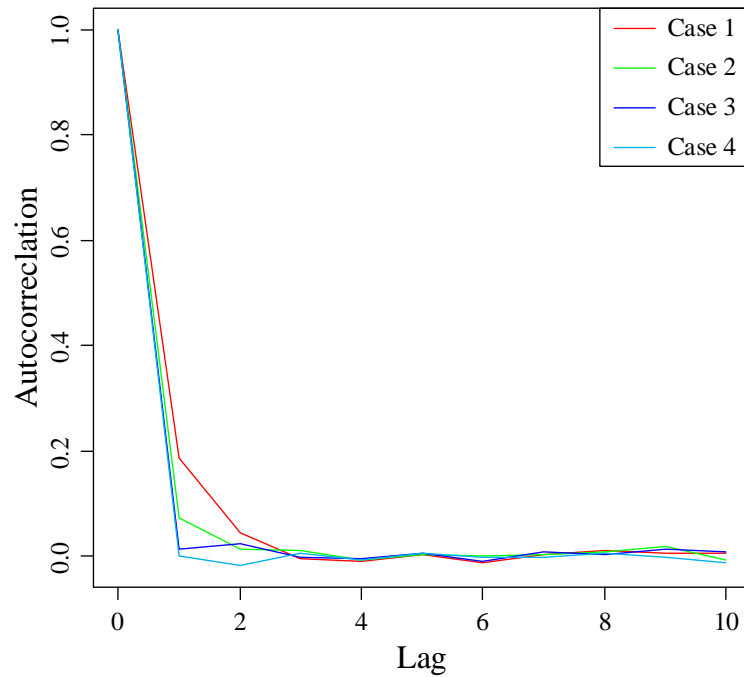
Figure 6.12 Autocorrelations of post-warmup samples in quantifying the random

uncertainty of flow measurements in each case

6.3.2.2. Posterior distributions of random uncertainties

The posterior distribution of random uncertainty of flow measurements in each case was

constructed using the corresponding post-warmup samples in Figure 6.11, as shown in

Figure 6.13. Corresponding to the posterior distributions, the numerical results are

presented in Table 6.5. For the quantified random uncertainty of flow measurements in

each case, its posterior mean was very close to its pre-set value (see Table 6.3). And the

95% Bayesian credible interval was narrow and contained its pre-set value. In addition,

the relative error of the posterior mean relative to its pre-set value was within 10%, such

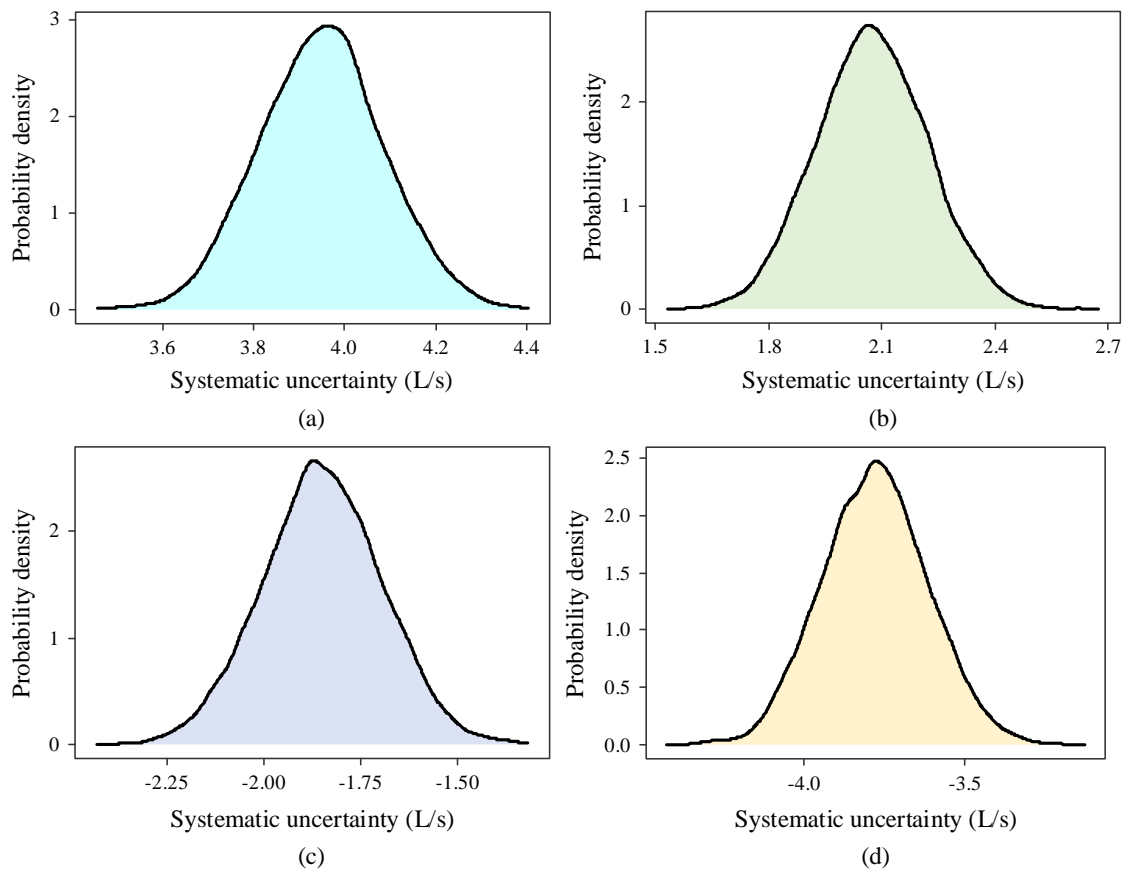a level of error was also acceptable in engineering practice.
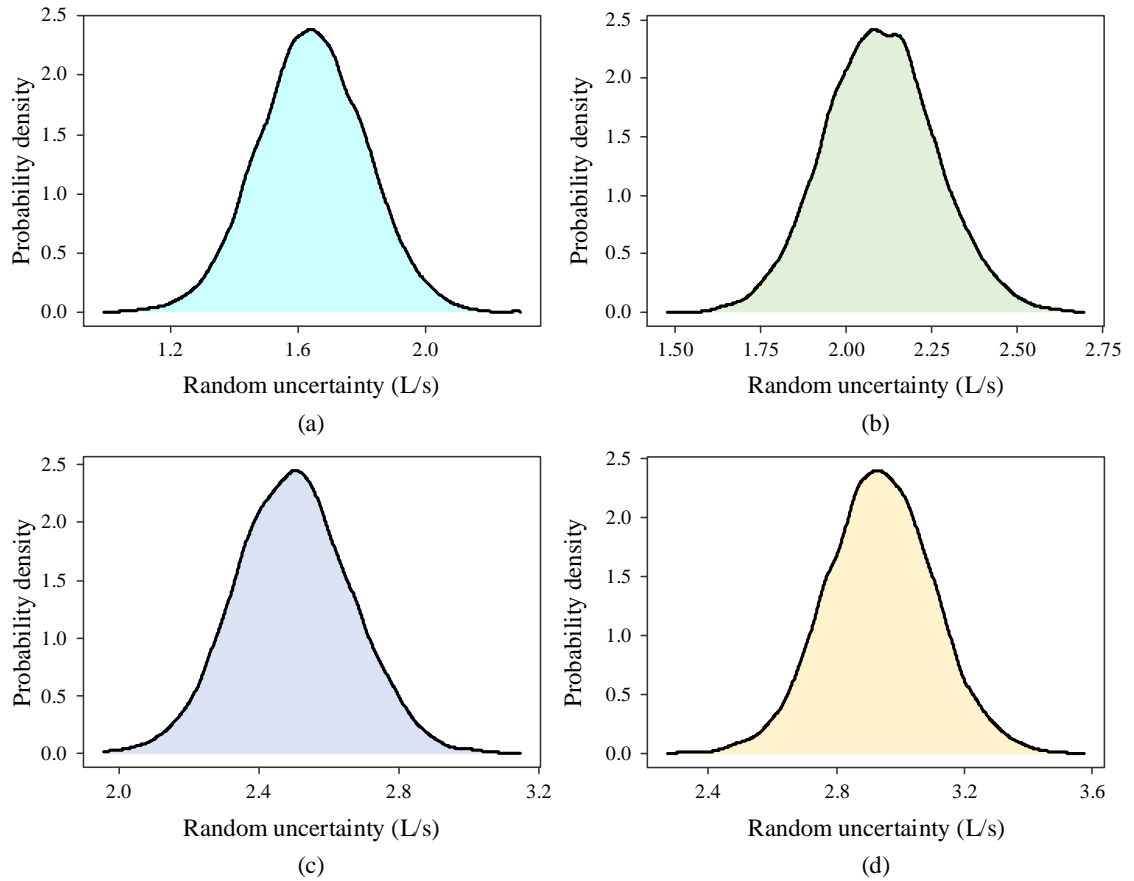
Figure 6.13 Posterior distributions of random uncertainty of flow measurements in (a)

Case 1, (b) Case 2, (c) Case 3 and (d) Case 4

Table 6.5 Numerical results of random uncertainty quantification

	Posterior mean (L/s)	95% Bayesian credible interval (L/s)	Relative error (%)
Case 1	1.64	[1.32, 1.97]	9.33
Case 2	2.10	[1.79, 2.42]	5.00
Case 3	2.50	[2.18, 2.82]	0.00
Case 4	2.94	[2.61, 3.26]	2.00

In summary, different levels of random uncertainties in flow measurements were quantified successfully using the proposed method, which indicates that the performance of the method in quantifying the systematic uncertainties of flow measurements was satisfactory.

6.4 Discussion

The validation results showed that the proposed method was effective to quantify flow measurement uncertainties. Different levels of flow measurement uncertainties, including the systematic and random uncertainties, could be quantified accurately. The performance of the proposed method in quantifying both systematic and random uncertainties of flow measurements was quite satisfactory. Compared with the physical model-based measurement uncertainty quantification method developed in Chapter 4, which performs poorly on negative systematic uncertainty quantification, the data-driven model-based method have a better performance on measurement uncertainty quantification. In addition, the data-driven model-based method has great advantages in model development, leading to greater application potential.

The accuracy of the proposed method in quantifying flow measurement uncertainties mainly depends on the data-driven benchmark regression model. Since the uncertainties quantified by the method are relative to the data used to train the regression model, the actual uncertainties in a dataset are the sum of the quantified uncertainties and the uncertainties in the training dataset. If the uncertainties in the training dataset are significant, the quantified results may be unreliable. Hence, the selection of the training dataset is of vital importance. The performance of the sensors/meters used is generally as expected after initial commissioning. It is recommended to use the data collected right after the systems/sensors are commissioned. In addition, the benchmark model or the training data can also be provided by the sensor/meter manufacturers.

In the test period, the case studies adopted a multiple quadratic non-linear regression model as the benchmark model. The regression model was not very accurate, the coefficient of determination was 0.92 and the standard deviation of residual was 11.39.

But this defect did not affect the performance of the method, because the error (residual) distribution of the benchmark model is considered in the Bayesian model. It is not necessary to develop a perfect regression model. The proposed method has strong adaptability. In addition, the data-driven regression model can be developed based on the available data, it is not necessary to install extra sensors for measuring more variables. There is almost no additional cost to implement this method. It shows great flexibility and economy.

The proposed data-driven model-based measurement uncertainty quantification method can be used for online sensor/meter calibration. It has a huge advantage compared with on-site calibration. The measurement uncertainty of a measuring instrument may change over time due to performance degradation. It is recommended that the measuring instruments should be calibrated on an annual basis (ASHRAE, 2014). But such measure is often not conducted due to the limitations of site conditions and high manpower costs. Online sensor/meter calibration is a promising and cost-effective solution to such practical problems. It can be done automatically as long as there are enough operation data. In addition, the interval of sensor/meter calibration can also be set flexibly according to the actual needs. The online sensor/meter calibration based on the proposed method is cost-effective and has great practical value.

6.5 Summary

A data-driven model-based flow measurement uncertainty quantification method is proposed in this study for enhancing the reliability and energy performance of HVAC systems. As the core of the proposed method, the data-driven regression model is the benchmark and is developed using the system's normal operation data. The flow measurement uncertainties are quantified based on the regression model using Bayesian

inference and Markov chain Monte Carlo sampling methods. The performance of the proposed method in quantifying flow measurement uncertainties is tested and validated systematically considering different levels of measurement uncertainties. Based on the validation results, the main conclusions are listed as follows.

- The proposed method can effectively quantify different levels of flow measurement uncertainties. It is applicable to quantify both the systematic and random uncertainties of flow measurements in HVAC systems.

- In the test period, the 95% Bayesian credible intervals contained the pre-set values of corresponding parameters, the difference between the posterior mean and the pre-set value of each parameter was very small, and the relative errors in quantifying flow measurement uncertainty were within 10%. The performance of the proposed method in quantifying flow measurement uncertainties was quite satisfactory.

CHAPTER 7   FRESH AIR CONTROL OPTIMIZATION STRATEGY FOR AIR HANDLING UNIT WITH MEASUREMENT UNCERTAINTIES PROCESSED BY DATA-DRIVEN MODEL-BASED METHOD

Fresh air control of air handling units plays an important role in maintaining indoor air quality and achieving energy savings for HVAC systems during transition seasons. Its performance is also affected by the uncertainties of the measurements used. Wrong control decisions are possible to be made and the aim of energy saving may not be achieved. This chapter quantitatively analyses the impacts of humidity measurement uncertainties on enthalpy-based fresh air control. An optimization strategy for the fresh air control is proposed to reduce the impacts, where the measurement uncertainties of relative humidity sensors are addressed by the data-driven model-based method developed in Chapter 6. And a systematic validation of the proposed control optimization strategy is conducted.

The organization of this chapter is as follows. Section 7.1 introduces the enthalpy-based fresh air control method of air handling units. Section 7.2 analyses the impacts of measurement uncertainties on enthalpy-based fresh air control. Then the fresh air control optimization strategy is proposed in Section 7.3. And it is validated systematically in Section 7.4. Finally, the conclusions are made in Section 7.5.

7.1 Enthalpy-based fresh air control of air handling units

An air handling unit (AHU) is one of the most important parts of an HVAC system and is used to provide cooling or heating for large-scale buildings (Yu et al., 2014). The air

(fresh air and return air) is conditioned by AHU and supplied to the indoor spaces for fulfilling the space ventilation and sensible/latent cooling functions (ASHRAE, 2020). Figure 7.1 shows the schematic diagram of an air handling unit (only cooling is provided). It mainly consists of a filter, a cooling coil, a supply fan, a return fan, and air dampers. The air dampers are modulated to control the quantities of fresh air (FA) and return air (RA). The fans are equipped with variable speed drives (VSD) and their frequency can be regulated to control the supply and return air flow rates according to the space cooling demand.
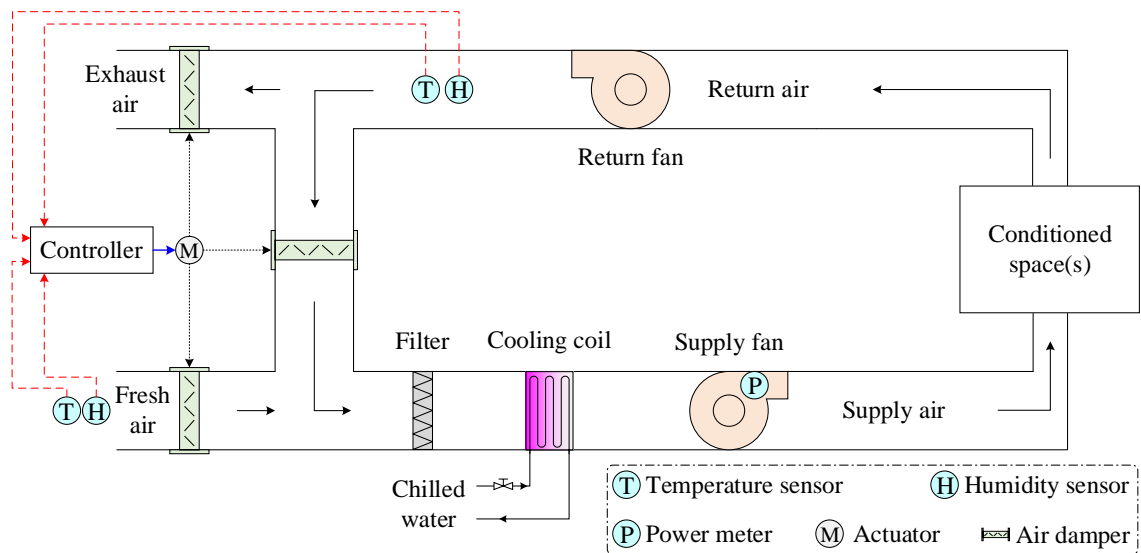
Figure 7.1 Schematic diagram and fresh air control system of an air handling unit

Figure 7.1 also shows the enthalpy-based fresh air control system. Fresh air control is very important for an AHU as the air quality of the conditioned space(s) highly depends on the quantity of fresh air intake. In addition, in the transition season, the energy consumption of mechanical cooling can be reduced by using the cooling of fresh air as much as possible. Generally, an air-side economizer is used to modulate the fresh air quantity according to the dry-bulb temperatures and/or enthalpies of the return air and fresh air.

The dry-bulb temperature-based fresh air control method applies to the regions with dry climates, while the enthalpy-based fresh air control method applies to the regions with hot-humid climates (Yao and Wang, 2010). In Hong Kong, the enthalpy-based fresh air control method is preferred as the ambient air is often moist. Figure 7.2 shows the enthalpy-based operating sequencing of an AHU in the cooling season. It is implemented by comparing the enthalpies of fresh air and return air. There are three cooling modes: (1) Total free cooling mode, (2) Partial free cooling mode, and (3) Mechanical cooling mode. In Mode 1, the enthalpy of the fresh air is small and less than that of the return air. The indoor space is cooled totally by fresh air, and no mechanical cooling is required, the return air is all exhausted. In Mode 2, the enthalpy of the fresh air is also less than that of the return air. The fresh air is also used to cool the indoor space, but the cooling of fresh air is not sufficient to meet the cooling demand. Mechanical cooling is required, and the return air is also exhausted. In Mode 3, the enthalpy of the fresh air is greater than that of the return air, which makes the cost of cooling fresh air higher than that of cooling return air. Therefore, the fresh air is modulated to the minimum, and the return air is recycled.
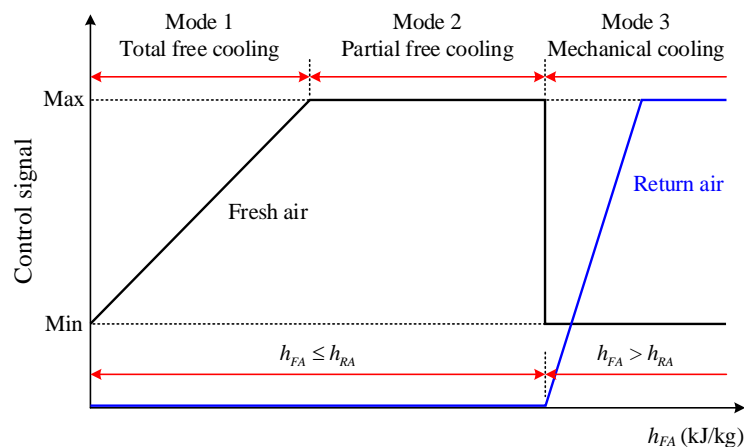
Figure 7.2 Enthalpy-based operating sequencing of an air handling unit in the cooling season

In general, the enthalpies of fresh air (h_{FA}) and return air (h_{RA}) are calculated by their dry-bulb temperatures (T_{FA}, T_{RA}) and relative humidity values (φ_{FA}, φ_{RA}). Corresponding sensors should be installed for measuring their enthalpies, as shown in Figure 7.1. According to 2021 ASHRAE Handbook – Fundamentals (ASHRAE, 2021), the enthalpy of moist air (h, kJ/kg) can be calculated by Eq. (7.1).

$$h = 1.006 \cdot T + d_m \cdot \left(2501 + 1.86 \cdot T\right) \tag{7.1}$$

where T is the dry-bulb air temperature in °C, and d_m is the humidity ratio of the moist air in kg$_w$/kg$_a$. The humidity ratio can be calculated by Eq. (7.2).

$$d_m = 0.621\ 945 \frac{\varphi \cdot p_s}{p - \varphi \cdot p_s} \tag{7.2}$$

where φ is the relative humidity of the moist air, p is the atmospheric pressure in Pa, and p_s is the corrected saturation water vapor pressure in Pa. The corrected saturation water vapor pressure can be estimated by Eq. (7.3), which is developed by Buck (1996).

$$p_s = 611.2 \cdot e^{\frac{\left(18.678 - T/234.5\right) \cdot T}{T + 257.14}} \tag{7.3}$$

7.2 Impact evaluation of measurement uncertainties on enthalpy-based fresh air control

The measurement uncertainties of both the temperature and relative humidity sensors may affect the performance of enthalpy-based fresh air control. Generally, temperature sensors are very stable and their accuracy can be maintained at an acceptable level for many years, but relative humidity sensors are difficult to maintain their accuracy, they even cannot meet the accuracy levels that their manufacturers claimed (Taylor and Cheng, 2010). In addition, relative humidity has large spatial variability, which leads to more significant

uncertainty (Hempel et al., 2018). This section, therefore, focuses on evaluating the impacts of measurement uncertainties of relative humidity sensors on enthalpy-based fresh air control, and it is conducted on a virtual platform.

7.2.1 Description of the system concerned and the virtual platform used

A virtual building system with an air handling unit is developed using TRNSYS, and the enthalpy-based fresh air controller is programmed using Python. As shown in Figure 7.3, the measurement uncertainties are introduced artificially. The measurements (i.e., the sum of the simulation outputs and introduced uncertainties) are input to the enthalpy-based fresh air controller. Then the control decisions are made, and the control signals are sent to the air handling unit. The actuator of the fresh air controller modulates the quantities of fresh air and return air according to the control signals.

The focus of this part is to evaluate the performance of the air handling unit considering measurement uncertainties. The cooling load of the air handling unit is simulated by the component of Type 88, which is a single zone building model with lumped capacitance. The cooling coil of the air handling unit is simulated by Type 752, whose cooling capacity is unlimited. The supply fan (variable speed) is modelled by Type 147, and the air enthalpy is calculated by Type 33 based on its temperature and humidity. Type 169 is used to connect Python to TRNSYS.

Table 7.1 shows the main parameters of the developed virtual system, including the thermodynamic parameters and the area of the building, the heat gains from lighting, equipment and occupants, the rated fan power and the overall coefficient of performance of the air handling unit. It should be noted that the overall coefficient of performance of the air handling unit is assumed to be a constant in this study, i.e., 2.5.
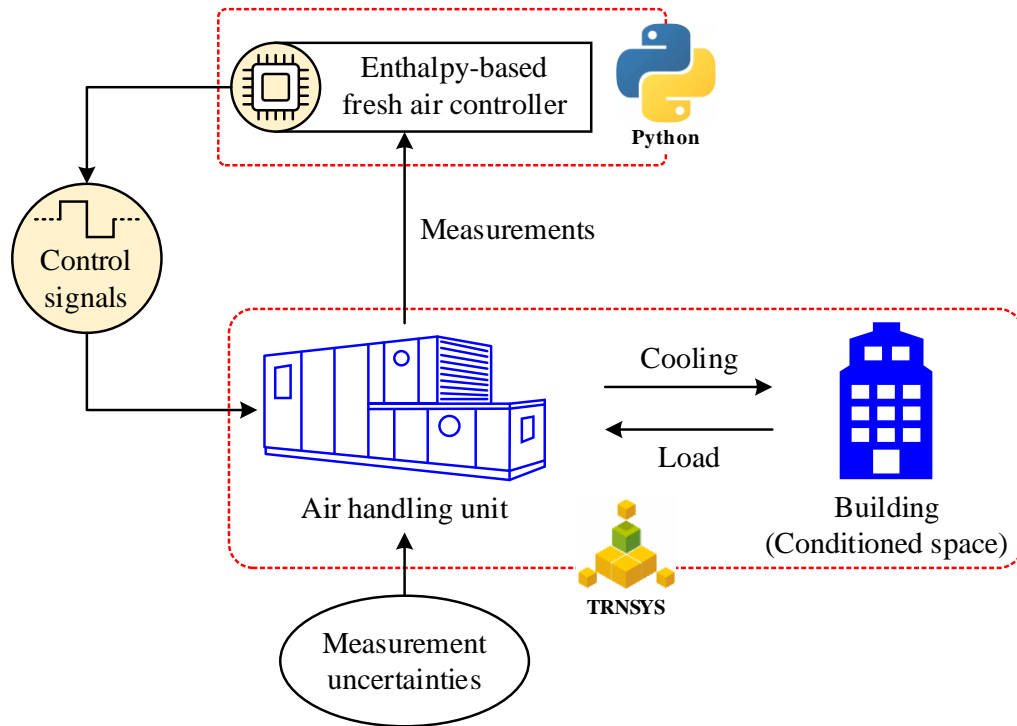
Figure 7.3 The system developed on a virtual platform

Table 7.1 Main parameters of the developed virtual system

Classification	Parameter	Value
Building	Overall energy loss coefficient	1.39 W/(m^2·K)
	Thermal capacitance	1 000 kJ/K
	Specific heat of building air	1.007 kJ/(kg·K)
	Density of building air	1.2 kg/m^3
	Floor area	1 000 m^2
	Occupant density	5/100 m^2
Load	Lighting load	13 W/m^2
	Equipment load	21.5 W/m^2
	Occupancy load	139 W/Occupant
AHU system	Rated power of supply fan	25 kW
	Overall coefficient of performance	2.5

7.2.2 Arrangements for the evaluation

Four cases with different levels of measurement uncertainties are used to evaluate the impacts of measurement uncertainties on enthalpy-based fresh air control. The measurement uncertainties of relative humidity sensors in each case are introduced artificially. They are generated randomly based on the parameters (mean and standard deviation) of a given normal distribution, as shown in Table 7.2. The measurements are simulated by adding the generated uncertainties to the simulation outputs of corresponding variables. A reference case without uncertainties is conducted and will be used as the benchmark. The main difference between the other cases is the plus-minus sign of systematic uncertainties. A positive systematic uncertainty tends to make the measured humidity greater than the actual humidity. On the contrary, a negative systematic uncertainty tends to make the measured humidity less than the actual humidity. These four cases cover all the possible scenarios in real applications, and the impacts of measurement uncertainties on fresh air control can be evaluated systematically based on them.

Table 7.2 Pre-set measurement uncertainties of relative humidity sensors (%)

	Fresh air humidity sensor		Return air humidity sensor	
	Systematic uncertainty	Random uncertainty	Systematic uncertainty	Random uncertainty
Reference	0	0	0	0
Case 1	8.0	3.0	6.0	1.5
Case 2	8.0	2.5	-6.0	2.0
Case 3	-8.0	2.0	6.0	2.5
Case 4	-8.0	1.5	-6.0	3.0

The running of the air handling unit system on a typical day is simulated. The states of fresh air on this day, including the relative humidity, dry-bulb temperature and enthalpy, are presented in Figure 7.4. The fresh air is suitable for cooling the indoor space and the purpose of evaluating the performance of fresh air control under measurement uncertainties can be achieved. The simulation time step is 10 seconds. The time interval of the data collection and control decision-making is 5 minutes.
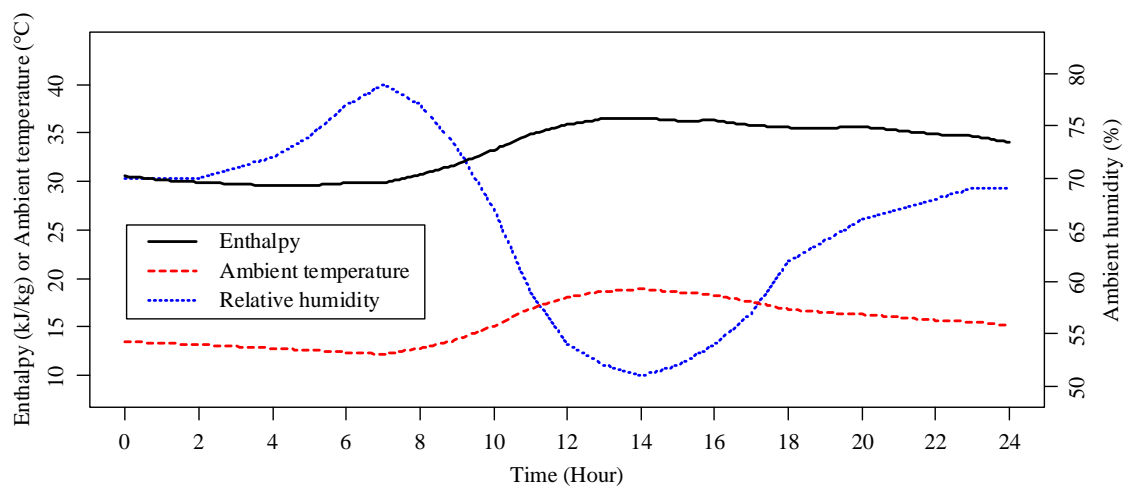
Figure 7.4 Fresh air states during the test period

7.2.3 Evaluation results and analysis

Table 7.3 shows the energy performance of the air handling unit system in each case. Compared with the reference case, the energy performance of other cases declines due to the existence of measurement uncertainties. In Case1, the cooling energy consumption increases a little and the fan energy consumption is reduced slightly, but the total energy consumption increases by 3.64%. In Case 2, the cooling energy consumption increases significantly (more than twice the reference value), but the fan energy consumption is reduced a little. It leads to a significant increment of 35.56% in total energy consumption. In Case 3, though the cooling energy consumption is reduced dramatically, the fan energy

consumption increases significantly, resulting in the total energy consumption increasing by 17.95%. In Case 4, the cooling energy consumption is reduced moderately, while the fan energy consumption increases significantly. The total energy consumption increases by 29.66%. Therefore, it can be concluded that the measurement uncertainties can affect the performance of fresh air control significantly and further decline the energy performance of air handling unit systems. The impacts cannot be ignored and should be addressed.

Table 7.3 Energy performance of the air handling unit system under different levels of humidity measurement uncertainties

	Cooling energy consumption (kWh)	Fan energy consumption (kWh)	Total energy consumption (kWh)	Increment (%)
Reference	42.67	88.36	131.03	-
Case 1	48.37	87.43	135.80	3.64
Case 2	89.72	87.90	177.62	35.56
Case 3	4.43	150.11	154.54	17.95
Case 4	26.77	143.13	169.89	29.66

The increment in energy consumption caused by the measurement uncertainties is different in different Cases, which is possibly related to the directions (plus-minus signs) of the introduced uncertainties. The uncertainties in Case 1 make the measured enthalpies of both fresh air and return air greater than their actual enthalpies. The impact is small as the results are often consistent when comparing the magnitudes of their measured or actual enthalpies. The uncertainties in Case 2 make the measured fresh air enthalpy greater than its actual enthalpy and the measured return air enthalpy less than its actual enthalpy, the air handling unit tends to operate under Mode 2 or 3, resulting in a significant increase in cooling energy consumption. On the contrary, the uncertainties in

Case 3 make the measured fresh air enthalpy less than its actual enthalpy and the measured return air enthalpy greater than its actual enthalpy, the air handling unit tends to operate under Mode 1, leading to a significant decrease in cooling energy consumption, but the fan energy consumption increases dramatically as more fresh air is needed to meet the cooling demand. The uncertainties in Case 4 make the measured enthalpies of both fresh air and return air less than their actual enthalpies. Possibly due to the influence of systematic uncertainties, the air handling unit tends to operate under Mode 1 or 2, causing an increase in fan energy consumption.

7.3 Fresh air control optimization strategy

The temperature and humidity of the return air are the same as those of the indoor air without considering the heat transfer in the air duct. Generally, an effective controller (for example, a feedback controller) makes the indoor air temperature always fluctuate around its setpoint. It means that the return air temperature is almost fixed. The return air temperature cannot take any effect to quantify the uncertainties of humidity measurements. Hence, it will be not used to develop the following models. The aim of the proposed fresh air control optimization strategy is to correct the relative humidity measurements of fresh air and return air online, and further they are used to calculate the enthalpies. The relative humidity of fresh air and return air are the target variables, and the auxiliary variables are the power consumption of the supply fan and the fresh air temperature.

7.3.1 Outline of the proposed fresh air control optimization strategy

The core of the measurement uncertainty quantification method developed in Chapter 6 is a data-driven benchmark model. Figure 7.5 shows the outline of the proposed fresh air control optimization strategy for air handling units. The data-driven benchmark model

should be developed firstly using the normal operation dataset. Then the method developed in Chapter 6 is used to quantify the uncertainties of fresh air and return air relative humidity measurements based on the historical operation dataset. Then the real-time relative humidity measurements are corrected online based on the benchmark model with known uncertainty distribution parameters. Finally, the enthalpies of fresh air ($h_{FA,cor}$) and return air ($h_{RA,cor}$) are calculated based on the corrected humidity and used to make control decisions. More details about the strategy are presented in Sections 7.3.2 and 7.3.3.

• Benchmark model development

Normal operation dataset

$$P_{fan} = f\left(T_{FA},\ \varphi_{FA},\ \varphi_{RA}\right) + e$$
$$= c_1 T_{FA}^2 + c_2 \varphi_{FA}^2 + c_3 \varphi_{RA}^2 + c_4 T_{FA} + c_5 \varphi_{FA} + c_6 \varphi_{RA} + c_7 + e$$

$\left\{P_{fan},\ T_{FA},\ \varphi_{FA},\ \varphi_{RA}\right\}$ where $e \sim N\left(0,\ \delta^2\right)$ $\Rightarrow \left\{c_1, c_2, c_3, c_4, c_5, c_6, c_7, \delta\right\}$

• Measurement uncertainty quantification

Historical operation dataset

$$\begin{cases} P_{fan} \sim N\left(c_1 T_{FA}^2 + c_2 \varphi_{FA}^2 + c_3 \varphi_{RA}^2 + c_4 T_{FA} + c_5 \varphi_{FA} + c_6 \varphi_{RA} + c_7,\ \delta^2\right) \\ \tilde{\varphi}_{FA} \sim N\left(\varphi_{FA} + \mu_{FA},\ \sigma_{FA}^2\right) \\ \tilde{\varphi}_{RA} \sim N\left(\varphi_{RA} + \mu_{RA},\ \sigma_{RA}^2\right) \end{cases}$$

$\left\{P_{fan},\ T_{FA},\ \tilde{\varphi}_{FA},\ \tilde{\varphi}_{RA}\right\}$ $\Rightarrow \begin{cases} \mu_{FA},\ \sigma_{FA} \\ \mu_{RA},\ \sigma_{RA} \end{cases}$

• Online correction of relative humidity measurements

Real-time operation data

$$\begin{cases} P_{fan,t} \sim N\left(c_1 T_{FA,t}^2 + c_2 \varphi_{FA,t}^2 + c_3 \varphi_{RA,t}^2 + c_4 T_{FA,t} + c_5 \varphi_{FA,t} + c_6 \varphi_{RA,t} + c_7,\ \delta^2\right) \\ \tilde{\varphi}_{FA,t} \sim N\left(\varphi_{FA,t} + \mu_{FA},\ \sigma_{FA}^2\right) \\ \tilde{\varphi}_{RA,t} \sim N\left(\varphi_{RA,t} + \mu_{RA},\ \sigma_{RA}^2\right) \end{cases}$$

$\left\{P_{fan,t},\ T_{FA,t},\ \tilde{\varphi}_{FA,t},\ \tilde{\varphi}_{RA,t}\right\}$ $\Rightarrow \begin{cases} \varphi_{FA,t} \\ \varphi_{RA,t} \end{cases}$

Calculating enthalpies and making control decisions

Figure 7.5 Outline of the proposed fresh air control optimization strategy

Similarly, the proposed fresh air control optimization strategy is validated on the virtual platform, as shown in Figure 7.6. Compared with the system developed in Figure 7.3, a component is added to correct the relative humidity measurements online with known distribution parameters of uncertainties. Then the corrected values are sent to the controller and make control decisions.
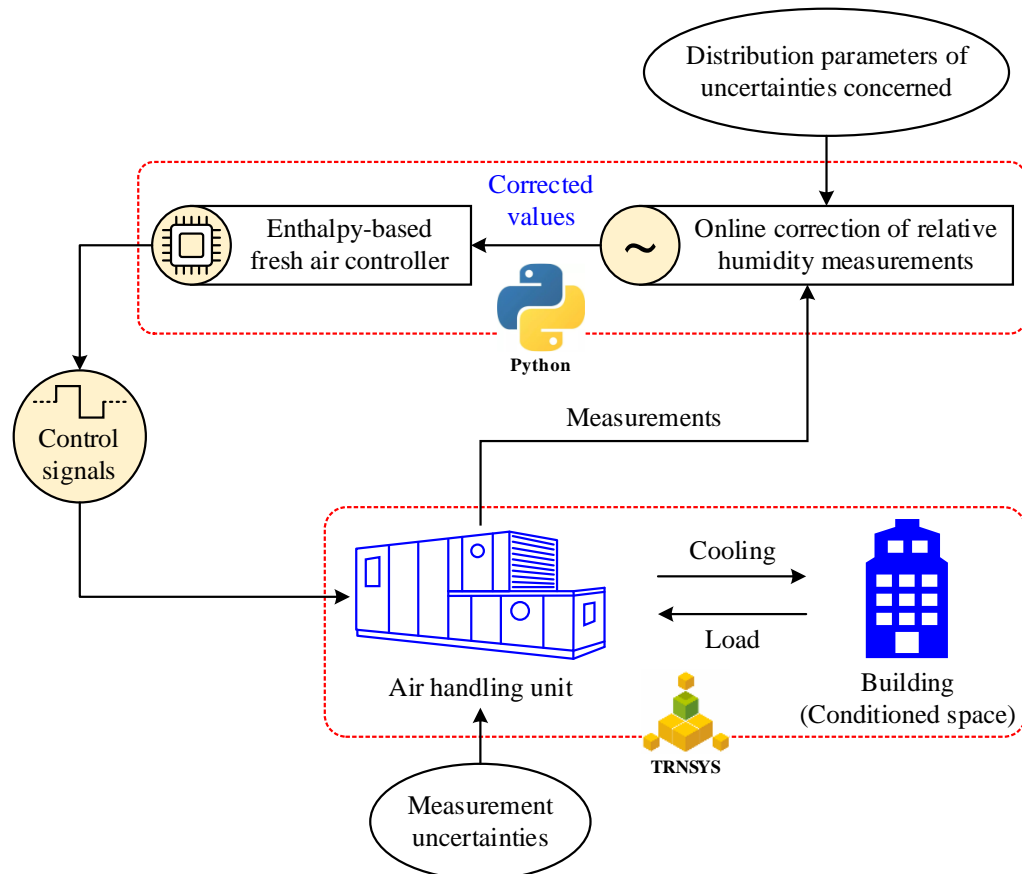
Figure 7.6 Validation of the proposed strategy on the virtual platform

7.3.2 Benchmark model development

A multiple quadratic regression model is developed as the benchmark model in this study. The fan power consumption (P_{fan}) is the dependent variable. The independent variables include the fresh air temperature (T_{FA}) and relative humidity (φ_{FA}), and the return air humidity (φ_{RA}). The model is expressed by Eq. (7.4). The coefficients of the model (a_{1-7}) and the standard deviation of the model error (δ) should be determined.

138

$$P_{fan} = f\left(T_{FA},\ \varphi_{FA},\ \varphi_{RA}\right) + e$$
$$= a_1 T_{FA}^2 + a_2 \varphi_{FA}^2 + a_3 \varphi_{RA}^2 + a_4 T_{FA} + a_5 \varphi_{FA} + a_6 \varphi_{RA} + a_7 + e,\quad e \sim N\left(0,\ \delta^2\right) \tag{7.4}$$

The model is trained by the simulation data of the reference Case, where no measurement uncertainties exist. The ordinary least squares method is adopted. The model is developed with an R^2 of 0.98, showing that the data fit the model well. These coefficients (including the standard deviation of the model error, which is replaced by the standard deviation of model residuals) to be determined are presented in Table 7.4.

Table 7.4 Coefficients of the developed data-driven model

Coefficient	a_1	a_2	a_3	a_4	a_5	a_6	a_7	δ
Value	-0.0592	0.0017	0.0913	2.3713	-0.2284	-3.9320	31.2957	0.1637

7.3.3 Online correction of relative humidity measurements and enthalpies

Once the benchmark model is developed, the uncertainty parameters of fresh air and return air humidity measurements can be quantified using the method developed in Chapter 6, it will not be repeated here. Of course, the uncertainty parameters can also be obtained by other methods, such as field calibration. The real-time relative humidity measurements can be corrected using Bayesian inference and Markov chain Monte Carlo sampling methods. The Bayesian models are shown in Eq. (7.5), where only the actual relative humidity of fresh air ($\varphi_{FA,t}$) and return air ($\varphi_{RA,t}$) are unknown and need to be estimated.

$$\begin{cases} P_{fan,t} \sim N\left(-0.0592T_{FA,t}^2 + 0.0017\varphi_{FA,t}^2 + 0.0913\varphi_{RA,t}^2 + 2.3713T_{FA,t} - 0.2284\varphi_{FA,t} - 3.932\varphi_{RA,t} + 31.2957,\ 0.1637^2\right) \\ \tilde{\varphi}_{FA,t} \sim N\left(\varphi_{FA,t} + \mu_{FA},\ \sigma_{FA}^2\right) \\ \tilde{\varphi}_{RA,t} \sim N\left(\varphi_{RA,t} + \mu_{RA},\ \sigma_{RA}^2\right) \end{cases}$$

$$\tag{7.5}$$

The Bayesian models in this study are coded using the *stan* programming language. The range of relative humidity is between 0 and 100. Therefore, a uniform distribution is used as the prior distribution of the relative humidity, as shown in Figure 7.7.
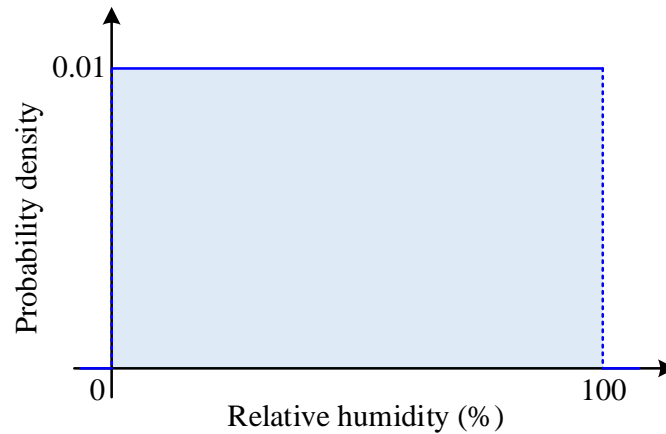
Figure 7.7 Prior distribution (uniform) of relative humidity

The posterior distributions of the fresh air and return air humidity measurements can be obtained. Their mean values are regarded as their corrected values and used to calculate/correct the enthalpies of fresh air and return air. Then the control decisions are made based on the corrected enthalpies.

7.4 Performance evaluation and test results of the fresh air control optimization strategy

The proposed fresh air control optimization strategy is tested using the Cases presented in Section 7.2.2. The strategy is implemented in each Case (other than the reference Case) and the results are presented in this section. The performance of the proposed fresh air control optimization strategy is evaluated by comparing the measured enthalpies and corrected enthalpies of fresh air and return air with their actual enthalpies and comparing the energy performance of the air handling unit before and after optimization.

7.4.1 Comparison of the measured enthalpies and corrected enthalpies

Figure 7.8-7.8 shows the enthalpies of fresh air and return air in each case during the test period, including the actual values, corrected values, measured values and 95% credible intervals. As can be seen from these figures, the measured enthalpies of fresh air and return air deviate from their actual enthalpies obviously due to measurement uncertainties of relative humidity, but the corrected enthalpies are very close to their actual values, and almost all the actual values are located within their 95% credible intervals.
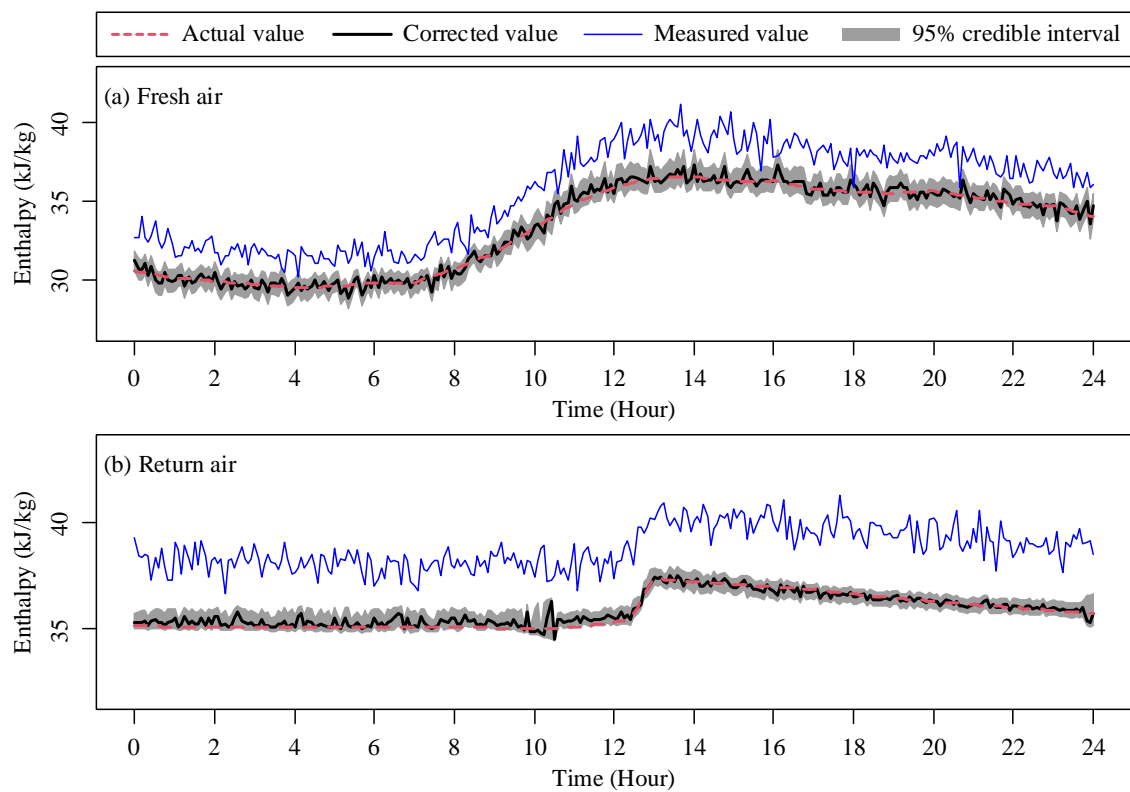
Figure 7.8 Enthalpies of fresh air and return air in Case 1 during the test period
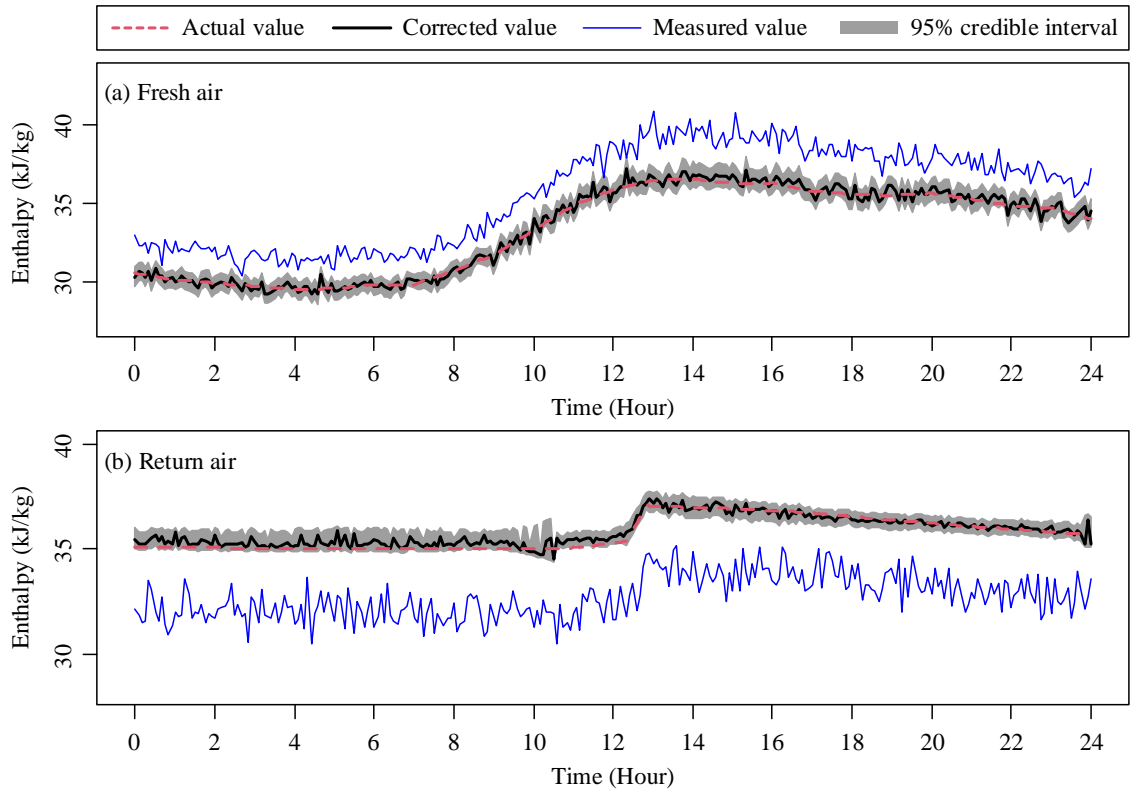
Figure 7.9 Enthalpies of fresh air and return air in Case 2 during the test period
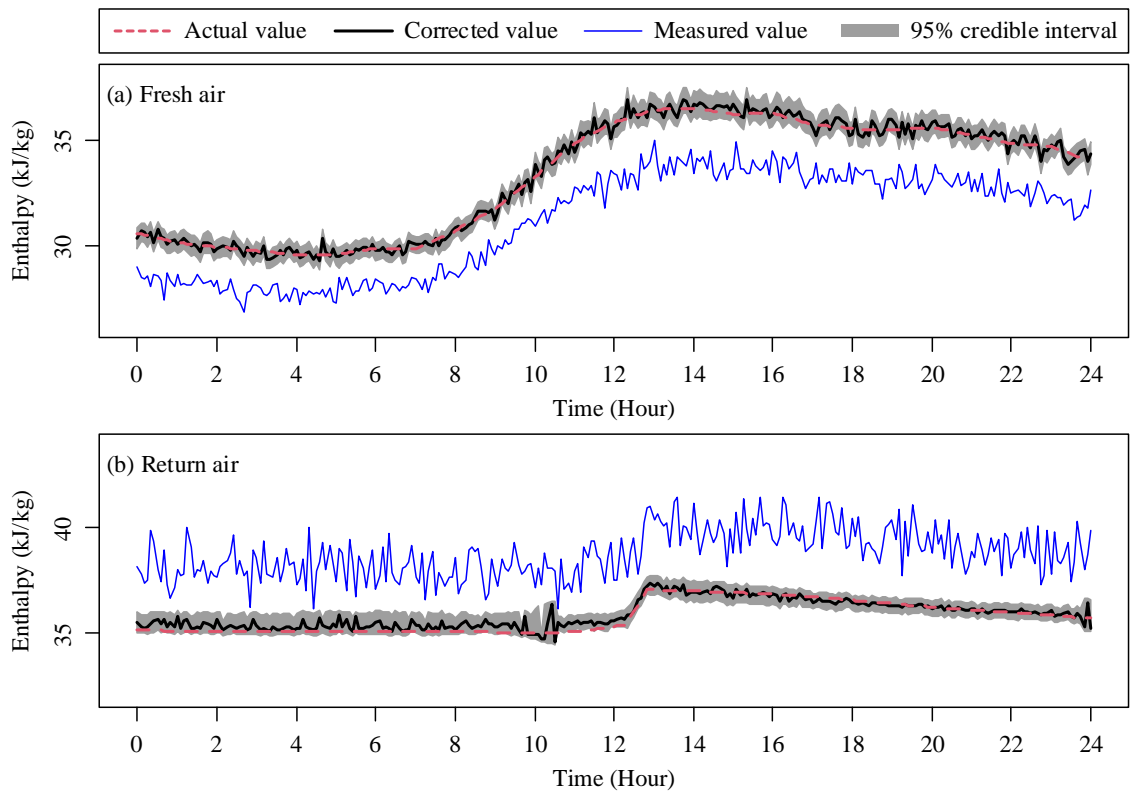
Figure 7.10 Enthalpies of fresh air and return air in Case 3 during the test period
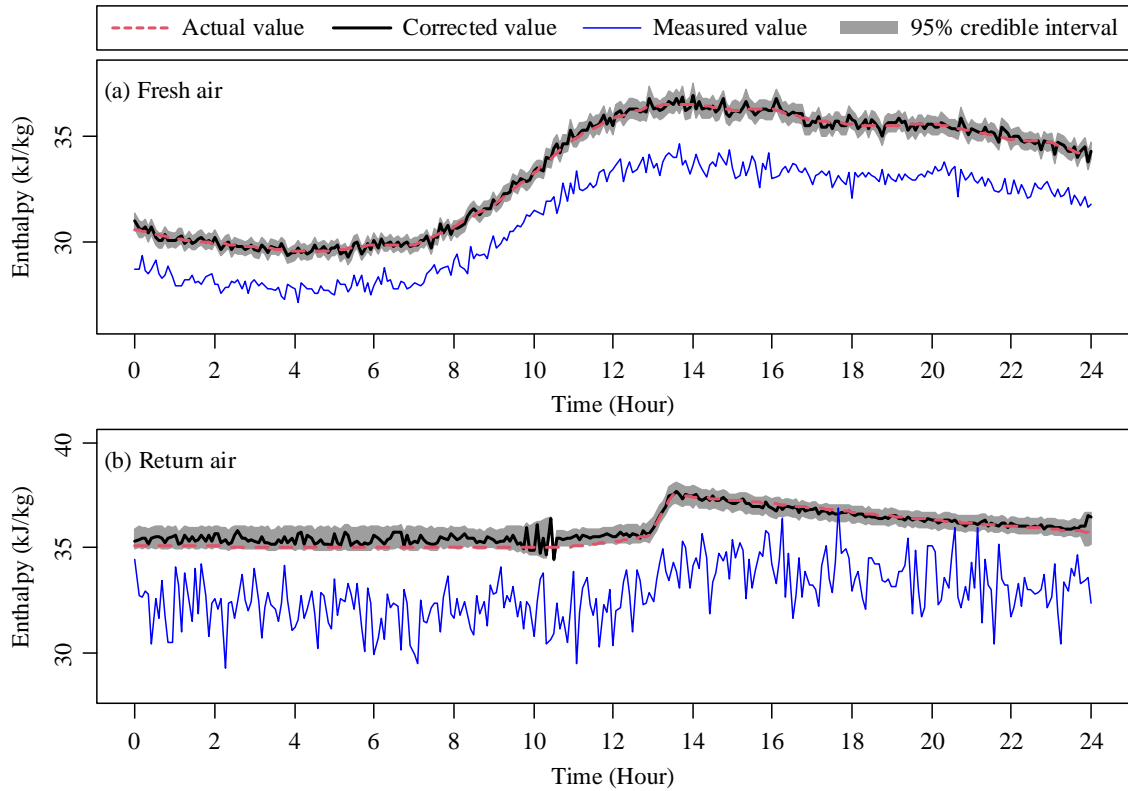
Figure 7.11 Enthalpies of fresh air and return air in Case 4 during the test period

The root-mean-square errors of the measured and corrected enthalpies are also calculated for conducting quantitative analysis, as shown in Table 7.5. The root-mean-square error of measured enthalpy in each Case is much greater than that of corrected enthalpy. Compared with the measured enthalpies, the average root-mean-square error of the fresh air enthalpy is reduced by 87.92% (from 2.2699 kJ/kg to 0.2813 kJ/kg) after correction, and the average root-mean-square error of return air enthalpy is reduced by 91.39% (from 3.1091kJ/kg to 0.2678 kJ/kg) after correction. The accuracy of the corrected enthalpy is enhanced significantly and is fully acceptable in real applications.

Table 7.5 Root-mean-square errors of the measured and corrected enthalpies

	Fresh air enthalpy			Return air enthalpy		
	Measured (kJ/kg)	Corrected (kJ/kg)	Reduction (%)	Measured (kJ/kg)	Corrected (kJ/kg)	Reduction (%)
Case 1	2.3791	0.3561	85.03	3.1051	0.2427	92.18
Case 2	2.3692	0.3153	86.69	3.0636	0.2470	91.94
Case 3	2.2576	0.2588	88.54	3.1441	0.2719	91.35
Case 4	2.2699	0.1950	91.41	3.1236	0.3094	90.09
Average	2.3190	0.2813	87.87	3.1091	0.2678	91.39

7.4.2 Energy performance of the air handling unit after optimization

Figure 7.12 compares the energy consumption of the air handling unit before and after optimization. Compared with the energy consumption before optimization, the energy consumption after optimization is reduced significantly by 1.02% - 24.58%. The energy savings are achieved after optimization. The conclusion can be drawn that the impacts of humidity measurement uncertainties are reduced significantly using the proposed fresh air control optimization strategy.
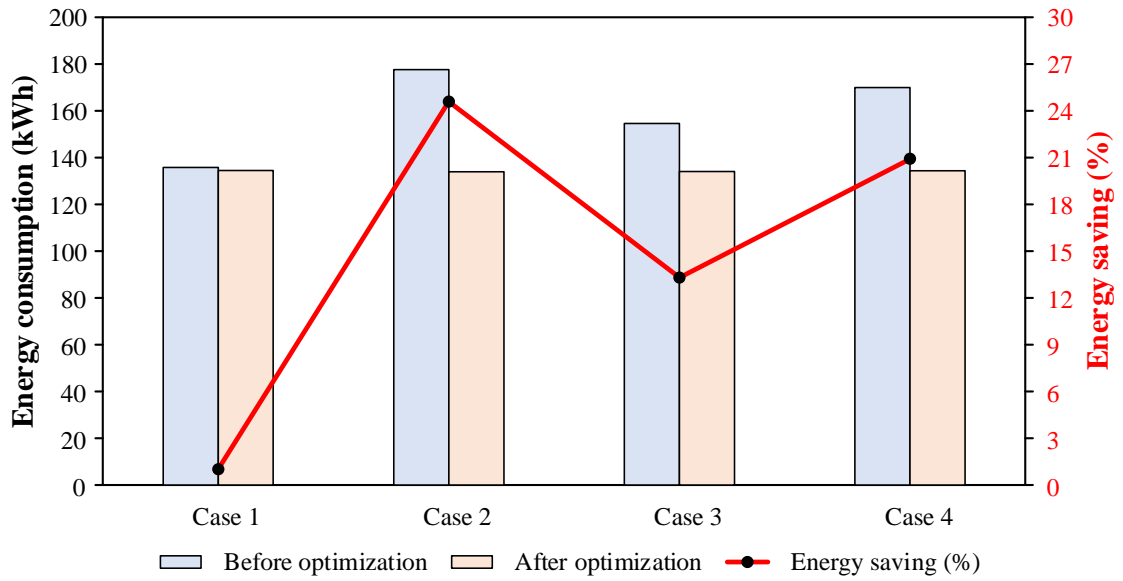
Figure 7.12 Energy consumption of the air handling unit before and after optimization

7.5 Summary

This chapter analyses the impacts of measurement uncertainties of relative humidity sensors on enthalpy-based fresh air control of air handling units. In order to reduce the impacts, a fresh air control optimization strategy is proposed, where the uncertainties of relative humidity measurements are processed by the data-driven model-based method developed in Chapter 6. The measured relative humidity of fresh air and return air is corrected online and used to calculate their enthalpies. The control decisions are made based on the corrected enthalpies of fresh air and return air. The proposed optimization strategy is validated systematically on a virtual platform. The main conclusions are as follows.

- The performance of the fresh air control method is affected significantly by the measurement uncertainties of relative humidity sensors (fresh air and return air). It may lead to an increase of up to 35.56% in the energy consumption of air handling units.

- The measured enthalpies of fresh air and return air deviate from their actual values due to the uncertainties of relative humidity measurements. The deviations can be reduced by correcting the relative humidity measurements online. Compared with the measured enthalpies, the average root-mean-square error of the fresh air enthalpy and return air enthalpy is reduced by 87.92% and 91.39% respectively after correction.

- The proposed fresh air control optimization strategy can significantly reduce the impacts of measurement uncertainties of relative humidity sensors. Compared with the energy consumption before optimization, the energy consumption of the air handling unit is reduced by 1.02% - 24.58% after optimization.

CHAPTER 8 CONCLUSIONS AND SUGGESTIONS FOR FUTURE RESEARCH

This PhD thesis proposed a physical model-based and a data-driven model-based measurement uncertainty quantification methods, and they are used to optimize the chiller sequencing control and enthalpy-based fresh air control under measurement uncertainties. The proposed methods and control strategies are tested and validated systematically. This chapter summarises the research work in this thesis, which is organized as follows. Section 8.1 presents the main contributions of this PhD study. Section 8.2 presents the conclusions drawn based on the work done in this thesis. Section 8.3 gives suggestions for future research.

8.1 Main contributions of this study

This study focuses on the quantification of measurement uncertainties for HVAC systems and the optimization of their control systems under measurement uncertainties. The main contributions of this study are summarised as follows.

i. A physical model-based and a data-driven model-based measurement uncertainty quantification methods are proposed. The measurement uncertainties of sensors/meters in HVAC systems can be quantified accurately using the methods. The energy efficiency and reliability of HVAC systems can be improved, and maintenance costs can be reduced.

ii. The proposed measurement uncertainty quantification methods provide a cost-effective and promising alternative for on-site sensor/meter calibration in

engineering practice, which facilitates the facility management and maintenance of HVAC systems.

iii. The proposed methods apply to the measurement uncertainties quantification of sensors/meters in most HVAC systems. It depends on the available information/data of the system in choosing between the physical model-based method and the data-driven model-based method.

iv. The measurements with significant/unacceptable uncertainties can be corrected online, which greatly enhanced the reliability of decisions made based on them. And the service life of corresponding sensors/meters can be extended dramatically as the sensors/meters with uncertainties can still be used.

8.2 Conclusions

On the physical model-based measurement uncertainty quantification method

- The physical model-based measurement uncertainty quantification method can effectively quantify the measurement uncertainties (including the systematic and random uncertainties) of chilled water and cooling water flow meters in multiple water-cooled chiller systems.

- The performance of the method in quantifying systematic uncertainties is satisfactory. The method is effective for validating flow meters and improving their measurement accuracy, and it can provide valuable and meaningful information in practical application.

- The random uncertainties can be quantified accurately by the proposed method no matter how significant they are. The method performs better in quantifying random uncertainties than systematic uncertainties.

- The levels of measurement uncertainties of different flow meters can be identified by the quantification method. It can be used to detect which flow meters need to be calibrated and assess the reliability of flow measurements, particularly concerning critical decision-making.

On the probability-based online robust chiller sequencing control strategy

- The proposed probability-based online robust chiller sequencing control strategy dramatically reduced the major impacts of both positive and negative flow measurement uncertainties on the multiple-chiller plants. Compared with the conventional total cooling load-based chiller sequencing control strategy, the total switching number of chillers was reduced by 35.71% under the positive flow measurement uncertainties, and the cumulative unmet cooling load was reduced by 31.22% under the negative flow measurement uncertainties.

- As the core of the proposed control strategy, the uncertainty processing model of flow measurements could quantify the chilled water flow rates accurately, which led to a significant decrease (about 79%) in the RMSE of cooling loads.

- The risks in the decision-making process could be quantified to evaluate the reliability of the proposed control strategy and the high-risk decisions could be avoided through double-checking by operators.

On the data-driven model-based measurement uncertainty quantification method

- The proposed method can effectively quantify different levels of flow measurement uncertainties. It is applicable to quantify both the systematic and random uncertainties of flow measurements in HVAC systems.

- In the test period, the 95% Bayesian credible intervals contained the pre-set values of corresponding parameters, the difference between the posterior mean and the pre-set

value of each parameter was very small, and the relative errors in quantifying flow measurement uncertainty were within 10%. The performance of the proposed method in quantifying flow measurement uncertainties was quite satisfactory.

On the fresh air control optimization strategy under measurement uncertainties

- The performance of the fresh air control method is affected heavily by the measurement uncertainties of relative humidity sensors (fresh air and return air). It may lead to an increase of up to 35.56% in the energy consumption of air handling units.

- The measured enthalpies of fresh air and return air deviate from their actual values due to the uncertainties of relative humidity measurements. The deviations can be reduced by correcting the relative humidity measurements online. Compared with the measured enthalpies, the average root-mean-square error of the fresh air enthalpy and return air enthalpy is reduced by 87.92% and 91.39% respectively after correction.

- The proposed fresh air control optimization strategy can significantly reduce the impacts of measurement uncertainties of relative humidity sensors. Compared with the energy consumption before optimization, the energy consumption of the air handling unit is reduced by 1.02% - 24.58% after optimization.

8.3 Suggestions for future research

This PhD study focuses on the direct quantification of measurement uncertainties in HVAC systems using Bayesian inference and optimization of their control systems under measurement uncertainties. Further efforts are suggested to be made in the following aspects for improving the quality of the studies conducted in this thesis and promoting the application of the developed methods and strategies in engineering practice.

- The measurement uncertainty quantification methods developed in this study can be regarded as a black-box model. The interpretability of the quantification results is poor. Further study should be conducted to figure out why the results are obtained. Especially the physical model-based method, as it performs very differently in quantifying different levels and types of uncertainties.

- This study evaluated the impacts of measurement uncertainties on HVAC systems and validated the performance of proposed control strategies, but the test period is short (a day or a week). A long-term test can be conducted in future for assessing the impacts of measurement uncertainties on the lifespan of equipment and the maintenance costs, etc.

- The data-driven models developed in this thesis using the ordinary least square method are multiple quadratic regression models. There are many other methods/algorithms that can be used to develop regression models, such as the support vector machine and the artificial neural network. The effectiveness and robustness of using other regression models to quantify measurement uncertainties are worthy of study, and the impacts of model accuracy and complexity on the quantification results should be studied further.

REFERENCE

Annis, J., Miller, B.J. & Palmeri, T.J., (2017). Bayesian inference with Stan: A tutorial on adding custom distributions. *Behavior research methods*, 49(3), 863-886.

ASHRAE, (2014). Guideline 14-2014: Measurement of energy, demand, and water savings.

ASHRAE, (2020). Handbook: HVAC systems and equipment.

ASHRAE, (2021). Handbook – Fundamentals.

Bae, Y., Bhattacharya, S., Cui, B., Lee, S., Li, Y., Zhang, L., Im, P., Adetola, V., Vrabie, D., Leach, M. & Kuruganti, T., (2021). Sensor impacts on building and HVAC controls: A critical review for building energy performance. *Advances in Applied Energy*, 4, 100068.

Booth, A.T. & Choudhary, R., (2013). Decision making under uncertainty in the retrofit analysis of the UK housing stock: Implications for the Green Deal. *Energy and Buildings*, 64, 292-308.

Booth, A.T., Choudhary, R. & Spiegelhalter, D.J., (2012). Handling uncertainty in housing stock models. *Building and Environment*, 48, 35-47.

Buck, (1996). Buck Research CR-1A User's Manual, Appendix 1: Humidity Conversion Equations.

Carpenter, B., Gelman, A., Hoffman, M.D., Lee, D., Goodrich, B., Betancourt, M., Riddell, A., Guo, J.Q., Li, P. & Riddell, A., (2017). Stan: A Probabilistic Programming Language. *Journal of Statistical Software*, 76(1), 1-29.

Castanedo, F., (2013). A Review of Data Fusion Techniques. *The Scientific World Journal*, 2013, 704504.

Chen, S., Friedrich, D., Yu, Z.B. & Yu, J., (2019). District Heating Network Demand Prediction Using a Physics-Based Energy Model with a Bayesian Approach for Parameter Calibration. *Energies*, 12(18).

Chen, Y.M. & Lan, L.L., (2010). Fault detection, diagnosis and data recovery for a real building heating/cooling billing system. *Energy Conversion and Management*, 51(5), 1015-1024.

Choi, Y. & Yoon, S., (2020). Virtual sensor-assisted in situ sensor calibration in operational HVAC systems. *Building and Environment*, 181.

Chong, A., Lam, K.P., Pozzi, M. & Yang, J.Z.J., (2017). Bayesian calibration of building energy models with large datasets. *Energy and Buildings*, 154, 343-355.

Chong, A. & Menberg, K., (2018). Guidelines for the Bayesian calibration of building energy models. *Energy and Buildings*, 174, 527-547.

Du, Z.M., Fan, B., Jin, X.Q. & Chi, J.L., (2014). Fault detection and diagnosis for buildings and HVAC systems using combined neural networks and subtractive clustering analysis. *Building and Environment*, 73, 1-11.

Fan, B., Du, Z.M., Jin, X.Q., Yang, X.B. & Guo, Y.B., (2010). A hybrid FDD strategy for local system of AHU based on artificial neural network and wavelet analysis. *Building and Environment*, 45(12), 2698-2708.

Gao, L., Li, D., Yao, L. & Gao, Y., (2022). Sensor drift fault diagnosis for chiller system using deep recurrent canonical correlation analysis and k-nearest neighbor classifier. *ISA Transactions*, 122, 232-246.

Gelman, A. & Rubin, D.B., (1992). Inference from iterative simulation using multiple sequences. *Statistical science*, 7(4), 457-472.

Goyal, S., Ingley, H.A. & Barooah, P., (2012). Effect of various uncertainties on the performance of occupancy-based optimal control of HVAC zones, 2012 IEEE 51st IEEE conference on decision and control (CDC). IEEE, pp. 7565-7570.

Guo, Y.B., Li, G.N., Chen, H.X., Hu, Y.P., Li, H.R., Xing, L. & Hu, W.J., (2017). An enhanced PCA method with Savitzky-Golay method for VRF system sensor fault detection and diagnosis. *Energy and Buildings*, 142, 167-178.

Hempel, S., König, M., Menz, C., Janke, D., Amon, B., Banhazi, T.M., Estellés, F. & Amon, T., (2018). Uncertainty in the measurement of indoor temperature and humidity in naturally ventilated dairy buildings as influenced by measurement technique and data variability. *Biosystems Engineering*, 166, 58-75.

Heo, Y., Augenbroe, G., Graziano, D., Muehleisen, R.T. & Guzowski, L., (2015). Scalable methodology for large scale building energy improvement: Relevance of calibration in model-based retrofit analysis. *Building and Environment*, 87, 342-350.

Heo, Y., Choudhary, R. & Augenbroe, G.A., (2012). Calibration of building energy models for retrofit analysis under uncertainty. *Energy and Buildings*, 47, 550-560.

Hoffman, M.D. & Gelman, A., (2014). The No-U-Turn Sampler: Adaptively Setting Path Lengths in Hamiltonian Monte Carlo. *Journal of Machine Learning Research*, 15, 1593-1623.

Hou, D., Hassan, I.G. & Wang, L., (2021). Review on building energy model calibration by Bayesian inference. *Renewable & Sustainable Energy Reviews*, 143.

Huang, G.S., Sun, Y.J. & Li, P., (2011). Fusion of redundant measurements for enhancing the reliability of total cooling load based chiller sequencing control. *Automation in Construction*, 20(7), 789-798.

Huang, G.S., Wang, S.W. & Sun, Y.J., (2008). Enhancing the Reliability of Chiller Control Using Fused Measurement of Building Cooling Load. *Hvac&R Research*, 14(6), 941-958.

Huang, G.S., Wang, S.W., Xiao, F. & Sun, Y.J., (2009). A data fusion scheme for building automation systems of building central chilling plants. *Automation in Construction*, 18(3), 302-309.

ISO/IEC Guide 98-3/Suppl.1, (2008). Uncertainty of measurement-Part 3: Guide to the expression of uncertainty in measurement (GUM: 1995)-Supplement 1: Propagation of distributions using a Monte Carlo method. ISO/IEC.

Jia, L.Z., Wei, S. & Liu, J.J., (2021). A review of optimization approaches for controlling water-cooled central cooling systems. *Building and Environment*, 203.

Julia, S., Carlos, C.D. & Christoph, F.R., (2017). Validation of a Bayesian-based method for defining residential archetypes in urban building energy models. *Energy and Buildings*, 134, 11-24.

Kang, J., Wang, S.W. & Gang, W.J., (2017). Performance of distributed energy systems in buildings in cooling dominated regions and the impacts of energy policies. *Applied Thermal Engineering*, 127, 281-291.

Kang, Y. & Krarti, M., (2016). Bayesian-Emulator based parameter identification for calibrating energy models for existing buildings. *Building Simulation*, 9(4), 411-428.

Karami, M. & Wang, L.P., (2018). Particle Swarm optimization for control operation of an all-variable speed water-cooled chiller plant. *Applied Thermal Engineering*, 130, 962-978.

Lee, P., Lam, P.T.I. & Lee, W.L., (2015). Risks in Energy Performance Contracting (EPC) projects. *Energy and Buildings*, 92, 116-127.

155

Li, G. & Hu, Y., (2019). An enhanced PCA-based chiller sensor fault detection method using ensemble empirical mode decomposition based denoising. *Energy and Buildings*, 183, 311-324.

Li, G.N., Hu, Y.P., Chen, H.X., Li, H.R., Hu, M., Guo, Y.B., Shi, S.B. & Hu, W.J., (2016). A sensor fault detection and diagnosis strategy for screw chiller system using support vector data description-based D-statistic and DV-contribution plots. *Energy and Buildings*, 133, 230-245.

Li, Q., Augenbroe, G. & Brown, J., (2016). Assessment of linear emulators in lightweight Bayesian calibration of dynamic building energy models for parameter estimation and performance prediction. *Energy and Buildings*, 124, 194-202.

Li, X., Liu, J., Liu, B., Zhang, Q., Li, K., Dong, Z. & Mou, L., (2021). Impacts of data uncertainty on the performance of data-driven-based building fault diagnosis. *Journal of Building Engineering*, 43, 103153.

Li, Z.W., Huang, G.S. & Sun, Y.J., (2014). Stochastic chiller sequencing control. *Energy and Buildings*, 84, 203-213.

Liao, Y.D., Huang, G.S., Ding, Y.F., Wu, H.J. & Feng, Z.B., (2018). Robustness enhancement for chiller sequencing control under uncertainty. *Applied Thermal Engineering*, 141, 811-818.

Liao, Y.D., Huang, G.S., Sun, Y.J. & Zhang, L.F., (2014). Uncertainty analysis for chiller sequencing control. *Energy and Buildings*, 85, 187-198.

Liao, Y.D., Sun, Y.J. & Huang, G.S., (2015). Robustness analysis of chiller sequencing control. *Energy Conversion and Management*, 103, 180-190.

Lim, H. & Zhai, Z.Q., (2018). Influences of energy data on Bayesian calibration of building energy model. *Applied Energy*, 231, 686-698.

Lu, X., O'Neill, Z., Li, Y. & Niu, F., (2020). A novel simulation-based framework for sensor error impact analysis in smart building systems: A case study for a demand-controlled ventilation system. *Applied Energy*, 263, 114638.

Luo, X.J. & Fong, K.F., (2020). Novel pattern recognition-enhanced sensor fault detection and diagnosis for chiller plant. *Energy and Buildings*, 228, 110443.

Ma, Z.J. & Wang, S.W., (2009). An optimal control strategy for complex building central chilled water systems for practical and real-time applications. *Building and Environment*, 44(6), 1188-1198.

Ma, Z.J. & Wang, S.W., (2011). Supervisory and optimal control of central chiller plants using simplified adaptive models and genetic algorithm. *Applied Energy*, 88(1), 198-211.

Mao, Q.J., Fang, X., Hu, Y.P. & Li, G.N., (2018). Chiller sensor fault detection based on empirical mode decomposition threshold denoising and principal component analysis. *Applied Thermal Engineering*, 144, 21-30.

Minasny, B. & McBratney, A., 2010. Conditioned Latin hypercube sampling for calibrating soil sensor data to soil properties, Proximal soil sensing. Springer, pp. 111-119.

Minasny, B. & McBratney, A.B., (2006). A conditioned Latin hypercube method for sampling in the presence of ancillary information. *Computers & Geosciences*, 32(9), 1378-1388.

Ng, K.H., Yik, F.W.H., Lee, P., Lee, K.K.Y. & Chan, D.C.H., (2020). Bayesian method for HVAC plant sensor fault detection and diagnosis. *Energy and Buildings*, 228, 110476.

Ohlsson, K.E.A., Nair, G. & Olofsson, T., (2022). Uncertainty in model prediction of energy savings in building retrofits: Case of thermal transmittance of windows. *Renewable and Sustainable Energy Reviews*, 168, 112748.

Omrany, H., Ghaffarianhoseini, A., Ghaffarianhoseini, A., Raahemifar, K. & Tookey, J., (2016). Application of passive wall systems for improving the energy efficiency in buildings: A comprehensive review. *Renewable & Sustainable Energy Reviews*, 62, 1252-1269.

Risch, S., Remmen, P. & Muller, D., (2021). Influence of data acquisition on the Bayesian calibration of urban building energy models. *Energy and Buildings*, 230.

Rysanek, A.M., Fonseca, J.A. & Schlueter, A., (2019). Bayesian calibration of a building energy model by stochastic optimisation of root-mean square error. *ETH Zurich*.

Shi, W., Jin, X. & Wang, Y., (2019). Evaluation of energy saving potential of HVAC system by operation data with uncertainties. *Energy and Buildings*, 204, 109513.

Song, K., Jang, Y., Park, M., Lee, H.S. & Ahn, J., (2020). Energy efficiency of end-user groups for personalized HVAC control in multi-zone buildings. *Energy*, 206.

Sun, S.B., Li, G.N., Chen, H.X., Guo, Y.B., Wang, J.Y., Huang, Q.Y. & Hu, W.J., (2017). Optimization of support vector regression model based on outlier detection methods for predicting electricity consumption of a public building WSHP system. *Energy and Buildings*, 151, 35-44.

Sun, Y.J., Wang, S.W. & Xiao, F., (2013). In situ performance comparison and evaluation of three chiller sequencing control strategies in a super high-rise building. *Energy and Buildings*, 61, 333-343.

Taylor, S.T. & Cheng, C.H., (2010). Economizer High Limit Controls and Why Enthalpy Economizers Don't Work. *Ashrae Journal*, 52(11), 12-28.

Thangavelu, S.R., Myat, A. & Khambadkone, A., (2017). Energy optimization methodology of multi-chiller plant in commercial buildings. *Energy*, 123, 64-76.

Tian, W., Heo, Y., de Wilde, P., Li, Z.Y., Yan, D., Park, C.S., Feng, X.H. & Augenbroe, G., (2018). A review of uncertainty analysis in building energy assessment. *Renewable & Sustainable Energy Reviews*, 93, 285-301.

Tian, W., Yang, S., Li, Z., Wei, S., Pan, W. & Liu, Y., (2016). Identifying informative energy data in Bayesian calibration of building energy models. *Energy and Buildings*, 119, 363-376.

Tian, W., Yang, S., Li, Z.Y., Wei, S., Pan, W. & Liu, Y.L., (2016). Identifying informative energy data in Bayesian calibration of building energy models. *Energy and Buildings*, 119, 363-376.

Vehtari, A., Gelman, A., Simpson, D., Carpenter, B. & Bürkner, P.-C., (2021). Rank-Normalization, Folding, and Localization: An Improved Rhat for Assessing Convergence of MCMC. *Bayesian Analysis*, 16(2), 667-718.

Wang, P., Han, K.H., Liang, R.B., Ma, L.D. & Yoon, S., (2021). The virtual in-situ calibration of various physical sensors in air handling units. *Science and Technology for the Built Environment*, 27(6), 691-713.

Wang, S., Zhou, Q. & Xiao, F., (2010). A system-level fault detection and diagnosis strategy for HVAC systems involving sensor faults. *Energy and Buildings*, 42(4), 477-490.

Xiao, F., Zhao, Y., Wen, J. & Wang, S., (2014). Bayesian network based FDD strategy for variable air volume terminals. *Automation in Construction*, 41, 106-118.

Yan, B., Li, X.W., Malkawi, A.M. & Augenbroe, G., (2017). Quantifying uncertainty in outdoor air flow control and its impacts on building performance simulation and fault detection. *Energy and Buildings*, 134, 115-128.

Yan, R., Ma, Z.J., Kokogiannakis, G. & Zhao, Y., (2016). A sensor fault detection strategy for air handling units using cluster analysis. *Automation in Construction*, 70, 77-88.

Yan, Y., Cai, J., Tang, Y. & Yu, Y., (2022). A Decentralized Boltzmann-machine-based fault diagnosis method for sensors of Air Handling Units in HVACs. *Journal of Building Engineering*, 50, 104130.

Yang, X.-B., Jin, X.-Q., Du, Z.-M. & Zhu, Y.-H., (2011). A novel model-based fault detection method for temperature sensor using fractal correlation dimension. *Building and Environment*, 46(4), 970-979.

Yang, X.B., Jin, X.Q., Du, Z.M., Fan, B. & Zhu, Y.H., (2014). Optimum operating performance based online fault-tolerant control strategy for sensor faults in air conditioning systems. *Automation in Construction*, 37, 145-154.

Yao, Y. & Wang, L., (2010). Energy analysis on VAV system with different air-side economizers in China. *Energy and Buildings*, 42(8), 1220-1230.

Yi, D.H., Kim, D.W. & Park, C.S., (2019). Parameter identifiability in Bayesian inference for building energy models. *Energy and Buildings*, 198, 318-328.

Yi, D.H. & Park, C.S., (2021). Model selection for parameter identifiability problem in Bayesian inference of building energy model. *Energy and Buildings*, 245.

Yoon, S., (2020). In-situ sensor calibration in an operational air-handling unit coupling autoencoder and Bayesian inference. *Energy and Buildings*, 221.

Yoon, S. & Yu, Y., (2018). Strategies for virtual in-situ sensor calibration in building energy systems. *Energy and Buildings*, 172, 22-34.

Yoon, S. & Yu, Y.B., (2017). Extended virtual in-situ calibration method in building systems using Bayesian inference. *Automation in Construction*, 73, 20-30.

Yoon, S.M. & Yu, Y.B., (2017). A quantitative comparison of statistical and deterministic methods on virtual in-situ calibration in building systems. *Building and Environment*, 115, 54-66.

Yu, F.W. & Chan, K.T., (2007). Optimum load sharing strategy for multiple-chiller systems serving air-conditioned buildings. *Building and Environment*, 42(4), 1581-1593.

Yu, Y.B. & Li, H.R., (2015). Virtual in-situ calibration method in building systems. *Automation in Construction*, 59, 59-67.

Yu, Y.B., Woradechjumroen, D.C. & Yu, D.H., (2014). A review of fault detection and diagnosis methodologies on air-handling units. *Energy and Buildings*, 82, 550-562.

Zhang, L., Leach, M., Bae, Y., Cui, B., Bhattacharya, S., Lee, S., Im, P., Adetola, V., Vrabie, D. & Kuruganti, T., (2021). Sensor impact evaluation and verification for fault detection and diagnostics in building energy systems: A review. *Advances in Applied Energy*, 3, 100055.

Zhao, T.Y., Li, J.T., Wang, P., Yoon, S.M. & Wang, J.Q., (2022). Improvement of virtual in-situ calibration in air handling unit using data preprocessing based on Gaussian mixture model. *Energy and Buildings*, 256.

Zhu, C.Q., Tian, W., Yin, B.Q., Li, Z.Y. & Shi, J.X., (2020). Uncertainty calibration of building energy models by combining approximate Bayesian computation and machine learning algorithms. *Applied Energy*, 268.

Zhu, Y., Jin, X. & Du, Z., (2012). Fault diagnosis for sensors in air handling unit based on neural network pre-processed by wavelet and fractal. *Energy and Buildings*, 44, 7-16.

Zhuang, C.Q. & Wang, S.W., (2020). Risk-based online robust optimal control of air-conditioning systems for buildings requiring strict humidity control considering measurement uncertainties. *Applied Energy*, 261.

Zhuang, C.Q., Wang, S.W. & Shan, K., (2020). A risk-based robust optimal chiller sequencing control strategy for energy-efficient operation considering measurement uncertainties. *Applied Energy*, 280.